POLITECNICO DI TORINO

Department of Mechanical and Aerospace Engineering

Class LM-21 Degree: BIOMEDICAL ENGINEERING

Master thesis in Biomedical Engineering

EFFECTS OF PATHOLOGIC AORTIC VELOCITY PROFILES ON CORONARY ARTERIES HEMODYNAMICS

Supervisor: *Prof. Umberto Morbiducci*
Co-Supervisor: *Dr. Diego Gallo*
Dr. Maurizio Lodi Rizzini

Master Student
Gabriele Birritta

Academic Year 2017-18

SOMMARIO

ABSTRACT

According to American Heart Association, *cardiovascular diseases* (*CVDs*) are the leading cause of morbidity, disability and mortality in developed world. Heart valve diseases are in third place, after hypertension and atherosclerosis, of *CVDs* with the highest prevalence.

Physiological aortic valve present three leaflet (*TAV*), but some people birth with congenital aortic valve alterations. In particular, the most prevalent anomaly (*1%* to *2%* in the developed world) is *bicuspid aortic valve* (*BAV*) in which the aortic valve presents only two flaps, of which one of these is the result of a fusion of two other leaflets. This pathology presents three different phenotypes: *LR-BAV*, *RN-BAV, NL-BAV*.

Aim of this master thesis is to mimic, starting from analytical formulations grounded in basic fluid mechanics, three-dimensional shapes of the velocity profile outing from bicuspid aortic valve, and, imposing them as inflow boundary conditions, studying if this alteration in blood velocity profile has an effect in coronary perfusion and hemodynamics. Three different velocity profiles configurations are prescribed, one for each of the three types of *BAV.* These *BAV*-like velocity profiles were compared with parabolic velocity profile considered as physiological baseline in our study.

In detail, a three-dimensional model of aorta and coronary arteries, reconstructed from clinical images acquired with a CT scan was considered as region of interest of this study. *Flow extensions* were added to each coronary outlet to minimize the impact of outlet boundary conditions, using *VMTK.* Then, a radius-based mesh was generated, using TetGen mesh generator implemented in the software *SimVascular.* Grid independence analysis was performed in order to find the best compromise between results accuracy and computational times.

BAV-like velocity profiles were generated using an ad-hoc python script implementing analytical formulations. The script estimated profile eccentricity based on pathological value of geometric orifice area. Two different velocity profiles were generated for each BAV configuration, one having only the forward flow and one having both *forward* and *backward* flow. TAV-like configuration was generated as parabolic profile using the Hagen-Poiseuille equation.

--- Abstract ---

Hemodynamics was simulated using the open-source code *SimVascular*, an ad-hoc computational fluid dynamics (CFD) solver based on the finite element method (FEM). Blood was considered as a Newtonian incompressible fluid. The different velocity profiles were prescribed as inlet boundary conditions, while a lumped parameter model completely resistive has been adopted as the outlet boundary condition. Blood vessels walls were assumed as rigid and no-slip condition was applied at walls.

Model hemodynamics was characterized both in term of wall shear stress and bulk quantities, such as velocity, vorticity and helicity, and the percentage differences between physiological-like inlet boundary condition simulation and BAV-like inlet boundary condition simulations were computed for each hemodynamic quantity.

The findings of this study suggest that coronary flows remain relatively unchanged, independent of the inflow velocity profile. In detail, marked differences in wall shear stress distribution were locally observed, in particular in left coronary artery, in correspondence of bifurcations. Overall, very low WSS percentage differences (less than 6% in LCA and less than 3,5% in RCA) from the physiological reference case were observed in BAV models, on average. Regarding velocity distribution it was observed that, depending on the shape of the imposed velocity profile at the inflow section, each coronary branch is influenced at different levels, but percentage differences from the physiological reference case remain low (less than 6% in LCA, less than 3,5% in RCA). Interestingly, the analysis of helical blood flow patterns also seems to suggest that the mimicked BAV conditions maintain the same helical flow structures as the physiologic case in two out of three configurations, *NR-BAV and NL-BAV.* Combining findings information from all helical flow descriptors, we note that RCA helical flow are not too distant from the physiologic case, but on contrary LCA percentage differences are very high in all BAV cases (LNH around 110%, h2 is 0%, h1, h3 and h4 around 450%). The main findings of the proposed study represent a good starting point for a better understanding of the hemodynamic modifications induced from heart valve pathologies on coronary arteries hemodynamics.

1. INTRODUCTION

1.1 CARDIAC ANATOMY AND PHYSIOLOGY

The **cardiovascular system** is a closed system of the *heart* and *blood vessels*. Its function is to deliver oxygen and nutrient rich blood to our tissues and to carry away waste products. The heart is the complex pump and the vessels, are tubes which carry blood to all the body districts. The importance of heart and the efficiency of the work of circulation are obvious, just think that, over one year, around 10000000 litres of blood are sent through this closed system [1-3].

The principal muscle, the heart, sits in the pericardial cavity, between lungs in the left centre of chest. It is divided in four chambers, the two top chambers are called *atria*, while the two bottom chambers are called *ventricles*.

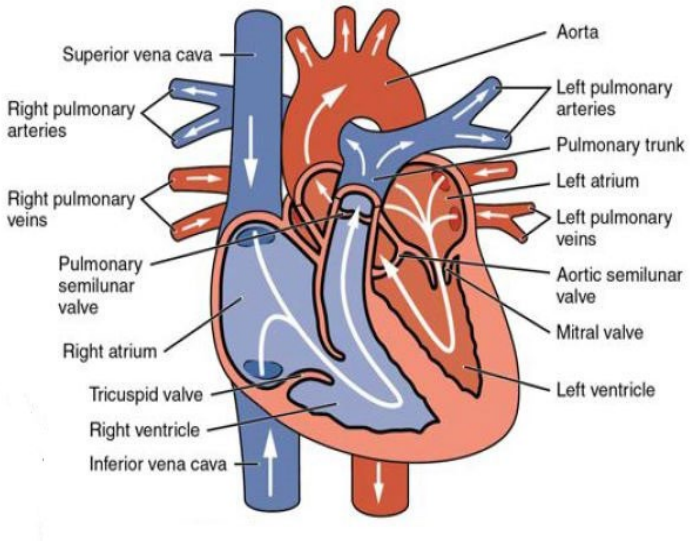

Figure 1-1: The normal heart [1].

In general, it is possible to speak about co-working, because the right side of the heart has the work to send deoxygenated blood to lungs, while the left side pump oxygenated blood to the rest of body. Based on this, two distinct circuits are highlighted: the pulmonary circuit and the systemic circuit. *In **pulmonary circuit, blood is*** transported to and from lungs, where it picks up oxygen and delivers carbon dioxide. *In **systemic circuit*** blood is transported to all tissues carrying oxygen and returns relatively deoxygenated to heart to be sent back to pulmonary circulation [1,2].

Main vessels are: *arteries* usually coloured in red because they carry oxygenated blood from heart to the rest of body, *veins* usually coloured in blue because they carry deoxygenated blood back to the heart and *capillaries* the smallest vessels, connecting the arteries to the veins, within the tissues where gas exchange take place [3]. Further details are provided in the next chapter.

The right atrium pumps blood into right ventricle. Then right ventricle pumps blood to pulmonary trunk, through pulmonary arteries, to lungs. From lungs, blood drains into left atrium and is then pumped into left ventricle. Then, left ventricle pumps blood into aorta which then distributes it to the rest of the body through other arteries [4].

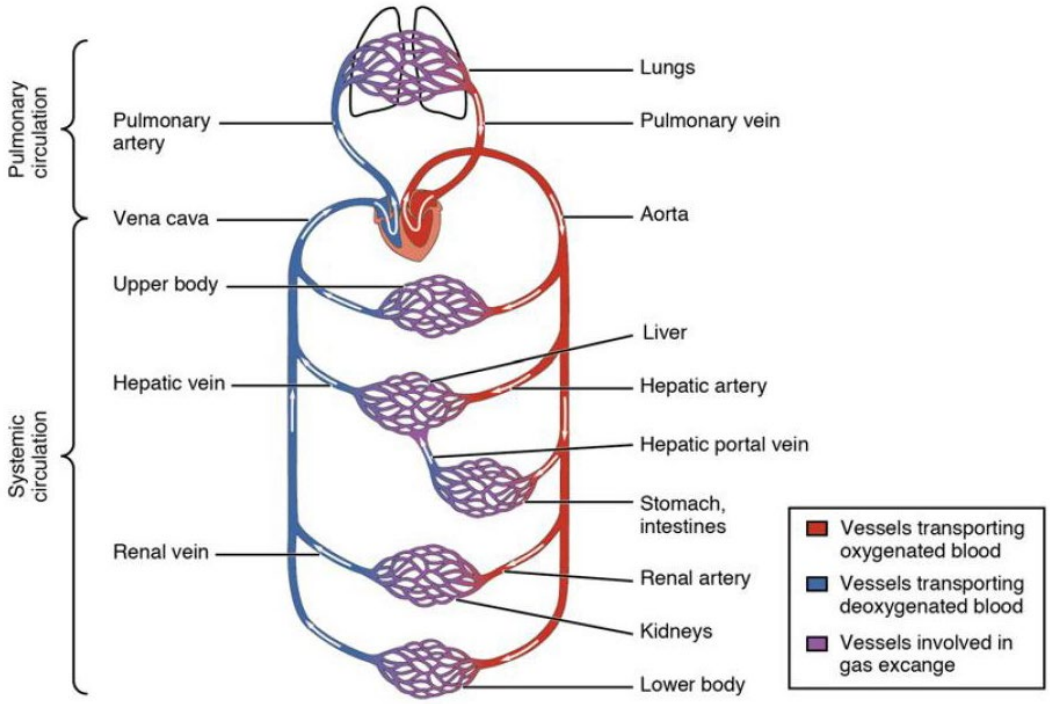

Figure 1-2: Cardiac circulation and its two circuits[1].

The pumping heart action results from myocardium contraction. Muscle cells wrap in an intricate way the four chambers and their contraction generate a complex swirling pattern, that push out the blood in an efficient way.

The ***cardiac cycle*** is a process that mixes electrical and muscular activity of the heart, to allow a correct perfusion of the body. Specialized conducting components such as the sinoatrial node, the internodal pathways, the atrioventricular node, the atrioventricular bundle, right and left bundle branches, and the Purkinje fibers, are the impulse generator that timing the sequence of the heartbeat event. Contracting phase is called *systole*, while the relaxing phase is called *diastole* [1,3].

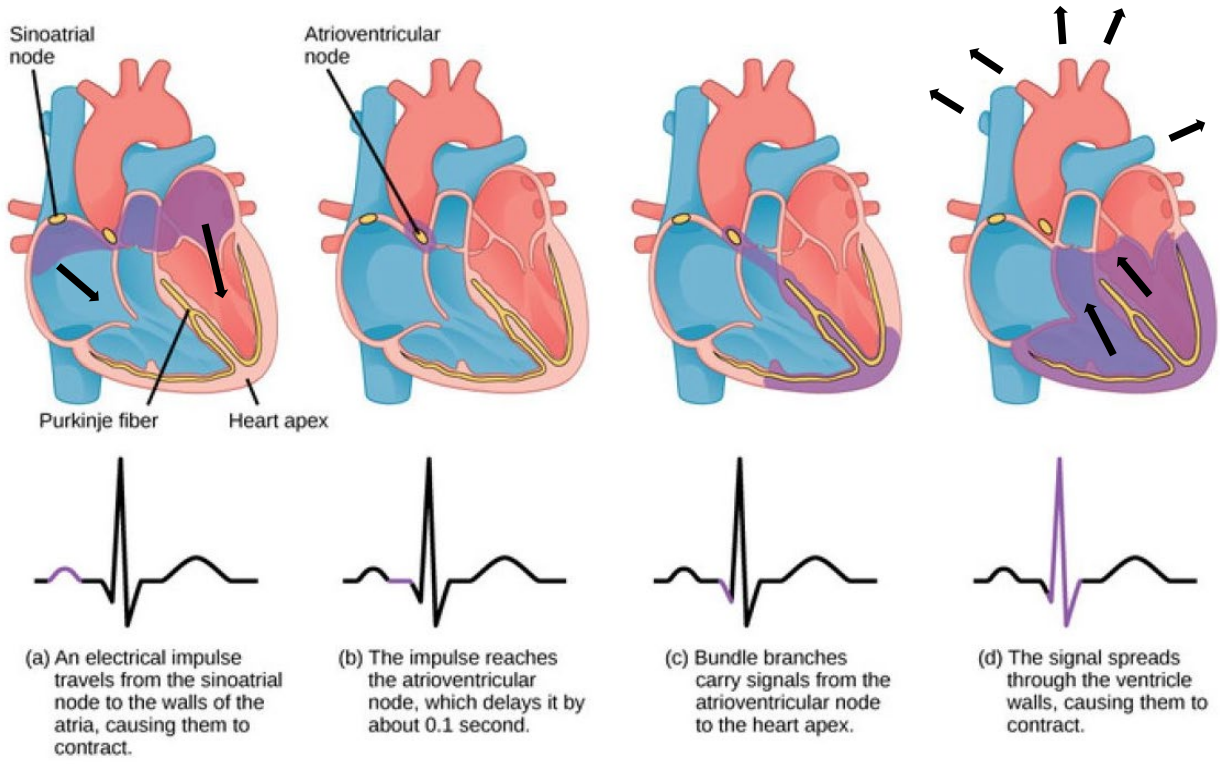

Figure 1-3: Cardiac cycle and relative ECG phase [2].

At the beginning of cycle both atria and ventricles are in diastole, so chambers fill with blood, then from the internal pacemaker start the electric signal that turn the atria state in systole, therefore blood pass from atria to ventricles. The next phase is ventricular systole, where both ventricles contract and pump blood into aorta (left side of heart) and pulmonary trunk (right side of heart). In this step atria are in diastole and receive new blood from pulmonary veins (left side of heart), and from superior vena cava and the inferior vena cava (right side of heart). After that, the following step is the ventricular diastole, and the cycle restart [1 ,4].

An observation to underline is the passage from atria to ventricles, which are separated by two *cardiac valves*, mitral (left side of heart) and tricuspid (right side of heart). They close and open to stop or allow the blood flow and ensure the unidirectional stream and avoid cardiac regurgitation. In the following chapters this topic will be described in detail [1, 4].

1.2 BLOOD VESSELS

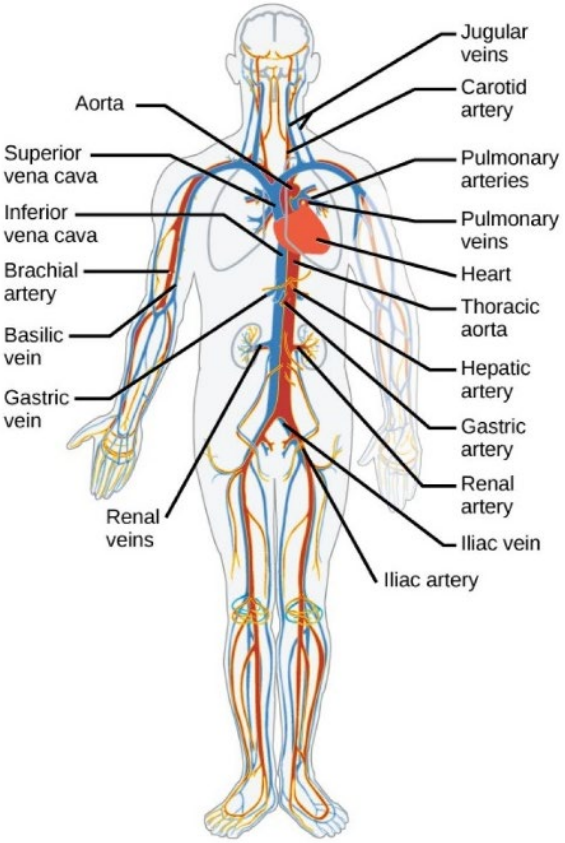

Figure 1-4: Blood vessels network, arteries (red) veins (blue) [2].

All parts of our body are sprayed by blood and this is possible thanks to the natural development in search to maximize the efficiency of the complex network which is the vascular system. Our lives depend on it, and using a simple and clear metaphor, it is a large tree with a million branches that varies in size, properties and role to reach every tissue, organ, muscle, cells in the body to provide nourishment and help in fighting diseases, stabilize temperature, and maintain the physiologic homeostasis.

Main vessels are divided between the arteries and the veins. They share the same function to transport blood, but at the same time they show important structural modifications based on their different role, such as the direction of delivery and the different blood pressure that flows through them in each district of the body [2].

Both arteries and veins have three distinct layers, called tunics, around the lumen where blood flows:

- *Tunica intima*
- *Tunica media*
- *Tunica externa*

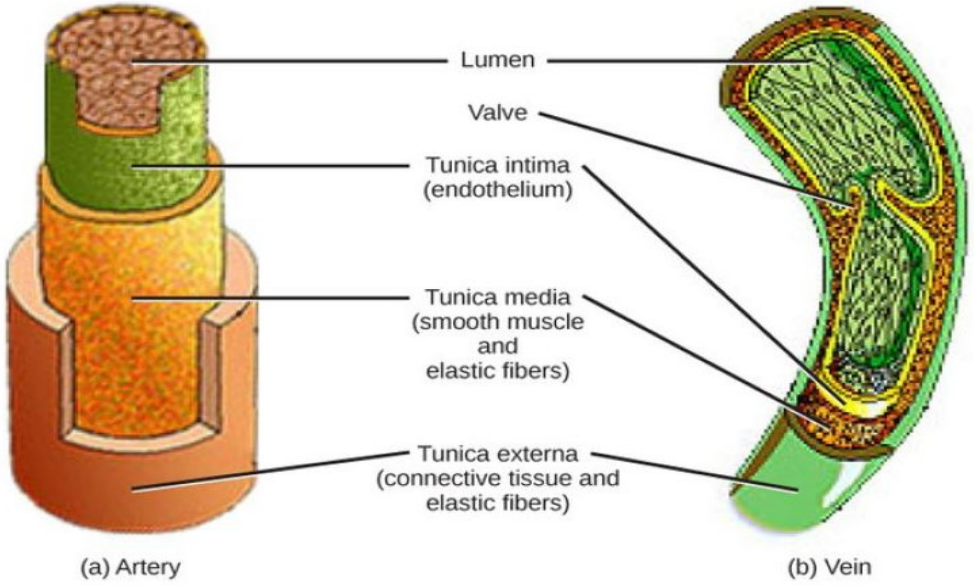

Figure 1-5: Arteries and veins layers [2].

Tunica intima, composed of epithelial and connective tissue, is the first boundary layer and the only one in direct contact with blood, so its integrity is of primary importance to avoid atherogenesis. This layer appears wavy due to constriction of smooth muscle in arteries, while it results smooth in veins. The endothelium is related to the connective tissue by the basal lamina, which has a structural and filter function to adjust the exchange [1, 5].

Tunica media is the thickest layer (much more in arteries than in veins), it is a mix of smooth muscle cells and elastic fibers and plays an important role in the propagation of the systolic pulse of the heart, using a continuous action of vasoconstriction and vasodilation regulated by vascular nerves [1, 5].

The last layer is ***tunica externa*** or ***adventitia***. Normally collagenous and elastic fibers predominate, in veins and smaller vessel there are also smooth muscle fibers according to the contraction/dilation regulation. A lot of nerve connections run along this layer mixing with the vasa vasorum [1, 5].

Vasa vasorum are micro blood vessels, located in the outer wall layers. In normal vessels, from the adventitia they grow into the media and actively regulate blood flow to the wall of these vessels. For this reason, vasa vasorum are considered the principal maintainer of normal structure and function to deliver nutrients and oxygen and to remove waste products, even considering that, the inner tunica media is a not blood irrorate layer. Note that, vasa vasorum

are not present in all vessels at the same way, but in arteries and veins they proliferate in response to wall thickness increase and release of angiogenic substances, to provide effective support [1,6-7].

About the compositions, these two types of vessels show two main differences: (1) arteries have the ***internal elastic lamina***, a thick and fenestrated layer of elastic fibers longitudinally arranged along the vessel to separate tunica intima and tunica media, while veins do not have it; (2)the ***external elastic lamina***, a wavy boundary between tunica media and tunica externa, which appears only in big arteries, not in arterioles or veins [1, 5].

1.2.1 An Overview of Arteries

Arteries (diameter 1–30 mm) are the blood vessels that deliver oxygen-rich blood from heart to tissues of the body (except for pulmonary arteries and umbilical arteries, that are the only arteries, belonging to the pulmonary circuit, that carry venous blood). The size and the composition of these vessels change proportionally by moving away from heart.

The largest arteries, which are also the closest to the heart, have the thickest walls and their tunica intima has a high percentage of elastin. Elastic fibers allow to these arteries to help heart in its pumping work. Therefore, their walls are able to be strong, flexible and resilient to expand and recoil so as to continuously adapt their resistance to blood flow and thus help maintain high blood pressures [8].

Farther from heart, it is possible to notice a decrease of elastin and an increase of muscle smooth fibers. This change in composition is explicable with the role that they play. When are distant from heart the push of blood, due to its contraction, is less efficient and weak and drop of pressure are frequently phenomes. Therefore, their ability to be elastic is less important, while having a higher number of smooth muscles allows to distribute blood to the vast network of arterioles, for this reason they are called also *distributive arteries* [8]

Arterioles (diameter 10–100 µm) are arteries smaller than the previous ones. These micro vessels are the same as the others, the only change is related to the thickness of the three layers and to their role, because the arterioles are the main site of resistance and regulation of blood pressure,

using constriction and dilatation movements, because of that they show a high prevalence of smooth muscle cells [1,5, 9].

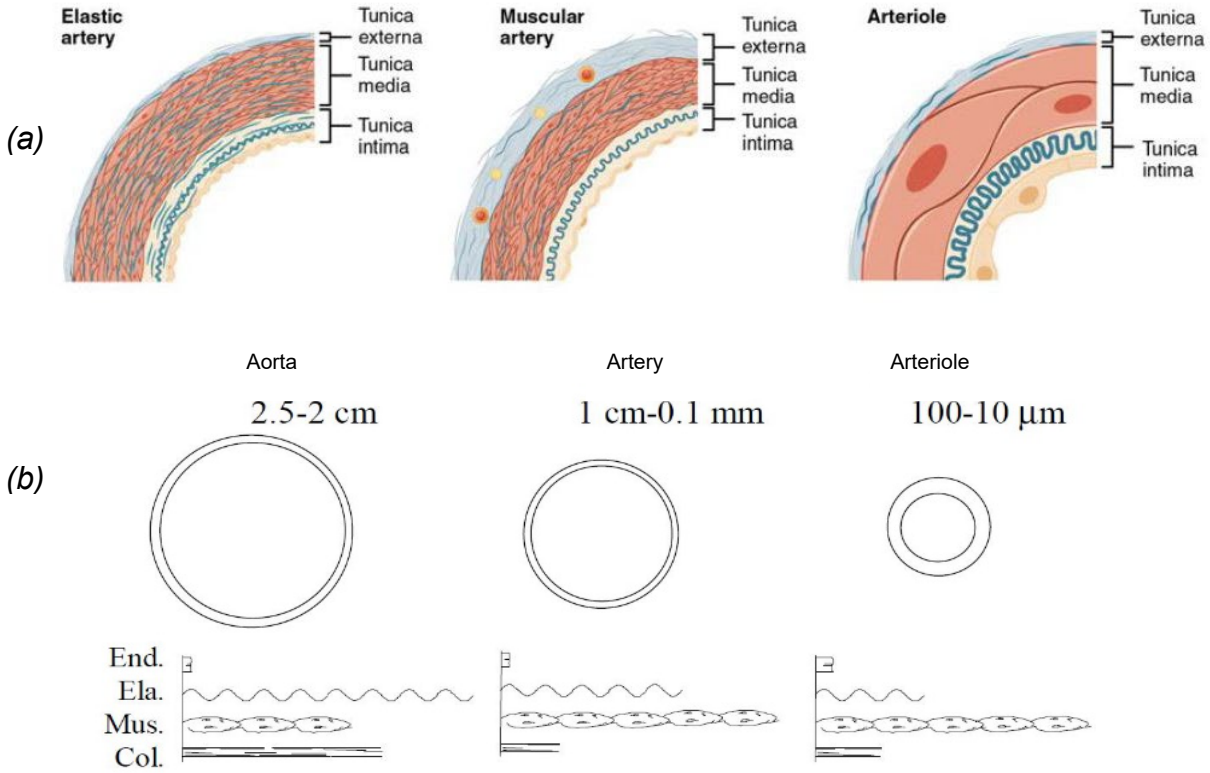

Figure 1-6: (a) Arteries and arterioles layers in details [1]*; (b) Aorta, arteries and Arterioles compositions* [5].

1.2.2 An Overview of Capillaries

Capillaries (diameter 4–40 µm) are vessels with extremely thin walls, the flow through them describe the microcirculation. Their walls show only one endothelial layer with occasional smooth muscle cells. The primary function of these micro vessels is to link smallest arteries with smallest veins. Therefore, they are the main characters of perfusion, a biunivocal gases and substances exchange. Oxygen and nutrient pass from blood to the tissue and carbon dioxide goes in the opposite way.

To allow this substances passage, their walls must be holey, and it is possible to discriminate three kind of capillaries: continuous, fenestrated and sinusoid.

Continuous capillaries show tight slots, where usually pass substances such as glucose, water, ions and hydrophobic molecules; ***fenestrated*** ones show pores for larger molecules; and the last ones, ***sinusoid*** capillaries are flattened with big gaps for the largest molecules such as plasma proteins or cells [1,2, 5,6].

(a)

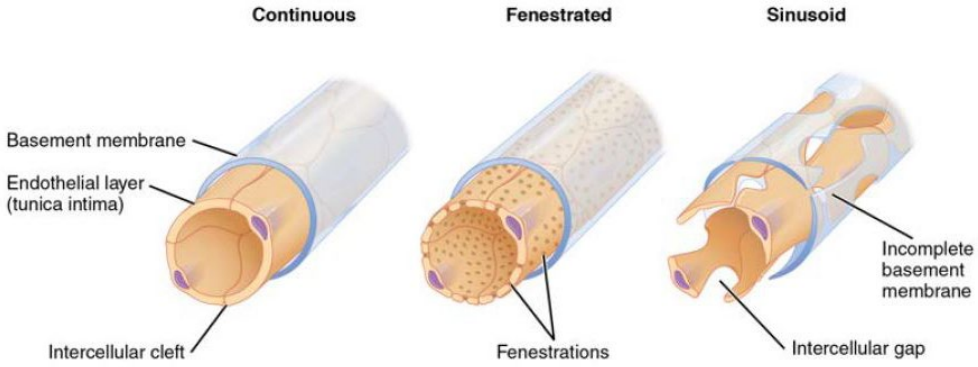

(b)

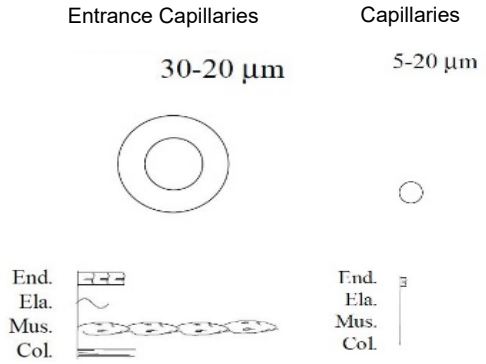

Figure 1-7: (a) Capillaries layers in details [1]*; (b) Capillaries composition* [5].

1.2.3 An Overview of Veins

Veins (diameter 1–25 mm) are blood vessels similar to arteries, but with an opposite role in the human circulatory system, in fact, they are used to carry dirty blood and clean up tissues from waste products. Their physiology shows that they have a large and irregular lumen and the same three layers previously described. Veins bring deoxygenated blood from the tissues to the heart. The exchange occurs at capillary level in the capillary bed, then through venules start the return begins and finally veins drain out the deoxygenated blood into the right heart side to send it to the lung and clean it.

It is important to note that the most important difference from the arteries is that the veins have a system of *valves* that is necessary to impose a unidirectional blood flow, since they are low pressure vessels and therefore differently from the arteries, the pressure is not useful in veins work [1].

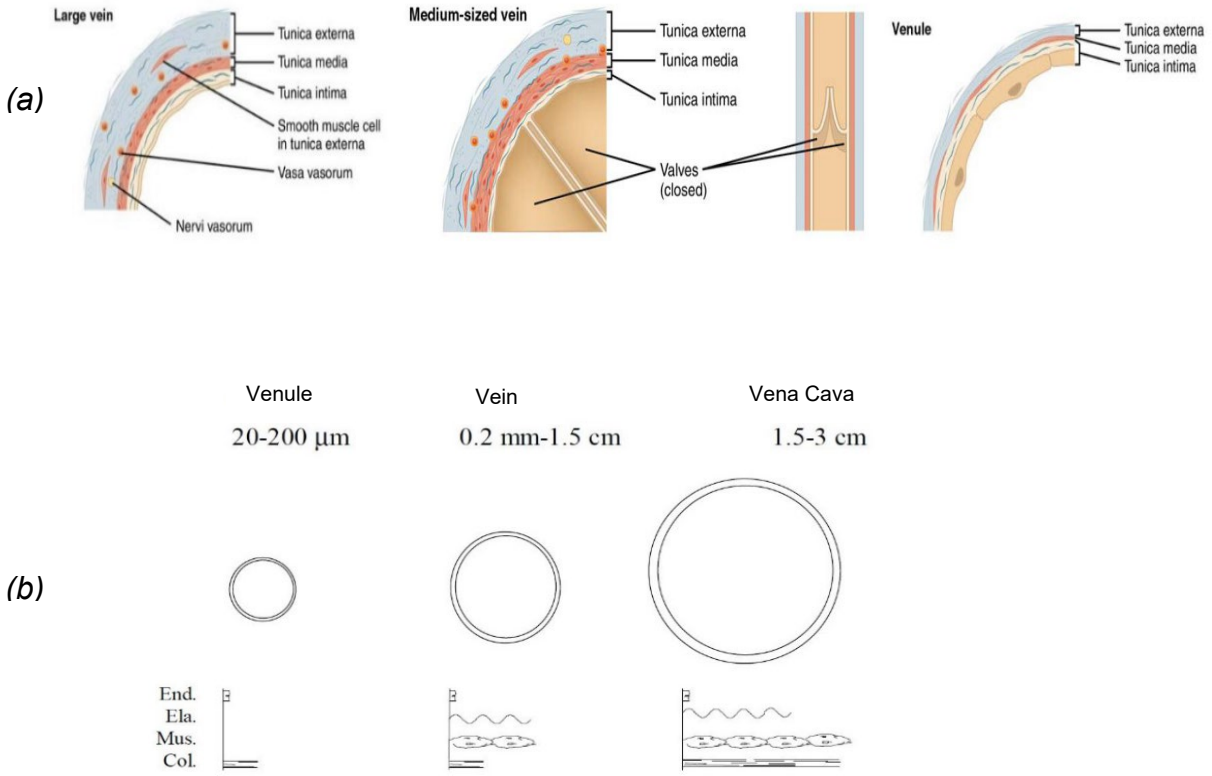

Figure 1-8: (a) Veins layers in details [1]*; (b) Veins composition* [5].

1.3 BLOOD

The circular system to perform the work described in the previous chapters efficiently, uses blood as a means of transport.

1.3.1 Components and Functions

The *blood* can be divided in two main parts: the ***fluid portion*** or plasma (yellow color) that is around 46-63% of the blood and the ***corpuscular portion*** (red blood cells, white blood cells and platelets) that is around the 37-54% [5].

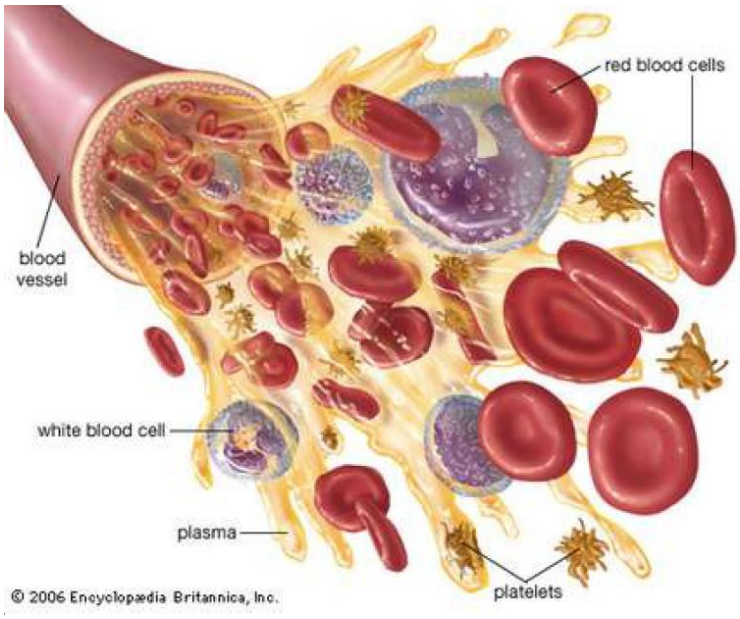

Figure 1-9: Illustration of all the components of the blood [10].

The ***plasma*** is a liquid or better it is classified as alkaline solution, composed by water in the 90% with inside numerous organic substances (such as proteins, hormones, lipids, vitamins, clotting factors ecc) and mineral substances, which can be find in suspension or dissolved. In general, the plasmatic proteins play a key role in the transport function of specific molecules, but at the same time some of these are nonspecific carrier proteins. Other important roles of the plasma are the immunological function (given that it has internal factors that help in the coagulation) and the enzymatic function [5,10].

The corpuscular components with the highest concentration are the ***erythrocytes*** or also commonly called *red blood cells*. They are anucleate cells with a form of biconcave disks, with a diameter size of approximately 8 µm and an external membrane called *stroma*. These elements transport gases in both two directions, from lungs to tissues and vice versa. They are constituted in the most percentage of ***haemoglobin***, which is the molecular that is able to bound to the oxygen atoms. In detail, the haemoglobin has four chains, where *heme group* is placed and using its iron atom, they involve reversible chemical links with oxygen. It should be noted that 90% of the oxygen is transported attached to the haemoglobin. They must to arrive in all tissues of the body, for this reason they are very flexible and able to modify their form to adapt to the specific canal size, travelling as *rouleaux* or in line one behind the other. These distortions generate on the erythrocytes cyclic structure stresses and they can allow to rupture. To avoid possible problems related to their haemolysis, they live for about 120 days. The red blood cells quantity is measured as a percentage of the volume, called *haematocrit* [1, 10-12].

White blood cells or also known as ***leukocytes***, are the corpuscular component involved in the defence of the organism. They are cells with nucleus and a cytoskeleton, that make them more rigid respect to the red blood cells. They are found inside and outside the bloodstream and they are a big group, where there are a lot of specialized types of cells that act in different way in relation of different enemies. The first subdivision is between granulocytes and agranulocytes. The ***granulocytes*** (approximately 12 µm in diameter) are called in this way because they show grains coloured and in this group are contained neutrophils, eosinophils, basophils. The ***agranulocytes*** (approximately 18 µm in diameter), instead, are without organelles and in this group are contained lymphocytes and monocytes [1, 10-12].

The last and smallest of the corpuscular components are the *platelets* or also known as ***thrombocytes***, they show a size approximately 3 µm in diameter and are without the nucleus. They are involved in the prevention mechanism to limit the loss of blood in injury. They immediately reach the rupture point and activated by chemicals messages and they aggregate together to coagulate or make a thrombus and stop the bleeding [1, 10-12].

Resuming, the functions that blood performs are a lot, important and involve all body, they can be grouped into three main categories [5,12]*:*

- *Transport*:
    - Carrying on oxygen from lungs to all tissue of every districts;

- Drain waste productions, such as urea and lactic acid that then are filtered by liver and kidneys;
- Providing of the nutrients, after the digestive action and their storage in the right sites;
- Removal carbon dioxide along the veins circulation;
- Leading hormones, enzymes and vitamins.

➢ *Protection*:

- Leukocytes or also called white blood cells, use the blood to arrive to the alien elements and destroy them or opposite them as first response for the immune system;
- In cases of injury, by the blood, platelet factors or thrombocytes run to initiate the haemostatic process and avoid huge haemorrhage.

➢ *Regulation*:

- Maintaining of the correct body temperature around 37/38 °C;
- Preserving the correct and physiologic pH level in the acid or basic area of the body;
- Regulating the water balance.

1.3.2 Rheology

The *rheology* is the discipline that work in the field of flow and deformation behaviour of the materials, both solid or fluid. Fluids, during their motions, are incessantly under the effects of the applied forces [5]. When speak about strengths, the application per unit area must be considered and, in this category, it is possible to differentiate two principal stress in the 3D space [5]*:*

➢ ***Normal stress*** σ: the force component in normal direction respect to the interested surface per unit area, also defined as a pressure.

➢ ***Shear stress*** τ*:* the force component in tangential direction on the interested surface per unit area.

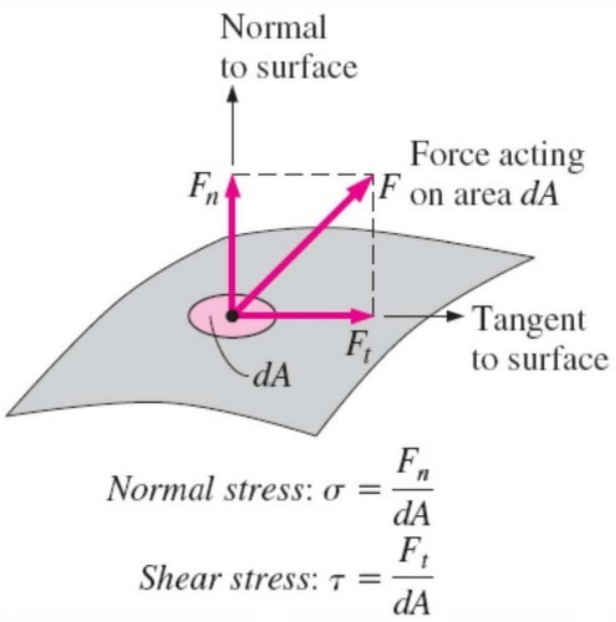

Figure 1-10: Stress acting per unit area [5].

The resistance of the fluid to the movement is quantifiable with the ***viscosity (μ)*** parameter, the rapport between shear stress and shear rate, and this factor of is fundamental importance to differentiate the two main groups of liquids: *Newtonian* and *Non-Newtonian* [13-14].

A ***Newtonian*** liquid is a fluid that shows direct proportionality in a shear rate-shear stress graph, so the viscosity is independent of variations. ***Non-Newtonian*** liquids show a different behaviour, their viscosity is not constant, but it is highly dependent on the shear rate or shear stress value and append to this they have a strong dependence on time [13-14].

$$\mu = [Pa \cdot s] = [N \cdot m^2 \cdot s] = 10^3 cPoise$$

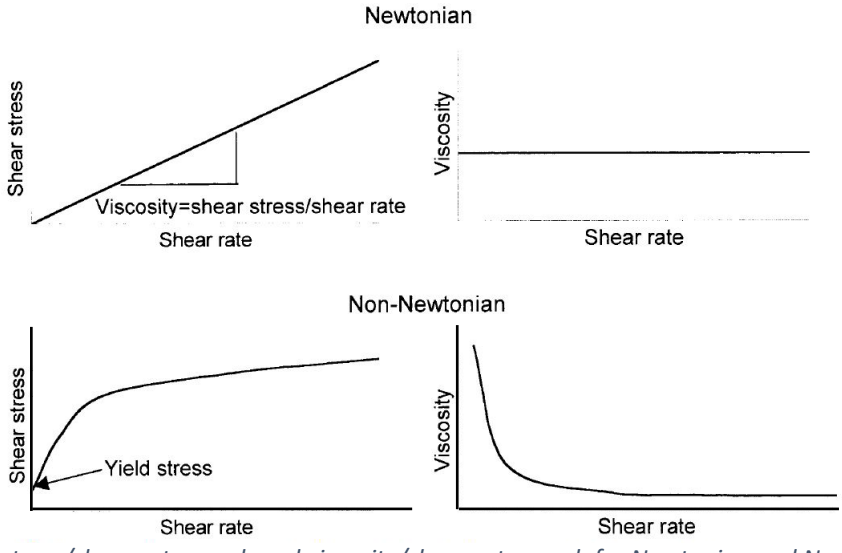

Figure 1-11: Shear stress/shear rate graph and viscosity/shear rate graph for Newtonian and Non-Newtonian fluids [12].

The blood can be classified how a Non-Newtonian fluid, due to its inhomogeneous characteristics. For this reason, its viscosity doesn't have a single value, but depends on the vessels size and the disease condition in exam. The plasma, in general, is a Newtonian liquid, but the main changes in behaviour are correlated to erythrocytes and their ability to deform their shape and to aggregate each other in rouleaux. For this reason, it is easy to observe that the blood viscosity is high in the field at low shear rate, because the stress is weaker and therefore help the red blood cells to combine and to create bigger surfaces that oppose the flow. In the field at high shear rate, the situation changes completely, the viscosity of the blood decreases, since the shear stress is more decisive in preventing aggregation and imposing to the blood cells to deform and to orient itself so as to give the lowest resistance [5,13-14].

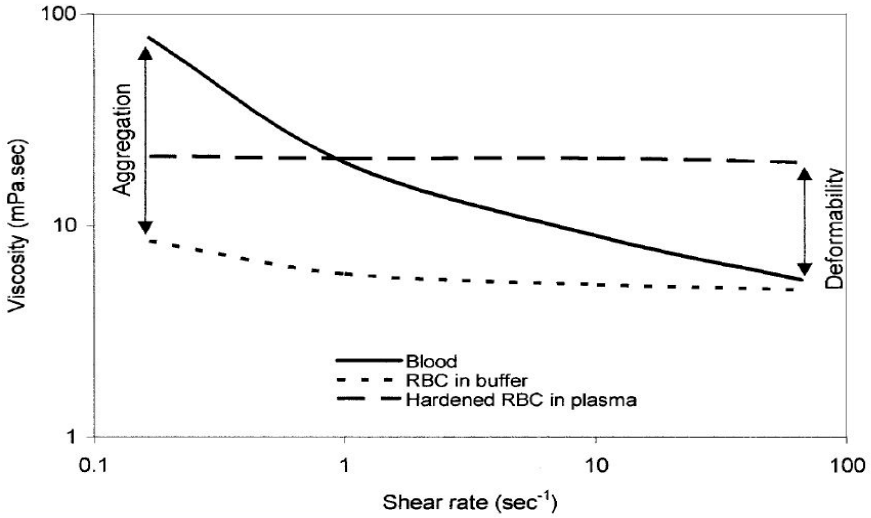

Figure 1-12: viscosity/shear rate graph for normal blood [12].

In first approximation, the value of shear rate about ***100 s^{-1}*** is used as separation line, where below this value the behaviour is Non-Newtonian (in detail pseudo-plastic) while above it the action is Newtonian [5].

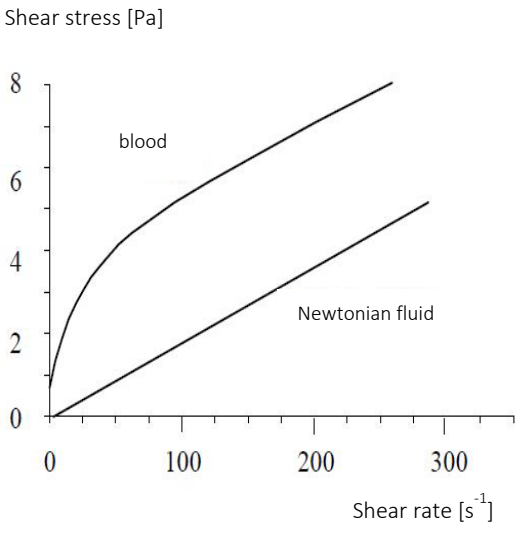

Figure 1-13: Shear stress/shear rate graph for blood [5].

Instead, if more detailed analysis is desired, more complex Non-Newtonian rheological models can be used to describe a more realistic blood viscosity, such as *Bingham* model or *Casson* model or *Carreau* model and more others [5].

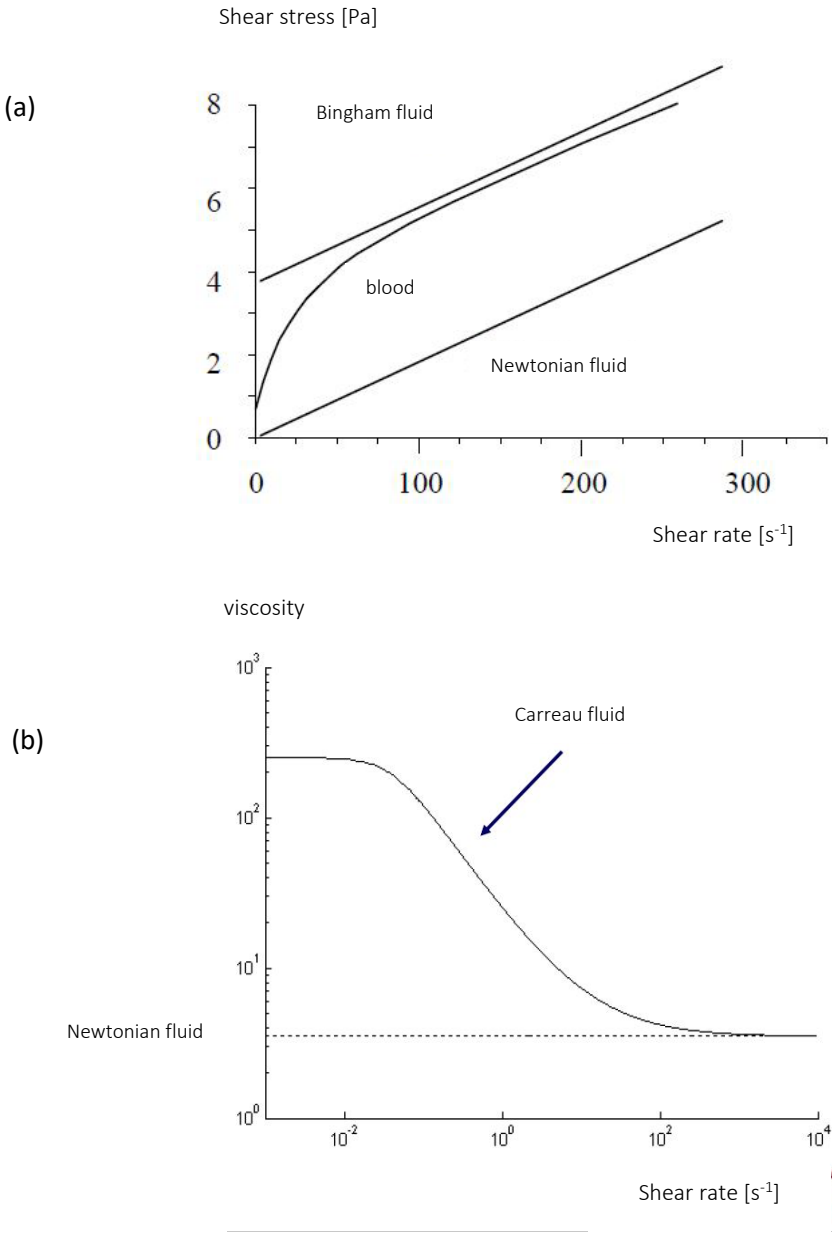

Figure 1-14: (a) Bingham model. (b) Carreau model [5].

1.4 ATHEROSCLEROSIS

All vessels described in previously chapters can be affected by different cardiovascular pathologies such as *angina, myocardial infarction, stroke, peripheral artery disease, congenital heart disease, valvular heart disease, coronary artery disease etc*. *Cardiovascular diseases* (*CVDs*) are a serious threat to both life and life quality, according to *American Heart Association,* it remains the leading cause of morbidity, disability and mortality in developed world [15-17].

It is important to clarify the distinction between similar terms that we hear every day about this argument: arteriosclerosis, arteriolosclerosis, and atherosclerosis [16].

- ***Arteriosclerosis***: describe a general phenomenon of hardening and loss of elasticity of medium and large arteries;
- ***Arteriolosclerosis***: describe a general phenomenon of hardening and loss of elasticity of arterioles;
- ***Atherosclerosis***: describe a general phenomenon of hardening and loss of elasticity of an artery, due to the atheromatous plaque growing.

This disease is an incurable consequence of the formation of *fatty plaques* in the vessel wall that obstruct the lumen and its blood flow, resulting in acute ischemic syndromes. Clearly, a narrowing of vessel lumen means a reduction of blood transported and oxygen to tissues (in the case of arteries) or heart (in the case of coronary arteries) with consequently illness or death [19-20].

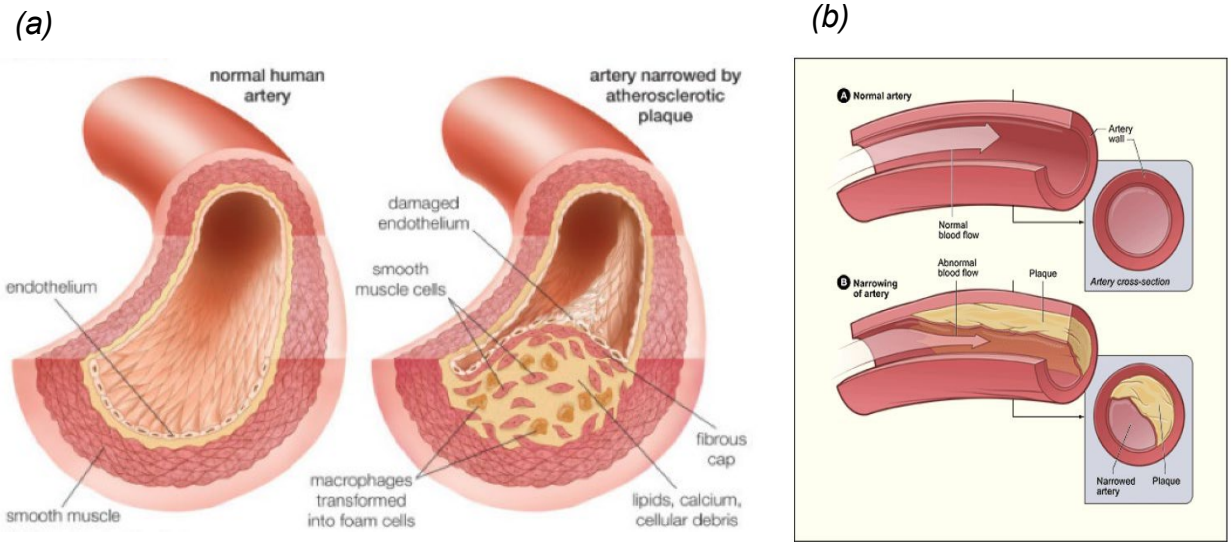

Figure 1-15: (a) Illustration of the fatty plaques components; (b) Illustration of the consequence of the formation of fatty plaques in the vessel [19].

From studies, it is evident that atherosclerosis is a process that begins in infancy and progresses slowly through all life, when can have some clinical manifestations after decades of asymptomatic growing. Usually speaking about the main arteries, the aorta and the carotids are the first vessels affected, then in puberty the pathology affects the coronaries and the cerebral arteries [17].

1.4.1 Pathogenesis and Classification

Nowadays, after many years of studies, the common hypothesis accepted from all scientific community is that the atherosclerosis is the "*response to injury*". It starts from an inflammatory process in the arterial endothelium, there, blood monocytes are chemotactically attracted to arterial wall, entering the subendothelial space where they are changed into macrophages. This change is associated with a retention of low-density lipoprotein (*LDL*), proportionally to size and complexity of the lesion. It is known that normally the LDL circulate in the vessels, but the threshold between normal and abnormal concentration has not been defined. However, if the retention of LDL increases or if its elimination from the circulation is delayed, they are trapped in the intima matrix and then oxidized or modified by macrophages, leading to the formation of isolated groups of foam cells (***Type I***) [16,19,22-23].

Then smooth muscle cells start to migrate from the middle layer, increasing the lipid droplets of foam cells, that became visible fatty streaks as yellow coloured streaks or spots on the intimal surface (***Type II***). It also true that not all type II lesion has this composition, for this reason two subgroups have been defined: ***Type IIa***, which collocates with specific adaptive intimal thickenings in predictable locations, and ***Type IIb***, which are found in intima that is thin and contains few smooth muscle cells. In this phase located mechanical forces play an important role, one of the most important is the low shear stress, typic of this district, because the increasing time of interaction between blood particles and endothelium, allows a major deposition and accumulation. To notice, that this step starts around age of 15 years old until the 60 years old, in the coronary arteries [16,19,22-23].

The following step of the progression is the "division line" between the clinically silent lesions, also called initial lesions, and the atheroma. Some of the LDL particles are not modified and

remain assembled with each other as fat droplets into the surface matrix (***Type III***). As demonstrated, these three steps are not necessarily sequential, but type III and type II can occur at the same time [19,24-25].

As the process evolves, now the lesions become more complex and more dangerous. Along the intima surface, a high presence of a lipid-rich necrotic core encapsulated by collagen rich fibrous tissue can be seen at naked eye. This lesion leads to intimal disorganization, artery diameter deformation and probably to advanced progressions. The fibrous cap consists of collagen, smooth muscle cells, and macrophages and lymphocytes (***Type IV***) [24-25].

The thickness of the fibrous cap distinguishes the fibroatheroma (relatively thick) from the thin fibrous cap atheroma (classic "vulnerable" plaque). Plaque rupture is responsible of 76% of fatal event and the reason for its breakage is poorly understood, for this reason a thinner cup is more unstable and the risk of pouring its content in the lumen is high (***Type V***) [24].

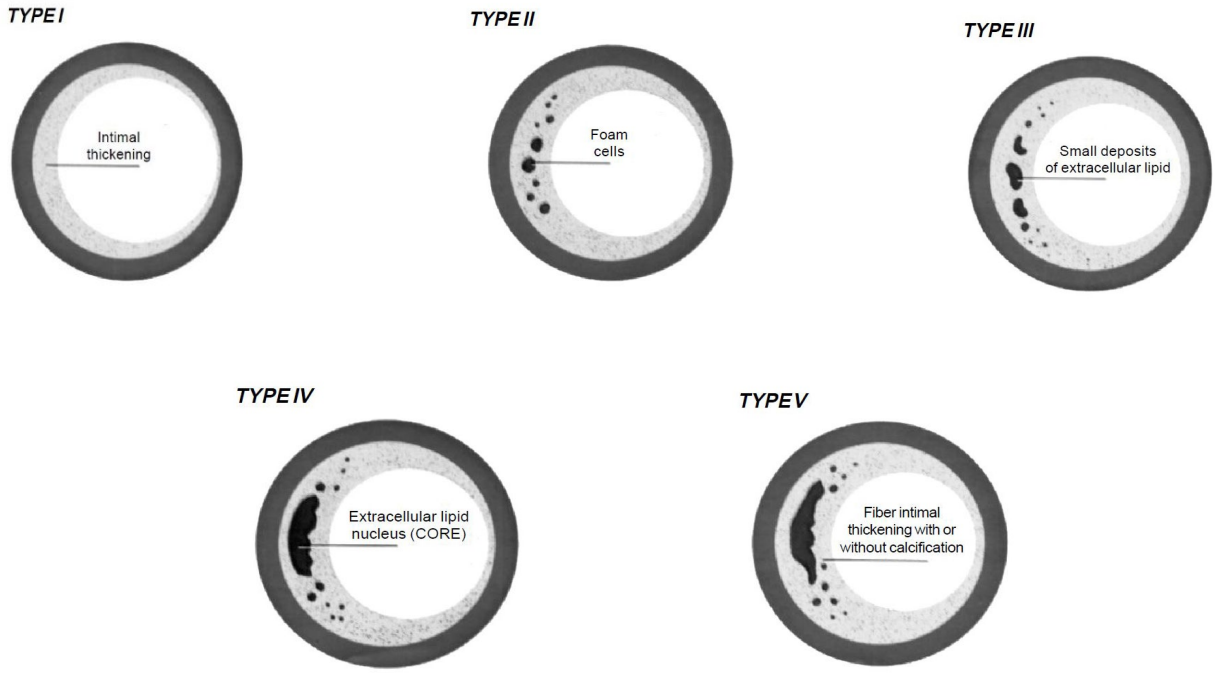

Figure 1-16: Histological type of atheromatous plaque [24].

Normally this last step starts around the fourth decade, and after that the most common possibilities are: producing stenosis, forming thrombus or aneurism and rupture [24,26].

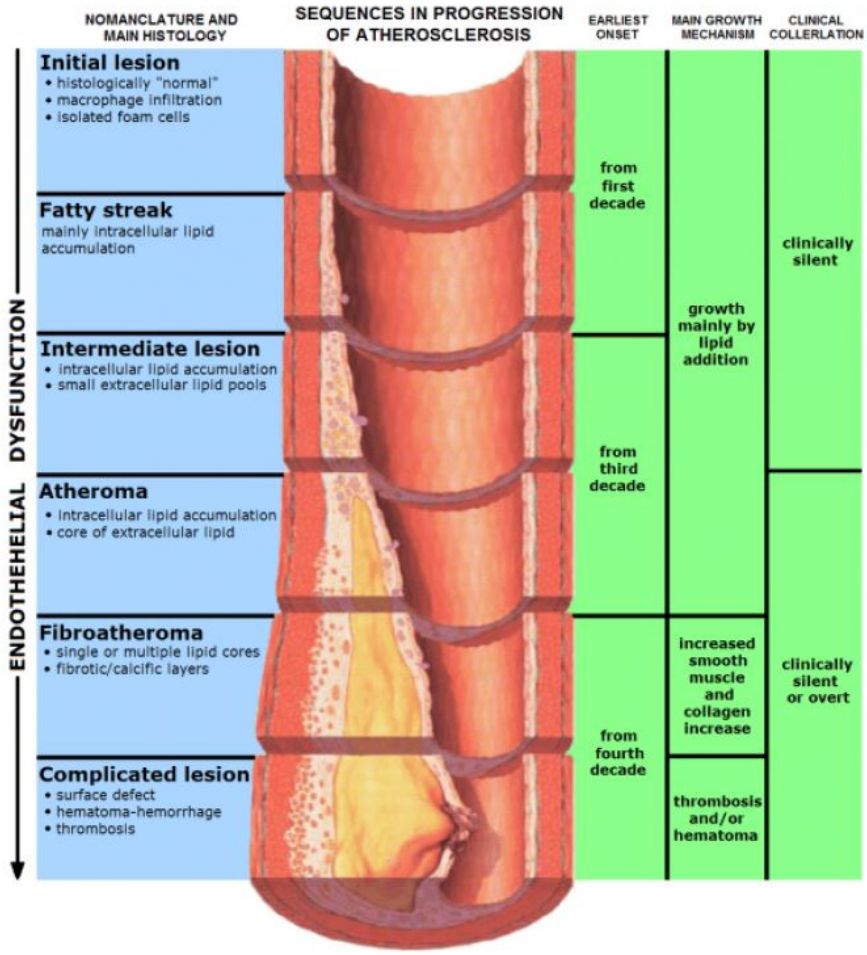

Figure 1-17: Description of the stages of endothelial dysfunction progression in atherosclerosis [19].

Stenosis is a partial or complete closure of the lumen and is a localized phenomenon. It is classified according to the luminal narrowing of the vessel and obviously the higher the degree, the more important is the reduction of blood flow and consequently hemodynamic problems. The stenotic areas tend to become more stable despite increased flow velocities at these narrowing, in according to this, is evident that most severe clinical events do not occur at plaques that produce high grade stenosis [26].

- *Grade 0 = Normal*
- *Grade I = 1-25% stenosis*
- *Grade II = 26-50% stenosis*
- *Grade III = 51-75% stenosis*
- *Grade IV = 76-100% stenosis*

While the forming of ***thrombus*** is an event related to the plaque rupture, due to the vulnerability of the unstable fibrous cap. When this cap breaks the inner lipid-rich core is poured in the lumen vessel and the contact between these elements whit the thrombogenic blood components activate the system coagulation, and therefore can also obstruct the blood flow acutely. It is important to highlight another aspect of the thrombus or fragments of these, that is, the possibility of passing through the bloodstream going to block distant blood vessels and damaging the related organs that are distant from the original site of the thrombus [5].

Thus, stenosis and thrombus are responsible for the obstruction of the blood flow and the lack of the necessary supply of oxygen and nutrients, which lead to the development of the myocardial infarction (heart attack) and the irreversible death of the interesting part of myocardial tissue (necrosis) [5].

All these event and modification of the vessel wall and layers obviously can't be overlooked, because they weaken and stretch the structure of the artery, causing its flattening and making it one of the perfect haemorrhage sites, or in other word causing ***aneurism*** and ***rupture*** of the blood vessel [5].

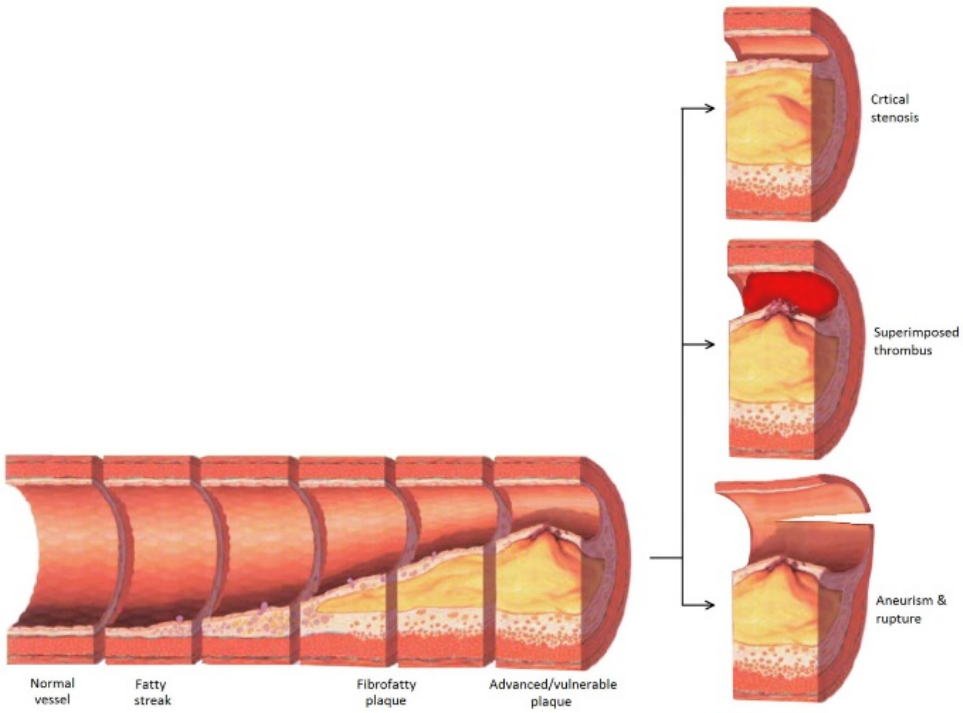

Figure 1-18: Possible complications of atherosclerosis in advanced states [19].

1.4.2 Risk Factors

As already said, the atherosclerotic process is not fully clear in all its complex aspects and some debates are yet opened [16,20]. Nowadays, the scientific community is agreed that the principal proved risk factors can be split into two main groups: modifiable and non-modifiable or also defined reversible and irreversible [5,28-30].

Reversible factors:

- *Diabetes*
- *Hyperlipoproteinemia*
- *Tobacco smoking*
- *Excessive alcohol*
- *Obesity*
- *Poor diet and alimental disorders*
- *Insulin resistance*
- *Hypertension*
- *Depression*
- *Chronic stress*
- *Sedentary lifestyle*

Irreversible factors:

- *Advanced age*
- *Gender*
- *Family history*
- *Genetic abnormalities*
- *Hypertension (genetic)*
- *Hypercholesterolemia (genetic)*
- *Obesity (genetic)*

Clearly, when speak about these factors and their incidence, it is impossible to evaluate the single event, but often the disease is the result of a gradually and complex combination of more of these aspects, where everyone plays a different role. It is possible that someone who present one or more of these factors does not develop atherosclerosis, but at the same time is also possible that he doesn't show clinical symptomatic occurrences. Although, it is proved that the individual, who has the right and random mix of these risk factors, has a higher and more predictable possibility of developing future vascular diseases.

1.4.3 Diagnosis

The long-time clinical silent development of the atherosclerosis is probably the worst feature of this cardiovascular disease, because it is often revealed only when it is at a critical level, with serious events such as *myocardial infarction*, *severe cardiac arrhythmias* or *other acute perilous syndromes*. For this reason, diagnosis is a difficult step that is continually being examined to obtain the best desirable performance [20].

There are a lot of tests that can help in the diagnosis, that include physical examination and medical testing. Some of these are more invasive and other less invasive [20,29].The most used and performing tests consist of:

- *Electrocardiography* (*ECG* or *EKG*) and *ECG - Stress test*: this test records the electrical heart activity and its rhythms [20,29].
- *Echocardiography* (*ECHO*): this imaging scan creates a video image of the pumping heart, using the ultrasound waves, to detect morphological changes [20,29].
- *Coronary angiography*: this test is a semi-invasive method. A small catheter is inserted into an artery to the coronary arteries and when it is in place a radiopaque contrast agent is injected to be seen on x-rays video screen [16,31].
- *Cardiac catheterization* (left heart catheterization): this procedure is also considered a semi-invasive method. It is the best way to have directly measure, a thin and flexible catheter is inserted to your coronary arteries and various microscopic instruments can be pass through the pipe to do different type of analysis [20,29,31].
- *Computed tomography scan* (*CT*) and *Magnetic resonance imaging* (*MRI*): these are two advantageous non-invasive methods to detect and to characterize eventually heart abnormalities [18].
- *Blood tests*: these are simple laboratory tests to evaluate blood cholesterol levels, LDL and HDL cholesterol levels, triglycerides, lipoprotein, homocysteine and others [20,29].
- *Family history.*

1.4.4 Treatments

If these exams give a positive result, then the individual has the atherosclerosis, some different treatments may be tried to reduce critical events, because it is clear that this disease can't be cured completely. Based on the level of danger, non-pharmacological treatments, drug therapies or surgery can be chosen [16,20]. Each action has the objective to reduce the reversible risk factors as much as possible, so helpful solution can be:

- *Lifestyle changes* [16, 29]*:*
  - Quit smoking tobacco
  - Quit drinking alcohol
  - Exercise regularly
  - Lose weight
  - Eat a healthy diet
- *Medications* [20, 32]*:*
  - Statins: demonstrated positive impact on reducing cholesterol.
  - Aspirin: reduces blood clotting.
  - Beta blockers and calcium channel blockers: used to reduce hypertension.
  - Drugs against diabetes mellitus.
  - Etc.
- *Surgery* [20,29,32]*:*
  - Balloon angioplasty and stent placement.
  - Coronary artery bypass graft surgery.
  - Laser surgery.

After this short excursus about the main aspects of the atherosclerosis and its diagnosis and treatments, it is right to say that the only solution to try to avoid this disease is a correct and persistent prevention, looking for the best way to reduce and to monitor all the responsible risk factors.

1.4.5 Biomechanical Factors and Effects

All the risk factors correlated to the atherosclerosis, combined with each other cause a *reduction of perfusion*, *weakening of vessels* and *changes in biomechanical parameters*. According to the severity of the condition can be induced to different symptoms or to death [5,8].

Endothelial vascular cells have been proven to be able to sense alterations in shear and response to mechanical stimuli. A large variety of biological elements have been proposed as potential *mechanoreceptors*. Over the years, many studies suggest a strong relationship between atherosclerosis and endothelial shear stress [5,8].

Wall Shear Stress or *WSS* plays a fundamental role in regulation of the progressive thickening of local atherosclerotic plaques [32]. It was demonstrated that local disturbed flow patterns with regions of ***low*** and ***oscillating WSS***, are common sites for the initiation of this pathology. Low WSS sites are usually *inner curves* and *bifurcations*, where the disturbed flow shows low velocity, which allows to endothelium cells to initiate the process of accumulation and plaque formation [5].

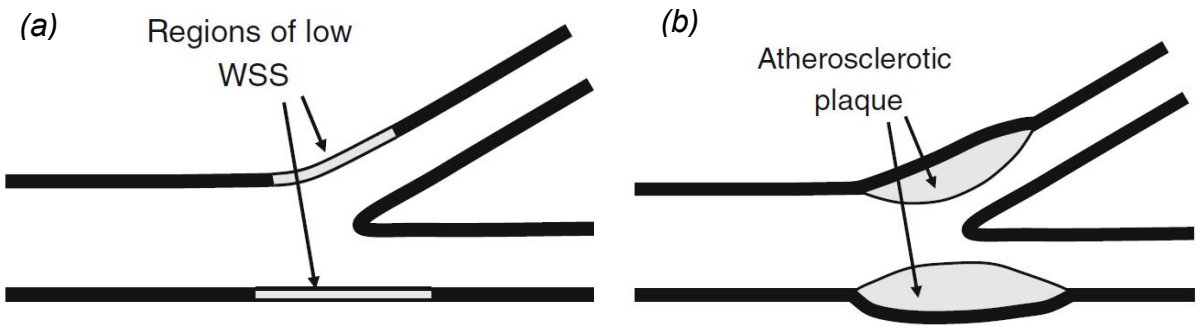

Figure 1-19: Illustration of a bifurcation: (a) before, high risk region in evidence; (b) after, plaque developed [8].

As mentioned above, the plaques grow over time and their gradual expansion means a *lower cross-sectional area* (stenosis) that leads to an increase in *velocity* (maximum in the *vena contracta* region), because the aim is to maintain a constant flow rate (*flow rare: Q = Area*velocity*), despite the plaque changes. As soon as atherosclerotic plaques have formed, wall shear stress increase in the stenotic region, while after stenosis, a flow separation occurs and, following the boundary layer region extinguishing downstream, a flow recirculation area with low WSS appears. Obviously, velocity changes mean changes in velocity profiles which are almost

plugged just after the stenosis, but returns to be the exact pattern with distance, when the wall viscosity activity makes the deformation effects insignificant [5,8].

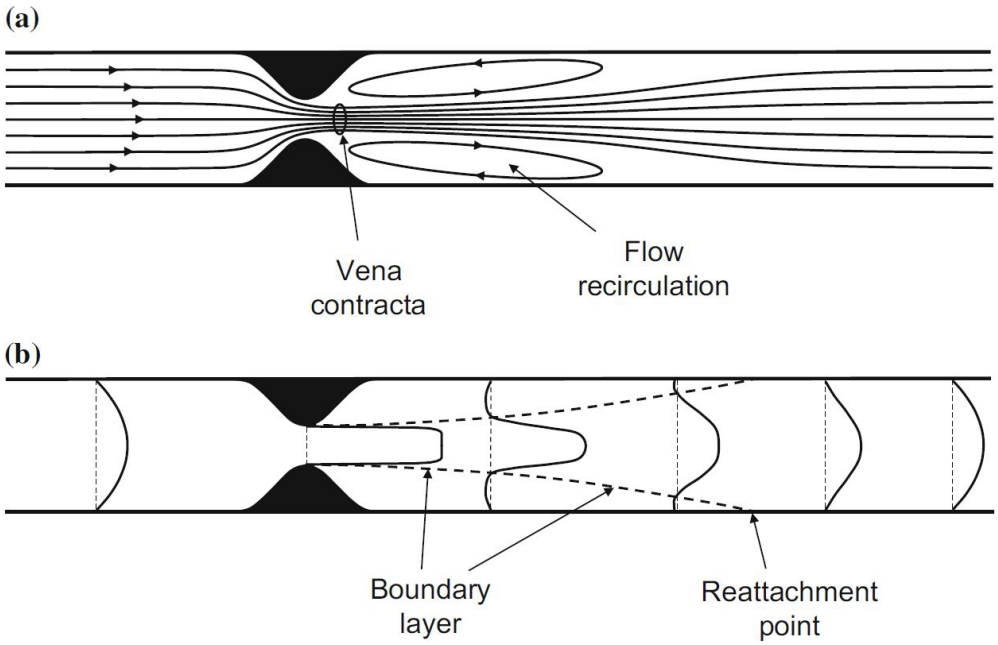

Figure 1-20: Schematic representation of how the stenotic plaque changes the flow distribution [8].

At the same time, even high levels of plaque stress are predicted as potential risk factors that may be involved in upstream plaque destabilization and be more prone to lead to rupture and therefore to cardiovascular events [8].

In summary, biomechanical stress could therefore potentially represent a useful tool for assessing the risk of plaque rupture, because it is clear that the WSS influences the plaque growth, but the presence of plaque influences in turn velocity field and so WSS patterns [8].

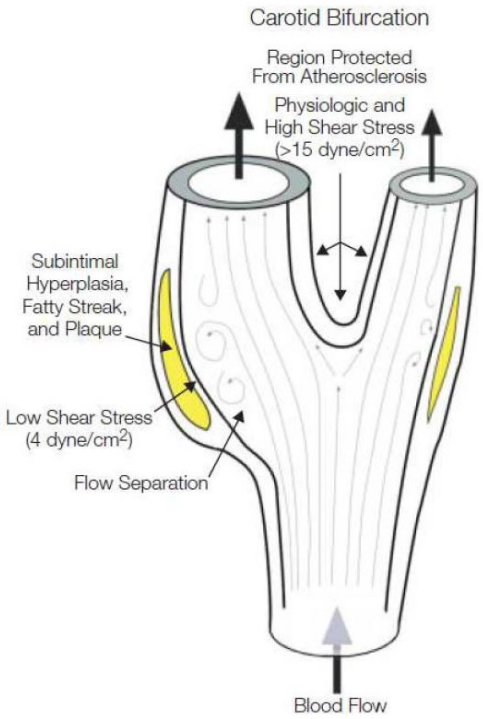

Figure 1-21: Illustration of carotid bifurcation with atherosclerotic plaques [5].

1.5 CORONARY CIRCULATION

From the previous chapters is not difficult to understand that the heart must work hard and constantly in every moment of our life. Therefore, blood vessels must deliver nutrient and drain away waste also at myocardium level and vessels used for this role are coronary arteries. The ***coronary circulation*** is a branched blood circuit that includes *coronary arteries* and *cardiac veins,* for oxygenate and deoxygenate blood, respectively.

1.5.1 Aortic Root and Sinuses of Valsalva

Observing the anatomy of the heart at the beginning of the aorta, just above the aortic semilunar valve and just below the ascending aorta, it can be defined the ***aortic root***. It is composed by the aortic valve leaflets, the leaflet attachments, the sinuses of Valsalva, the interleaflet trigones, the sinotubular junction and the annulus [34-35].

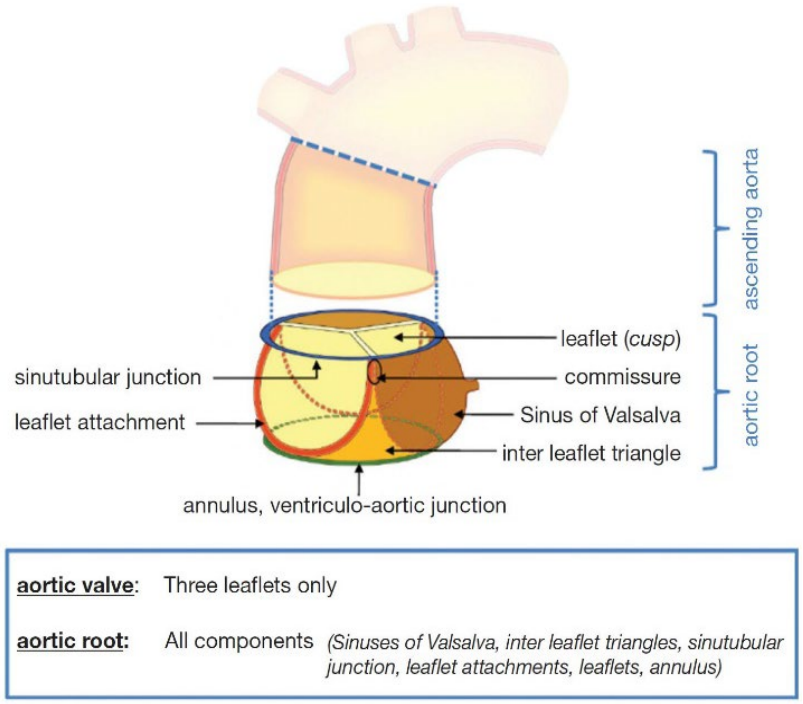

Figure 1-22: Aortic root components [33].

Now, these elements will not describe in detail, but it is important to know that each component has a specific function such as maintain the laminar flow, reduce the resistance or reduce the tissue stress and its damage to able to response to every hemodynamic situation in the best way.

We focus on the expanded portion of the aortic root, the *sinuses of Valsalva*, where there are three distinct bulges. Two of this give rise to the coronary arteries, therefore they are called right (***RCC***) and left sinuses (***LCC***), respectively. Instead, from the third doesn't originated any vessel, thus it is called the non-coronary sinus (***NCC***) [34-37].

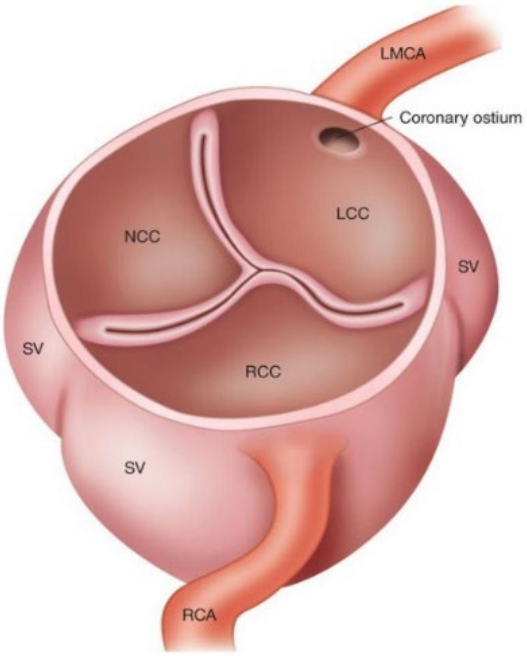

Figure 1-23: Transverse section of the aortic root [36].

The precise function of the sinuses of Valsalva is still unclear. In recent year, numerous studies have confirmed the hypothesis of its role in optimization of the aortic hemodynamic and of the aortic valve functions (opening and closing mechanism). The sinuses mitigate the flow instabilities (vortices) produced by the *vena contacta* effect, leading to stress reduction and allow complete physiological leaflets expansion, minimizing drop pressure and reducing the loss of energy [35-39].

It is also important to note that the position of the coronary orifices is not random and many studies demonstrate the functional advantage of this orientation. Generally, the coronary ostia are positioned just above the sinotubular junction and the aortic valve leaflets rest on them by tapping them in the opening phase [38]. An example of abnormal condition, that supports the considerations of previous studies, is the *high take-off coronary artery* pathology (the prevalence

in the general population is around 0.202%), which usually has a small clinical significance, but in different cases may be part of a more complex arteria variations [34-41].

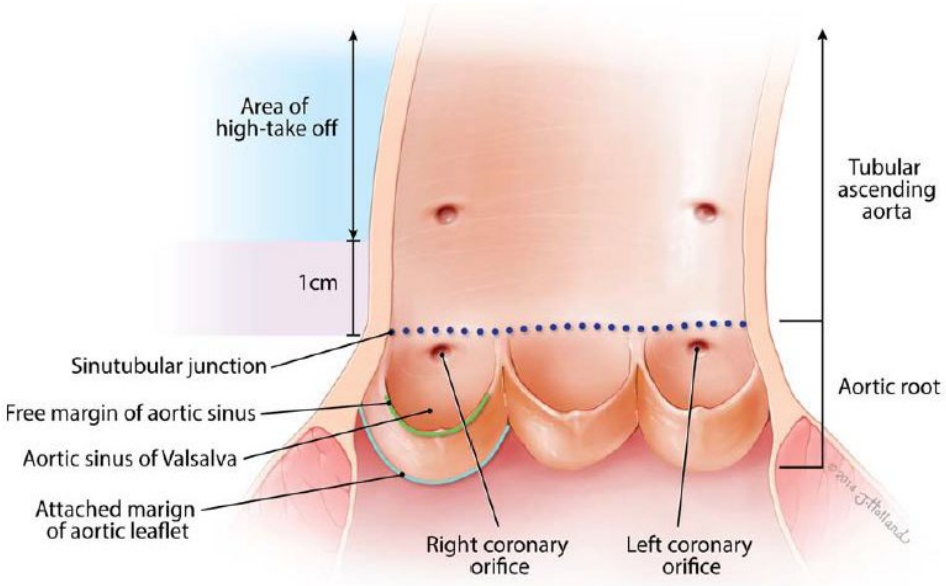

Figure 1-24: Illustration of the aortic root with simulation of the high-take off coronary arteries [33].

1.5.2 Coronary Arteries

Diffusion phenomena of blood which fills the four heart chambers are not fast enough to supply also the heart wall, so, a dedicated diffusion system is necessary to perfuse oxygenated blood into ***epicardial surface*** and deeper into ***myocardium tissue*** too, this is the coronary circulation.

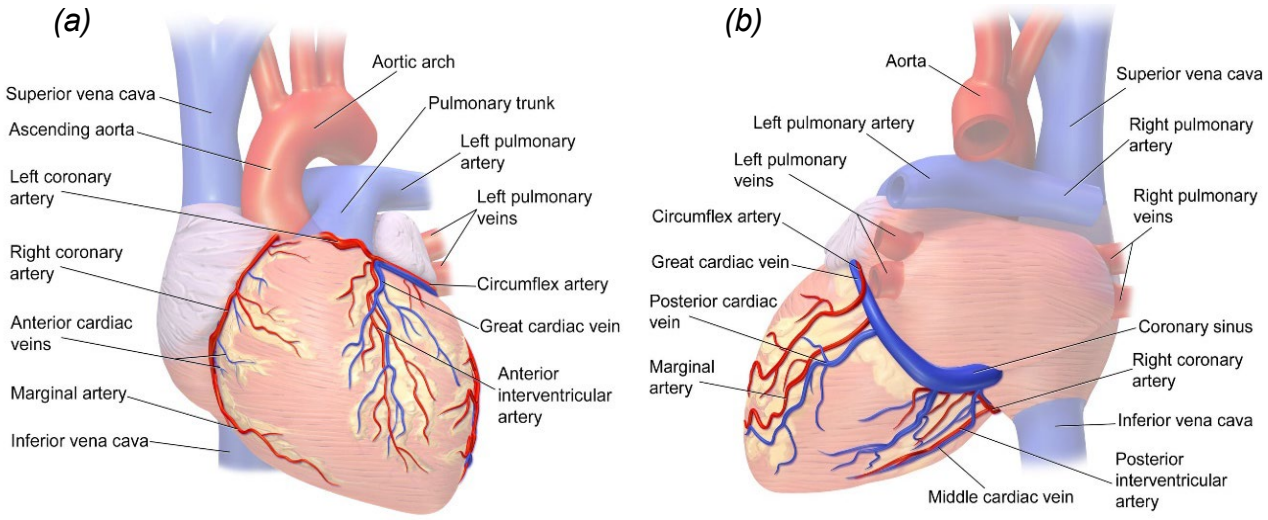

Figure 1-25: Coronary circulation: (a) anterior heart section; (b) posterior heart section [34].

Coronary arteries rise from the ascending aorta, near the sinuses of Valsalva, and surround the whole heart.

As suggested by the *American Heart Association* (*AHA*), it is possible to discriminate two main branches, the right and the left, which then they are divided in other small branches, counting from 15 to 29 segments [40].

The ***left coronary artery*** (***LCA***) starts from its respective sinus, passes between the pulmonary trunk and left atrial appendage, curving anteriorly toward the anterior interventricular sulcus. The initial *common trunk,* also called left main coronary artery (***LM***) segment divides into the *left anterior descending* (***LAD***) and the *left circumflex* (***LCX***). In 37% of the population, is estimated the presence of a third intermediate branch (can be more than only one), called *diagonal left ventricular artery*, it also born from the common trunk and is positioned in the middle, between the *LAD* and the *LCX* [40-42].

In detail, the following figure help to locate each section. Left anterior descending is dived into *proximal LAD* (L2 and L5) and *mid-distal LAD* (L3, L4, L6) [40[41][41]]. Left circumflex includes *proximal* and *mid LCX* (C1 and C3), tree *obtuse marginal* (C3, C4 and C5) and some *grouped distal LCX* (C6, C7 and C8) [40[41][41]].

The *LAD* branch carries blood to the interventricular septum and the anterolateral wall of the left ventricle. In detail, it splits into three sections that extends: the first toward the first septal branch, the second section until the third septal branch or the second diagonal branch and the third section reaches the apex [1-19].

The *LCX* branch supplies most of the left atrium and part of the left ventricle. In detail, it is divided into three sectors: the first and second groups goes from the origin to the first, second and, if is present, the third marginal branches, while the third sector follow the extinction of the vessel [1-19].

The ***right coronary artery*** (***RCA***) starts from right ostium in the right sinus, proceeds along the coronary sulcus and then curves posteriorly. Its calibre is smaller than the *LCA*. It splits into three branches, starting from the origin, known as *proximal*, *mid* and *distal RCA* that supply blood to the right atrium, right ventricle. At this point, the right coronary artery divides into its two *marginal arteries*, called *posterior descending artery* (*PDA*) and *posterolateral groups* (*PLV*), which are engaged in the irroration the diaphragmatic portion of the left ventricle [40-42].

In detail, in the following figure it possible to distinguish proximal, mid, distal RCA (R1, R2 and R3) and some posterior right groups (R4 and R5) [40[41]].

This classification is the most frequent configuration, but anatomical variations are usual. *LCA* supplies exclusively to the left side of the heart, while *RCA* deliver action is expanded to both sides, this is defined *right dominance* with a prevalence of 50% of cases; in the 20% of cases was found *left dominance* and in the rest 30% of cases was observed a *co dominance*[1] [42-43].

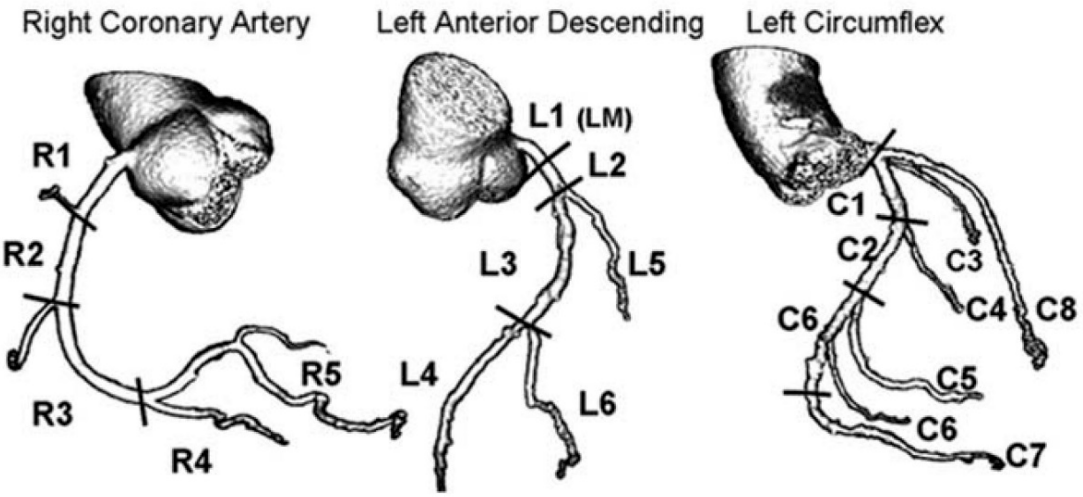

Figure 1-26: Segmentation model with 19 segments [40[41]].

1.5.3 Coronary Perfusion

Since coronary arteries must deliver blood to heart tissue, the coronary perfusion must be proportional to the cardiac work. At rest condition, the coronary flow is around the ***5%*** of the cardiac output about *60-80 ml/min* (per 100 g of tissue), while during activities the flow increases around the *200-300 ml/min* (per 100 g of tissue) [44-45].

Changes in coronary perfusion follow aortic pressure, which increases or decreases during the cardiac cycle. Myocardium contraction (during systole) leads to an extravascular compression that increases coronary resistances and reduces blood flow, version the contrary in the diastolic phase when the heart muscle is relaxed, coronary resistances are lower blood is facilitated to flow through coronary arteries [43].

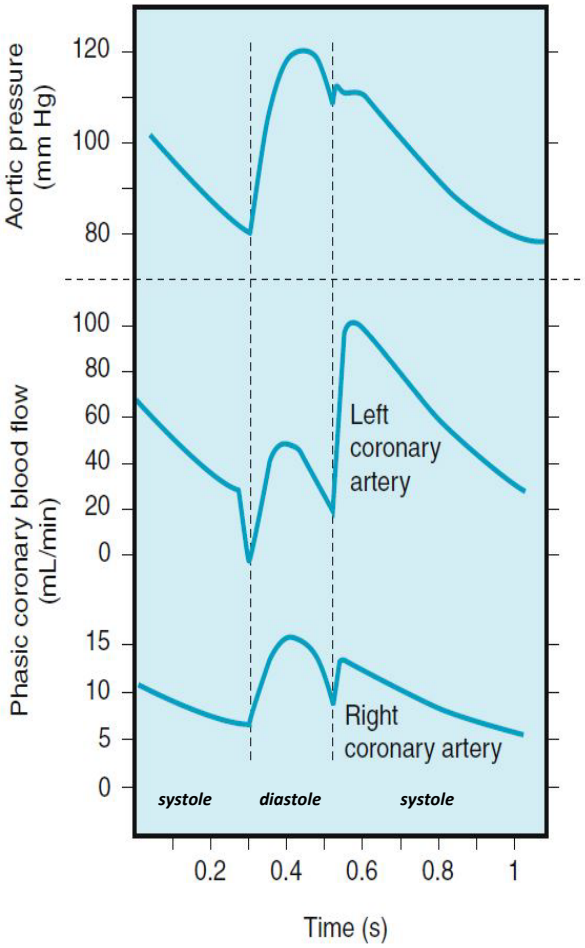

Figure 1-27: Comparison of phasic coronary blood flow in the left and right coronary arteries [44].

The aortic pressure is probably the principal responsible of coronary perfusion alterations, but there are also other factors that contribute to implementing changes, such as metabolic, neural or hormonal factors. These are all expression of the same phenomenon, the autoregulation of blood flow [43].

1.6 HEART VALVES

In the previous chapters, the importance of some valves along the bloodstream, inside the heart and through vessels, has already been mentioned. In this chapter they are showed more in detail, a good starting point is to distinguish their anatomy, position and main differences [45].

The heart has four different valves, two of these regulate the flow between atrial and ventricular chambers, while the other two control the stream from heart to pulmonary trunk and to aorta [45].

The role of each valve is to guarantee the ***unidirectional blood flow***, avoiding *backward leakage*, opening and closing of these is synchronized with the cardiac cycle phases. Between atrium and ventricle, valves movements are muscular, that means that closing and opening is determined by contraction and relaxation of the papillary muscles. On the other hand, movements of valves that regulate flow from heart to aorta and pulmonary trunk, are not muscular, but their activity is passive, so their closing and opening is determined by the pressure changes, which are consequences of the contraction or relaxation of the relative chamber [19,46].

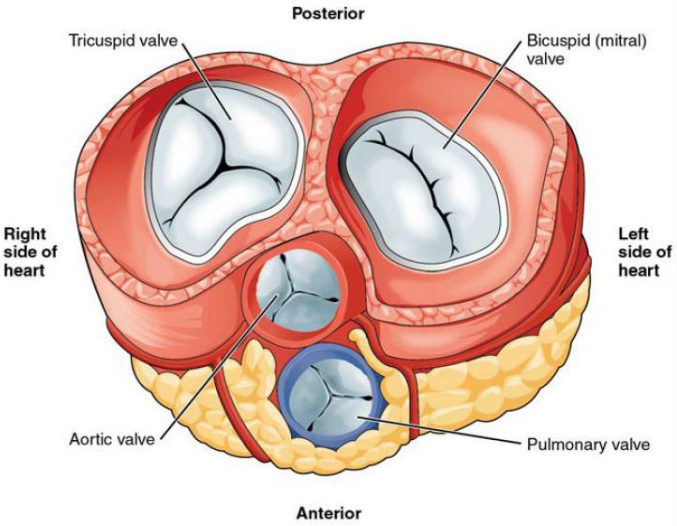

Figure 1-28: Illustration of heart valves with the atria and major vessels removed [1].

The ***tricuspid valve***, also called the *right atrioventricular valve*, regulates the pumped flow from the right atrium to the right ventricle. On the left side, the same role of controlling bloodstream from atrium to ventricle, such as the previously valve is done by the ***bicuspid valve***, also named

mitral valve or *left atrioventricular valve*. About the valves related to the blood vessels, there is the ***pulmonary semilunar valve***, also known as the pulmonic valve or the *right semilunar valve*, it controls the blood flow through the tract between right ventricle and the pulmonary trunk.

1.6.1 The Aortic Valve

The last valve is also the most important for the development of this work, it is the ***aortic semilunar valve*** or *left arterial valve*. It controls the correct unidirectional blood flow, from left ventricle to ascending aorta [1]. Anatomically, this valve is trifoliate, this means that it has three semilunar and symmetric leaflets, called *left*, *right* and *posterior* [19]. Their name come from the corresponding orientation of the bulges of the underlying Sinus of Valsalva (look the Coronary Circulation chapter for more information). In all hearts, the sinuses that give origin to the coronary arteries are nearly always the aortic sinuses that are adjacent to the pulmonary valve. As with the pulmonary valve, there is a small thickening on the centre of the free edge of each cusp, at the point where the cusps meet [46-48].

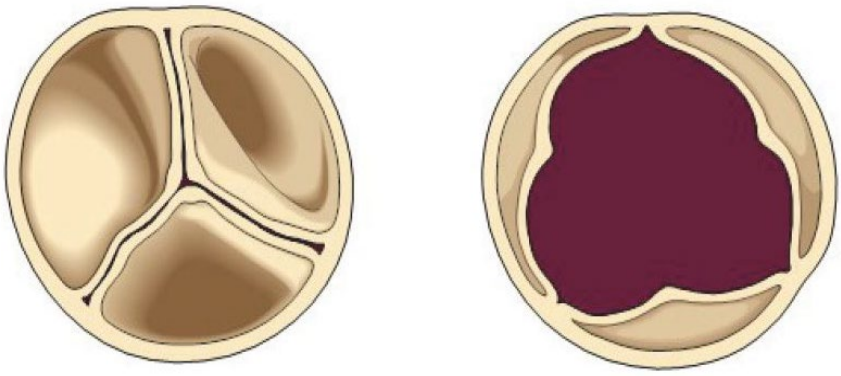

Figure 1-29: Aortic semilunar valve opened and closed [47].

The average height, measured from the base of the centre of leaflet to its free edge, for right coronary, noncoronary, and left coronary cusps was 14.1, 14.1, and 14.2 mm, respectively. When height of each individual leaflet was expressed as a percentage of its width, right coronary, noncoronary, and left coronary leaflets varied between 39% and 82%, 34% and 87%, and 34% and 113%, respectively. Obviously, these are average measurements, because the three flaps are not perfectly equal, many intra-individual and inter-individual differences have often been found [38].

Histologically, the leaflets are composed of an internal collagen matrix, organised in three distinct layers of fibrosa, spongiosa and ventricularis type. The *fibrosa* with its dense connective tissue oriented in circular way, that provides strength. The *spongiosa* with its loose matrix of glycoproteins provides a cushion to resist mechanical forces and to allow the movements of other two layers. The *ventricularis* comprehends radially oriented elastin and provides elasticity for changes of shape during opening and closing. Normally, these three layers are not vascularized, but they are innervated [48-50].

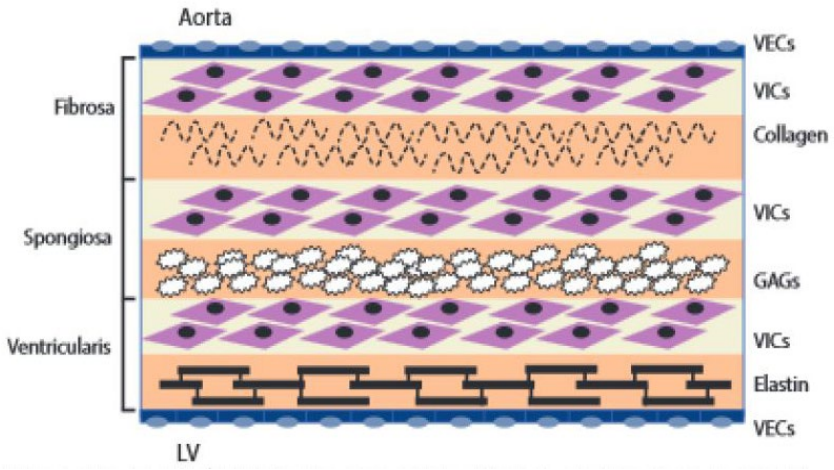

Figure 1-30: Cellular structure of the valve [29].

When the valve opens, leaflets fall back into their sinuses with the potential of occluding coronary artery ostioles positioned behind two of the leaflets, while when they are closed, the flaps meet blocking the backward bloodstream in the left ventricle cavity from blood in aorta.

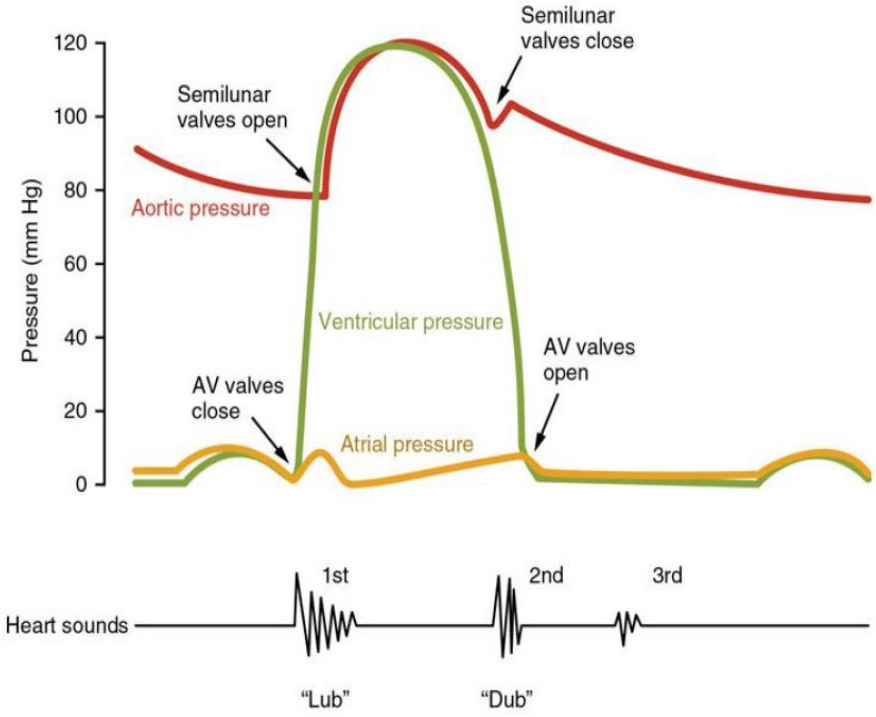

Figure 1-31: In this illustration, the x-axis reflects time with a recording of the heart sounds. The y-axis represents the pressure of the chambers in a cardiac cycle. It is possible to identify the opening and closing instants of valves [1].

Their movements of closing and opening, how already said, are determined by the pressure to which they are subjected and the direction of pressure pushing. The closure of the aortic valve contributes to hear the second heart sound [46].

Resuming, the valves system to be efficient must work in perfect harmony, synchronized with each step of the cardiac cycle, following this timeline.

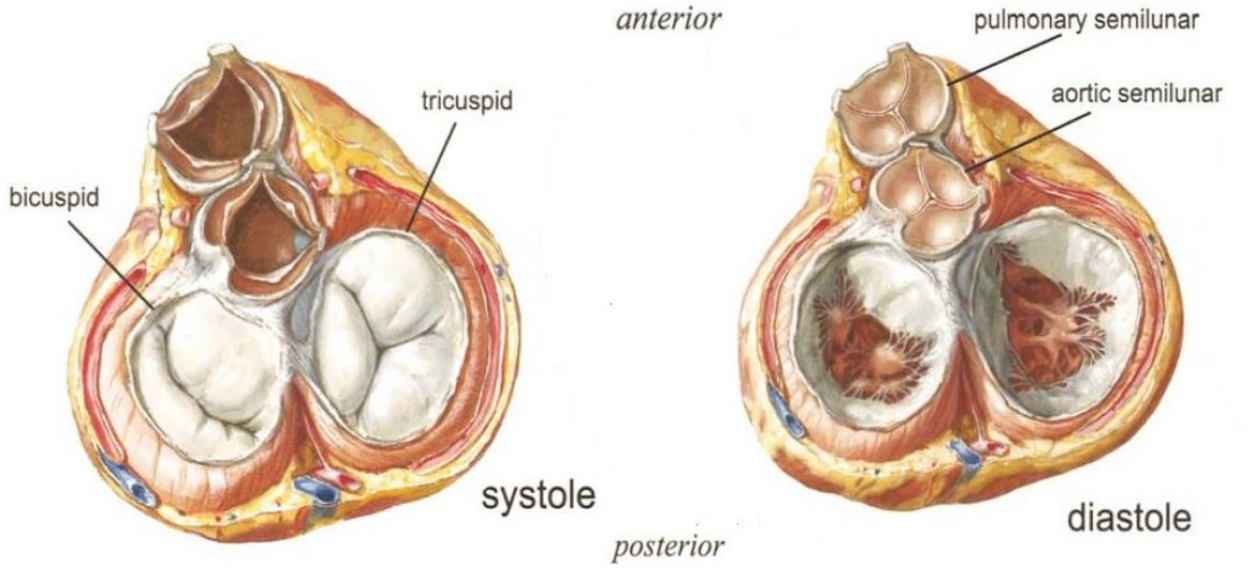

Figure 1-32: - Valves of the heart, during ventricular systole and ventricular diastole [35].

Tricuspid and Bicuspid Valves	***Pulmonary and Aortic Valves***	***Atria***	***Ventricles***
OPENED	*CLOSED*	*RELAXED*	*RELAXED*
OPENED	*CLOSED*	*CONTRACT*	*RELAXED*
CLOSED	*OPENED*	*RELAXED*	*CONTRACT*

Table 1: Opening and Closing of the aortic valve during heart cycle.

1.6.2 Biomechanics of Heart Valves

All four heart valves, although positioned at four different heart sites, have the same role that is to regulate the fluid stream and ensure the correct *unidirectional transit* during the cardiac cycle. Around $3 * 10^9$ cycles of closing and opening have been estimated over 70 year of life, to meet the continuous blood demand and, nowadays, it clear that a lot of aspect are related to the

valvular hemodynamic function, so the best method to understand the valvular mechanics is to take an "integrated" approach [51-52].

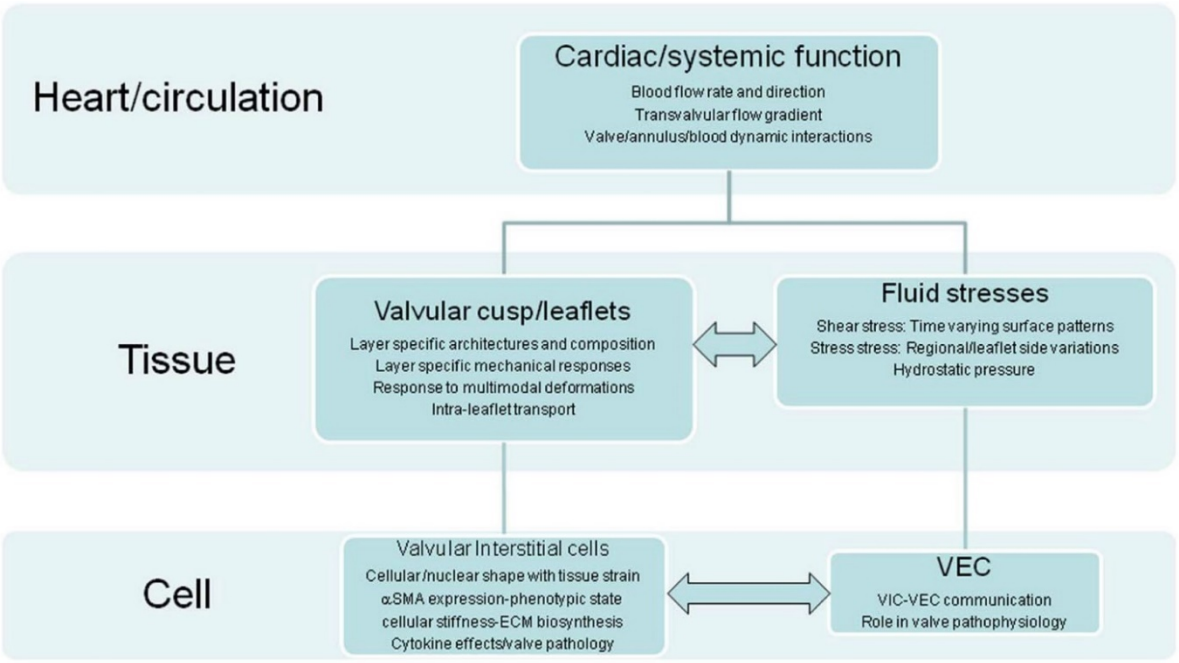

Figure 1-33: Approach to the biomechanics of heart valve function [50].

Biomechanics factors can be resumed in three elements: flexure, shear and tension. Flexure is referred to opening and closing movement, shear is referred to effects of blood flow on the wall vessels, while tension is connected with dynamic leaflets deformability [49].

Abnormal shapes disturb local flows, so specific characteristics such as valve size or effective orifice area are important to be considered. Sinus morphology is physiological perfect to give rise to vortices, which are necessary to make efficient the closing of the valve, and thus avoid excessive losses. Therefore, an abnormal valve shape leads to disturb local flow that can damage biomechanical behaviour. Therefore, specific characteristics such as valve size or effective orifice area are important to be considered to understand hemodynamic differences from physiological valve.

About leaflets properties, studies have demonstrated a highly complex and anisotropic mechanical behaviour and a high capacity to resist to irregular stretches and deformations for interactions with blood during opening and closing phases [53-54].

Over time, many studies have been conducted on hemodynamic valve characteristics, but some of these are only estimated and still quite unknown, due the obvious difficulties to do reliable and exact measurements. In a healthy human valve, the shear stress is predictable about 10 – 80 dyne/cm^2, physiological transvalvular pressure is included between 10 – 80 mmHg (considering

all four valves) and 3 – 5 l of blood are pumped in each cycle through aortic valves, which means high flow velocity about 1.35 ± 0.3 m/s [51].

1.6.3 Heart Valve Disease

How already seen, the heart can be considered a functional unit, so its performances are correlated to work in harmony of each components. Therefore, some diseases are due to single or multiple elements dysfunction. The valves can be considered one of the problems with the major incidence. In industrial countries heart valve diseases are at the third place, after hypertension and atherosclerosis, of CVDs with the highest prevalence. There are several possible causes of valvular disorders, the most common are: *rheumatic fever*, *scarlet fever*, *endocarditis*, *ageing*, results of *traumatic process* or even *congenital birth malformations*.

In general, there are two types of functional abnormality: *stenosis* and *regurgitation*, but it is not unusual to find subjects with a combination of both.

1.6.3.1 Valve Stenosis

Valve Stenosis is an obstruction that does not allow the valve to open properly, limiting the bloodstream. This is a disease that all four cardiac valves can develop. Due to this condition, the heart must pump harder than normal, so there is an overload pressure. The flow backing up causes unnatural mechanical stress and strain on the walls of the myocardium that can induce cardiac weaknesses or diseases or, in advanced stages of the disease, can lead to heart failure [1,46,54].

Clinically, it is possible to distinguish three type of stenosis:

- *Congenital aortic stenosis*: this type, unlike the others, can be detected and treated already in the first years of live. It is probably the worst type, because kids who have this kind of stenosis often die in childhood, or, if they survive, need surgery to replace aortic valve. To notice that the congenital aortic stenosis does not lead to heart failure, the most

plausible reason is that concentric hypertrophy seems compensates for the existing pressure overload [53].

- *Rheumatic valve disease (RVD)*: nowadays this cause is very rare in developed world, but at same time in other countries, it remains one of the types with a great incidence. The RVD is the result of an infection process by a bacterium, the *Streptococcus pyogenes* [1,55-56].

- *Calcific aortic stenosis* (*CAS*): this type of stenosis, show many aspects similar to atherosclerotic factors seen above. It is considered the third heart disease in developed countries (about 2% of people over the 65 years old). The process begins with an initial sclerosis and over the decades becomes a stenosis, passing from a valvular thickening without obstruction to a fully calcification and to the subsequent blocking of the flow. Obviously, the clinical evidences increase progressively over time and are totally absent in the early years. The CAS starts as *response to injury*, with a consequently osteoblastic transformation of the interstitial active cells, that is mainly responsible for calcium deposition leading to deposition of calcified nodules that essentially consist in accumulation of crystals of hydroxyapatite, osteopontin and osteocalcin [49-50]. This observation is another point shared between atherosclerosis and CAS, which suggests, as already mentioned, that this disease is an active and regulate process. Therefore, the result is the loss of leaflets flexibility, valve stiffening and subsequently incapacity to open and close properly, causing several hemodynamic changes about flow and shear stress, in details, CAS is characterised by pulsatile shear stress on the ventricular side and low and reciprocating shear stress on the aortic side [55,57].

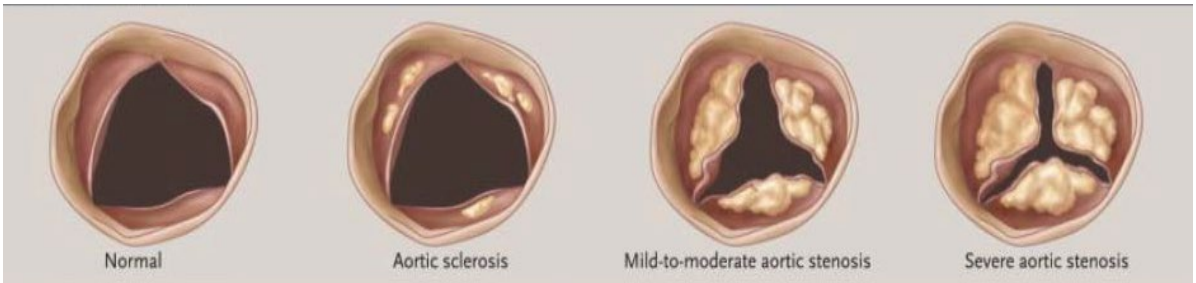

Figure 1-34: Degeneration of calcific aortic stenosis [48].

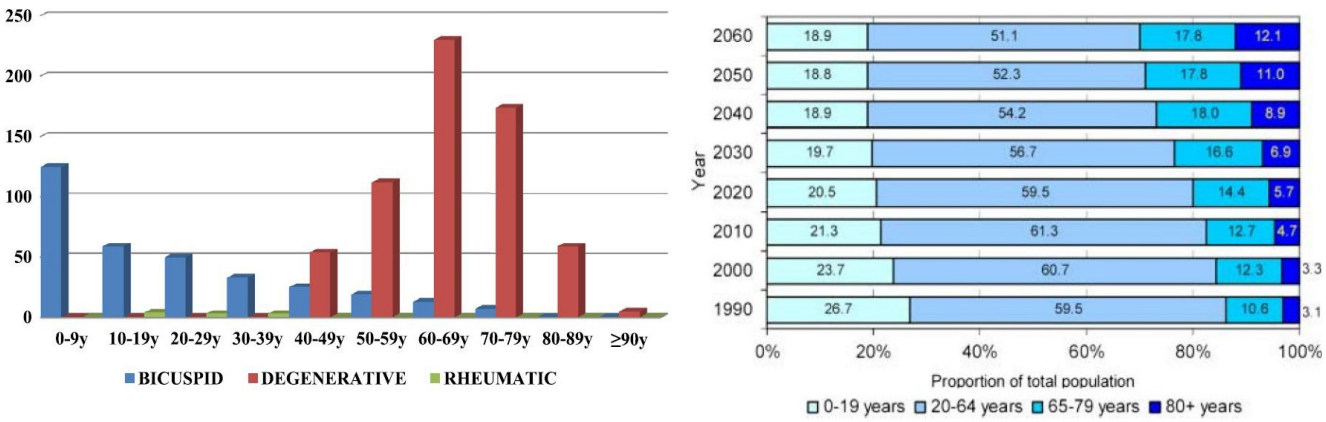

Figure 1-35: on the left the age and ethology-wise distribution of cases of isolated aortic stenosis, on the right a prediction of the evolution of age structure [48].

1.6.3.2 Regurgitation

In addition to stenosis, the other important functional irregularity is the ***regurgitation***. It is a valvular insufficiency or incompetence, which means that the valve involved shows an incapacity to complete correctly the closing movement. Therefore, during diastole, after contraction of ventricle, the chamber pressure changes direction, this condition leads the blood to flows backward in the reverse direction. Then, the *door job* of valve is less efficient, and the heart pump must work harder. This insufficiency causes both heart volume and heart pressure increase. Based on the disease level, a chronic aortic insufficiency may lead to heart failure and it is possible to see systolic pressures diminish [45].

This disorder can be classified into three categories, which maybe coexist at the same moment: *leaflet abnormality*, *variation of root shape* and *loss of commissural support*.

When speak of flap abnormalities, it can be caused by perforation, tearing, prolapse or even congenital anomalies in relation to their size or number. Normally, leaflets have a shape and size bigger than the true aortic root orifice, so it is easy that due to possible variation of root shape such as vasodilation, endocarditis, yielding of the endothelium walls, possible flaps modifications or a combination of both, radically changes physiological hemodynamic [48,58].

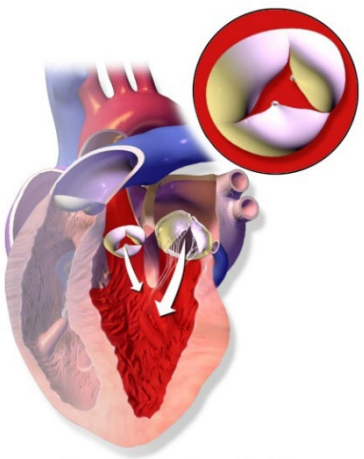

Figure 1-36: – Illustration of the aortic regurgitation [55].

1.6.4 Bicuspid Aortic Valve

One of the most important cardiac defects is the ***bicuspid aortic valve*** (***BAV***). It falls into the group of congenital disease and nowadays it has a high diffusion in the developed world; on average its incidence is around the *1-2%* of the entire population, with a male predominance (3:1) [59-60].

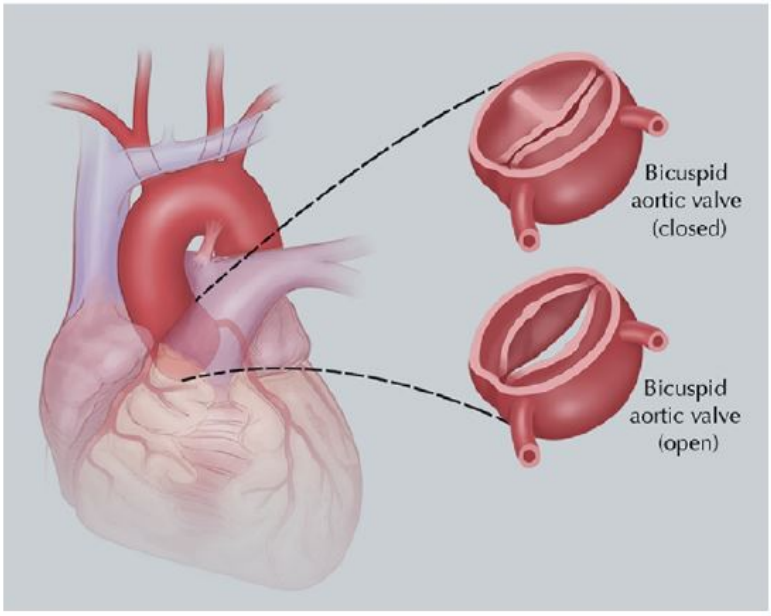

Figure 1-37: Illustration of a typical bicuspid aortic valve arrangement [58].

Normally, the aortic valve has three leaflets (***TAV***), but people birth with this anomaly presents only two flaps of which one of these is the result of a fusion. BAV can be classified in three different phenotypes groups [59,62]*:*

- ***Type I*** = fusion between left and right coronary leaflets (***LR-BAV***) with a repeatability of about 80%, also called antero-posterior arrangement, in this case coronary arteries arise both from the anterior sinus.
- ***Type II*** = fusion between right and non-coronary leaflets (***RN-BAV***) with a repeatability of about 17%, in this case coronary arteries arise from each opposite sinus.
- ***Type III*** = fusion between left and non-coronary leaflets (***NL-BAV***) with a repeatability of about 2%, this case is the same of the type II about coronary orifices.

The two resulting leaflets have the characteristics that they do not have equality size and they are dome shaped. The fusion can be happened in two way, with "*raphe*" or "*pure*" (it is rarer). The difference is at the level of the union, where there usually is a connecting cord, thicker and wider, at the centre of the join of the two interested flaps, while if this merging line is not so evident, it is called pure, because the union is perfect and looks like a single flap [60-65].

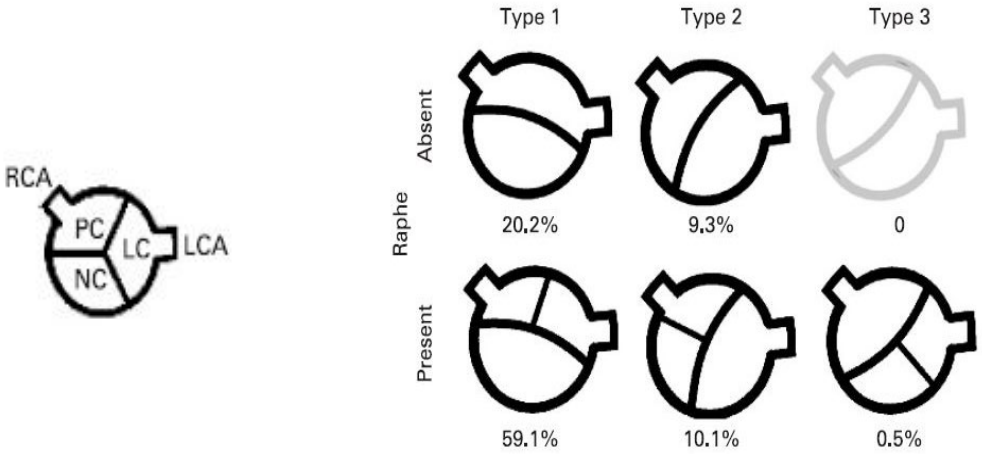

Figure 1-38: BAV leaflets fusion morphology, with relative coronary arteries origin and raphe [59].

It is considered the first risk factor for secondary heart disorders or aortopathy, because although this heart malformation is in the most cases asymptomatic in the first years of life until the adolescence, in adulthood, instead, people with BAV show a high tendency to developed cardiac diseases [61]. In general, good estimates say us that BAV leads to *aortic stenosis* in the 15% ÷ 71% of the cases, to *aortic regurgitation* in the 1.5% ÷ 3%, *infective endocarditis* in the 9.5% ÷ 40% and *aortic dissection* in the 5% of the cases. It is clear that those are wide, but it is explicable considering the different age of occurrence (the aortic stenosis arises in middle aged people, while infective endocarditis is typical in young aged people) [64,66].

It is clear, that the complications seen above are rarely an isolated clinical event, but it is easier for them to be mixed up with each other. Therefore, based on the risk profile of each patient,

the frequency of the occurrence of significant clinical events is estimated in the following graph [58]:

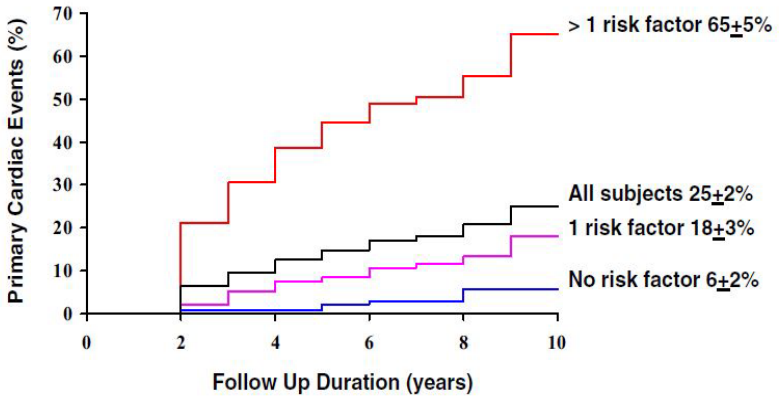

Figure 1-39: Trend curves of adverse clinical events related to the risk profile of adult patients [60].

Physiologically, this different number of leaflets forces valves to be less functional, because in the opened state the resulting orifice, through which the bloodstream passes, results smaller and asymmetric than the naturally. For this reason, valves can be more *inflexible* or *leaky*, so to be unable to open or close properly, inducing adverse hemodynamic events. The flow impinges on the flaps, stretching them, and they often are incapable to support the pressure load in both direction incoming and outcoming. Therefore, the natural compensation process leads to find alternative solutions, such as to deform the leaflets arrangement (*dome shaped*), trying to obtain a better match and delay valvular failure. Observe the *degree of folding* can help us to understand the grade of distortion of the hemodynamic stress magnitude, it is the main sign of correlation between cause and effect. [46,65]

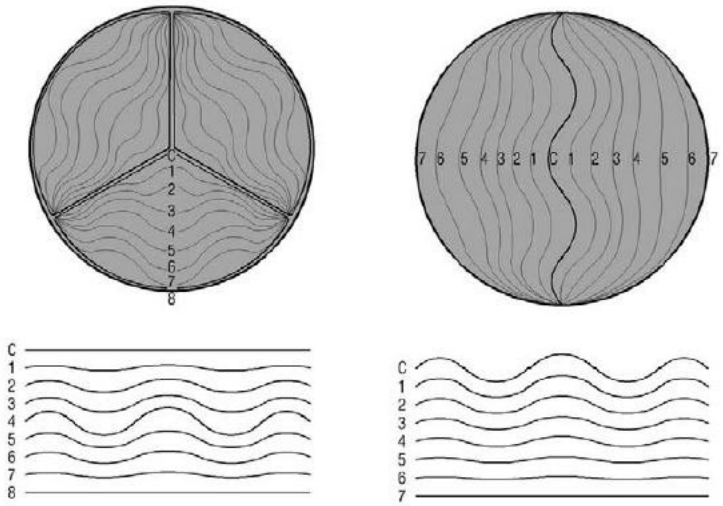

Figure 1-40: Degree of folding of each leaflet in TAV (on the left) and in BAV (on the right) [60].

Depending on the condition seen above, it not a surprise to find a *turbulence* state associated with a bicuspid aortic valve disorder. Turbulent flow may also cause significative impingement in different zones of the aortic wall inducing dilatation, aortic dissection or other complications. Several studies show how unphysiological flow and hemodynamic forces impacts with important changes in endothelium layers, given start to phenotypic expression of aortopathy, proven the known cells ability to respond to any abnormal sensing [59,65].

From a biomechanical point of view, clinical signs and anatomical features of BAVs result in important variations of the main hemodynamic parameters, which over the years have been detected and classified by different studies. The observed factors are the *flow* in *direction* (eccentricity), *magnitude*, *displacement*, *angle*, *velocity* and *asymmetry*, the wall shear stress force along the interested districts in terms of *magnitude*, *direction* and *frequency*, the *helicity* or other possible *hemodynamic indices* that can quantify the desired information necessary to understand how the pathological features affect concretely the fluid dynamics [59,61].

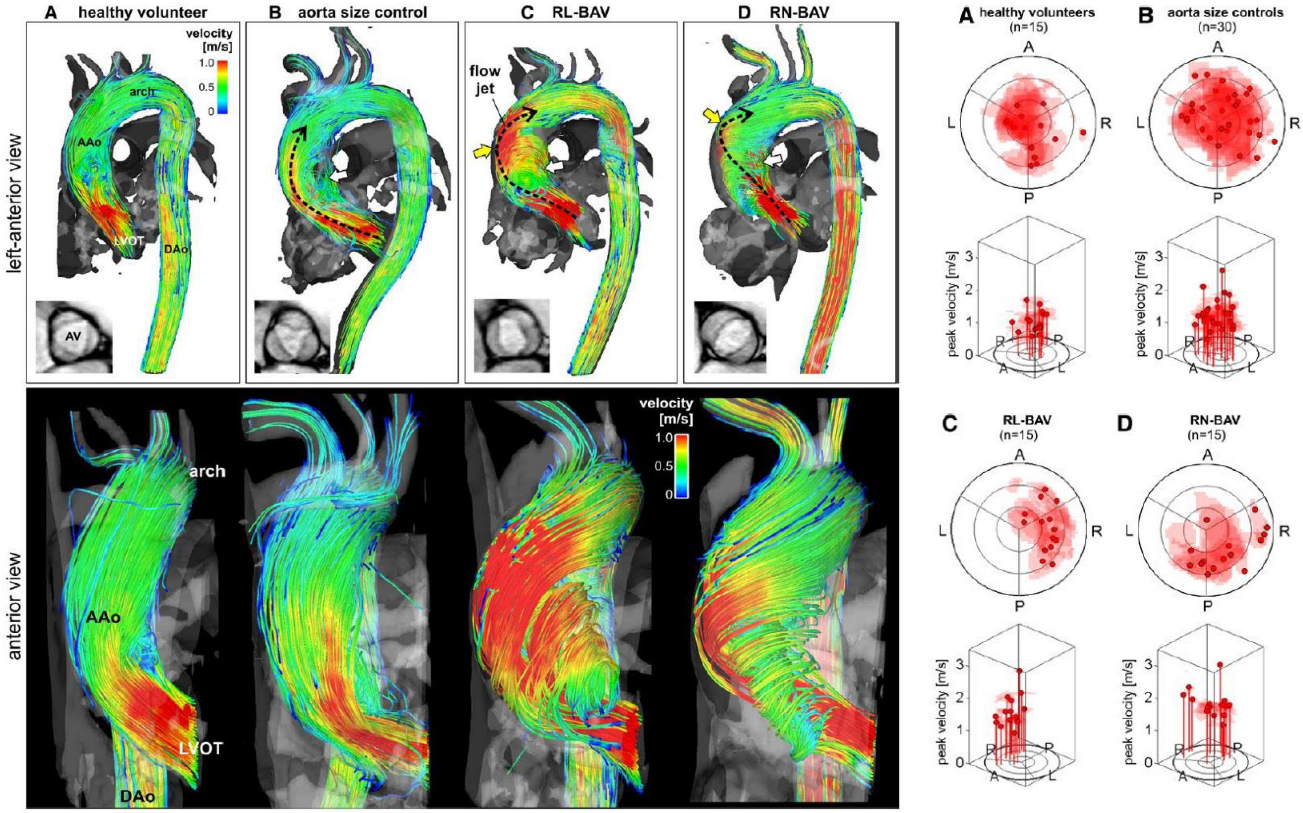

Figure 1-41: Top: Visualization of the blood flow streamlines on four types of aortic valve, using 4D PC-MRI. Middle: Visualization of the bloodstream in detail in the left ventricular outflow tract, in the ascending aorta, in the aortic arch. On the right: Comparison of the different flow profile asymmetric direction [61].

2. 3D MODEL and MESH OPTIMIZATION

2.1 3D MODEL

A three-dimensional model of aorta and coronary arteries obtained from coronary CT-scans is the object of this study. The complete model in exam be made up of: the ***aortic root***, where the three sinuses are clearly distinguishable; a portion of ***ascending aorta***; left and right coronary arteries. The model present one inlet surface in the lower part of the model, in correspondence of aortic anulus, and six outlet surfaces: one relative to aorta, and the others relative to coronary arteries.

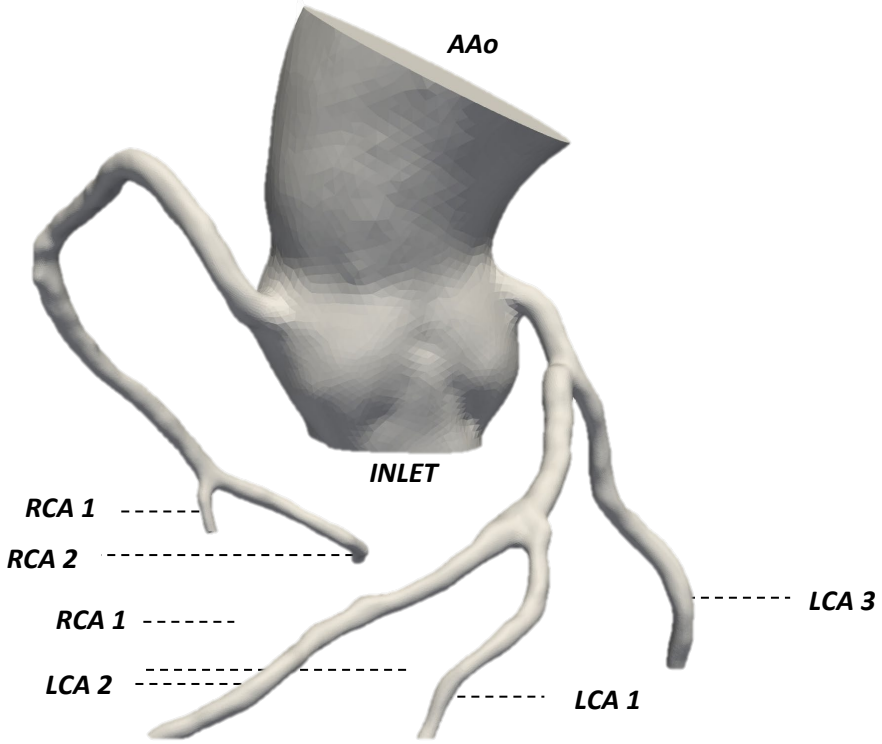

Figure 2-1: 3D Model.

2.2 PRE-PROCESSING

Before mesh generation, it is important to ensure that boundary conditions do not affect fluid dynamics results in the region of interest (*ROI*), so at each coronary outlet flow extensions were added.

To size of *flow extensions* were considered the distance necessary to have a fully developed flow, using the formula[64]:

$$L_h = 0.05 * Re * D$$

Reynolds number (***Re***) is one of the key concepts that governs the fluid field and is expressed as [64]:

$$Re = \frac{\rho \cdot \overline{v} \cdot D}{\mu} = \frac{Inertial\ forces}{Viscous\ forces}$$

where:

- ρ is the blood density $\left[\frac{g}{cm^3}\right]$
- μ is the blood viscosity $[\ Poise\ ]$
- D is the characteristic length of geometry, it is the diameter in case of circular section [cm]
- $\overline{v}$ is the mean blood velocity $\left[\frac{cm}{s}\right]$, calculable as $\frac{Q}{Area}$

It describes how the internal particles of the fluid stream along the channel, under the movement action of the flow. In a slow flow condition, it is possible to observe that the liquid moves parallel to the duct wall and this type of movement is called ***laminar*** flow, while if the flow is completely irregular and chaotic, condition that occurs when the speed increases, it is possible termed this condition as a ***turbulent*** state [5,12]. The standard ranges to establish the regime of flow are:

- *Laminar regime*: $\mathrm{Re} < 1000$
- *Turbulent regime*: $\mathrm{Re} > 2000$

- *Transition regime*: $1000 < \mathrm{Re} < 2000$

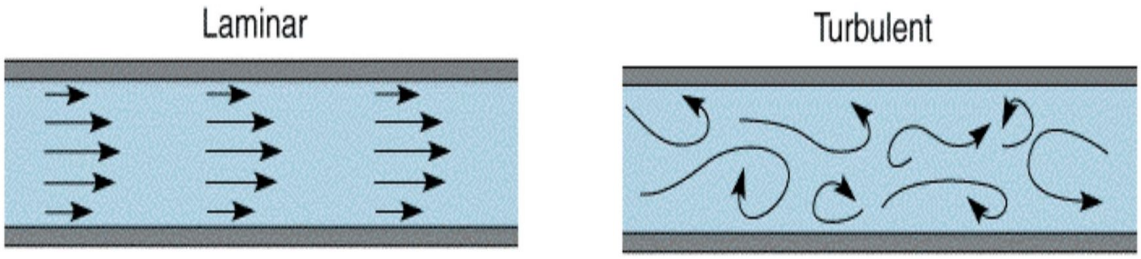

Figure 2-2: Illustration of the different movements between turbulent and laminar flow [12].

Practically, the ***Vascular Modeling Toolkit*** (*VMTK*) [65] was used to automatically compute vessels ***centerlines*** using a Voronoi diagram based algorithm which maximize the distance from boundary surface [65][66]. This mathematical characterization results to be a robust approximation in almost all cases, even in bifurcation or zones with complex geometry [66].

Figure 2-3: VMTK centerlines.

The model, was then imported into ***SimVascular***, an open source software used for CFD analysis[67]. Using this software, is possible to extract the surface area (cm^2) of each outlet

cap and, after a steady-state CFD simulation, flow values for each coronary artery can be obtained and Reynolds numbers subsequently calculated.

Now, all factors needed are known, so hydraulic quantities described above are quantifiable:

Cap Name	***Cap Area (cm^2)***	***Reynolds***	***Extension Ratio***	***Entrance Lenght (cm)***
LCA_1	0,021735	90,442	4,52210	0,75228
LCA_2	0,020966	88,802	4,44009	0,72544
LCA_3	0,052817	160,330	8,01649	2,07887
RCA_1	0,025416	100,123	5,00613	0,90055
RCA_2	0,040251	133,236	6,66181	1,50812

Table 2: Hydralic quantities for each coronary outlet.

Finally. starting from centerlines and lengths previous computed, flow extensions were added at each coronary outlets (Figure 2-4)[65].

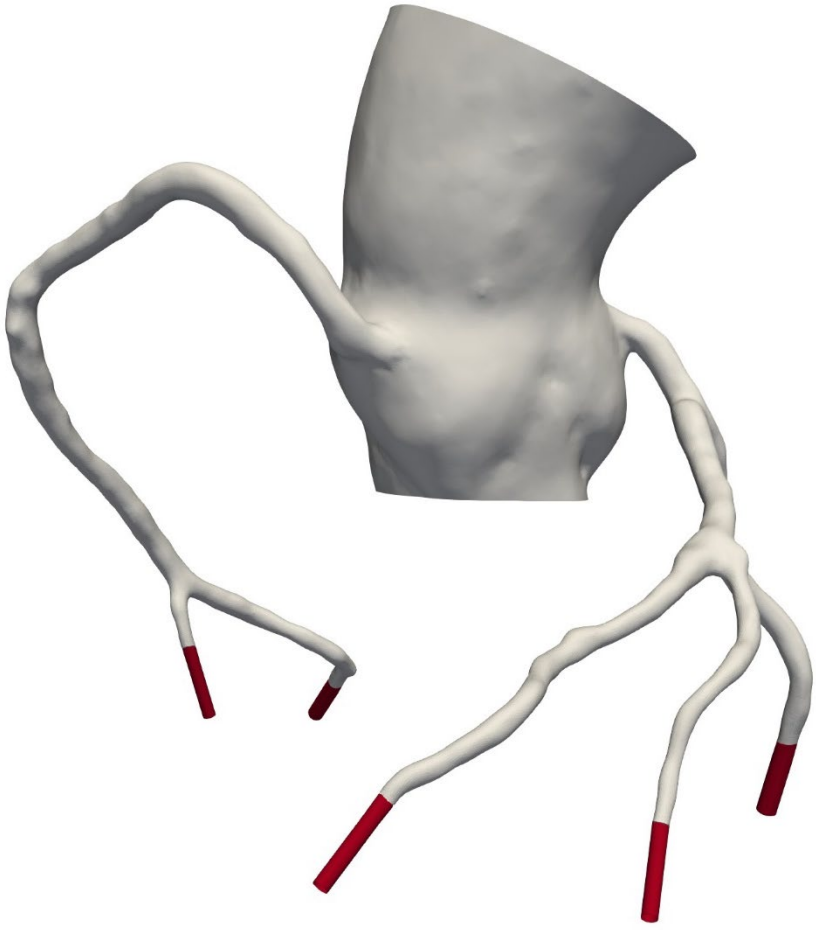

Figure 2-4: 3D Model with flow extensions.

2.3 MESH GENERATION

The last thing essential to do, before CFD simulations, is to create an appropriate computational grid on 3D model.

The discretization phase is necessary to allow the numerical solution of the *partial differential equations (PDEs)* [67]. Nowadays, a lot of commercial software exist and each of them can use different algorithms that have been developed over time. Each pieces of mesh are called ***elements*** and based on their shape, it is possible to differentiate, for example, a grid formed by *tetrahedral* or *hexahedral* elements. The choice of the shape and size of the elements is related to the need to be able to approximate the flow domain in the best way.

In this project ***TetGen*** [71-72], a tetrahedral mesh generator that uses *3D Delaunay Triangulation* has been used, because it is considerate an algorithm which provides flexible options for refinement, so produces the best shape in most cases, even the most complex ones, being able to adapt to the geometry and guarantee ***robustness***, ***good mesh quality***, and ***computational efficiency*** [71].

Often when simulating blood flow, interesting phenomenon can occur near the vessel walls. Under laminar flow, for example, ***boundary layers*** can form with great velocity and pressure gradients near the wall and it is advantageous to have a higher mesh density in the areas of high gradients. For this reason, near-wall boundary layer mesh has been generated [67], setting the adequate parameter in the *Boundary Layer Meshing* checkbox:

- ***Portion of Edge Size***: the portion of the edge size to use as the size for the initial boundary layer.
- ***Number of Layers***: the number of layers desired, too many layers can cause self-intersections on smaller vessels.
- ***Layer Decreasing Ratio***: the amount of the size decrease between successive boundary layers.

TetGen and ***MeshSim*** [70] are an open-source and a commercial mesh generators respectively, and they are already implemented in SimVascular. They are useful because

allow to custom many advanced options such as the boundary layer, previous mentioned, but also allow to easily obtain both isotropic and anisotropic meshes.

Isotropic mesh is so called because all its elements are the same *Global Max Edge Size*. It is possible to specify the size manually or rely on automatic estimate. The alternative is to generate an ***anisotropic mesh***, where different model portion show different mesh size.

A lot of models contain vessels with different dimensions, so in these cases it is desirable to compute a finer or larger mesh in the different vessels. The software allows to choose whether to compute a *radius-based mesh*, where the size of the mesh is automatically scaled in order to be proportional to the size of each vessel, or to compute a *local mesh size refinement,* where spheres can be added manually to increase the mesh density in specific regions of the model [67]. This last two solutions have been chosen and combined in this work. So, a radius-based mesh was generated based on coronary artery dimension and a regional refinement was imposed through several spheres in the aorta region.

2.4 CFD SIMULATIONS

CFD simulations were performed using the open-source software Nowadays, the CFD is a tool commonly applied in many fields such as industrial or clinical research, with the same scope for solving fluid problems of modelled physical cases without an invasive approach.

Fluid motion is governed by two fundamental equations, known as ***Navier-Stokes equations,*** these two equations describe the conservation of two quantities: *mass* and *momentum* [5]:

$$\begin{cases} \frac{\partial \rho}{\partial t} + \nabla \cdot (\rho \vec{v}) = 0 \\ \rho \left(\frac{\partial \vec{v}}{\partial t} + (\vec{v} \cdot \nabla) \vec{v} \right) = -\nabla P + \nabla \cdot \tau_{ij} + \vec{g} \end{cases}$$

Where the member before the equal sign is the inertial contribution, subdivided in the contribution of the *unsteady acceleration* $\left(\rho\frac{\partial\vec{v}}{\partial t}\right)$ and *convective acceleration* $\left(\rho\left(\vec{v}\cdot\nabla\right)\vec{v}\right)$, while the contribution after the equal sums the *pressure force* $(-\nabla P)$, *viscous forces* $(\nabla\cdot\tau_{ij})$ and *gravitational force* $(\vec{g})$.

If the fluid is Newtonian and incompressible, the two equations became:

$$\begin{cases} \nabla\cdot\vec{v} = 0 \\ \rho\left(\frac{\partial\vec{v}}{\partial t} + \left(\vec{v}\cdot\nabla\right)\vec{v}\right) = -\nabla P + \mu\nabla^2\vec{v} + \vec{g} \end{cases}$$

Nowadays, an analytical solution for these equations was not still found, for the most complex three-dimensional domains, so, they must be resolved through numerical methods, which found an *approximate solution* (temporal and spatial approximation), using the high computational power available today.

Generally, the most know numerical methods used to solve the Navier-Stokes equations are *finite volume* or *finite elements*, SimVascular solver, used for this work is based on ***Finite Element Method*** (***FEM***) [71]. CFD analysis performs on mesh elements, resolving individually the equations on each one until iteratively they reach *convergence*. Many control strategies can be set, such as "***Residual Criteria***" [67], which means that svSolver calculates residual error and checks that is smaller enough than an imposed reference value, if it is verified the solver continue to the next step, otherwise it need to compute other iterations to ensure the request.

2.5 SENSITIVITY ANALYSIS

An increase in mesh density means better accuracy of results but means also a significant increase in computational time (considering both mesh generating and following CFD processing). Contrary, if the number of elements that discretize the model volume and surfaces geometry is not enough, the results will be dependent from the quality of the mesh. Therefore, these two aspects can often be considered a non-negligible limit.

So, the choice of the mesh is a fundamental aspect, because it is necessary to find the best compromise between:

- ***High quality of the results***
- ***Reasonable computational times***

It is right to say that in this work, from the beginning, another obligatory limit is imposed on the maximum number of elements, due to the processing power of the personal computers we have available. So, we decided to set the highest threshold of discretization of the model to about ***5 million elements***.

To find the best solution, it was decided to perform a *sensitivity analysis*, facing the problem with an approach based on two steps:

Step 1) ***Optimization of the mesh size on coronary arteries***

Step 2) ***Optimization of the mesh size on aorta***

The strategy of paying more attention to only one section at a time, is chosen because we want to be sure that the aortic root does not influence too much the results about the smaller coronary branches in the first step and vice versa in the second step.

Note that all following meshes show an equal ***boundary layer*** set as:

- *Portion of Edge Size = 0.5*
- *Number of Layers = 2*
- *Layer Decreasing Ratio = 0.5*

2.5.1 CFD Boundary Conditions and Solver Parameter

To understand which one the most appropriate mesh is, ***steady-state flow simulations*** in SimVascular [67] were performed and from these some hemodynamic data extracted and used in the sensitivity analysis. It is important to note that the same simulation must be done for each mesh in question, because the results must be comparable to each other.

A generic ***aortic inflow waveform***, in ***.flow*** file format, is prescribed at the aorta inlet face. It quantifies the flow coming out from the aortic valve and coming in in the initial portion of the ascending aorta.

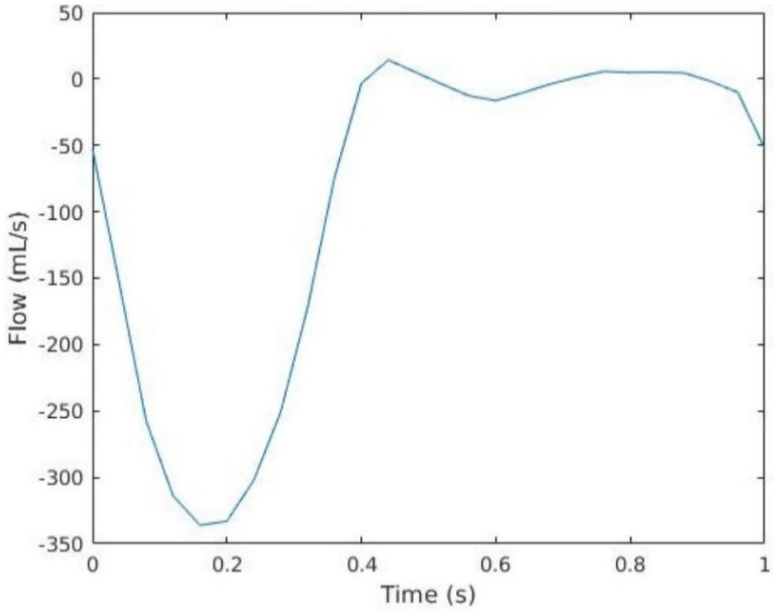

Figure 2-5: Aortic inflow waveform [67].

The flow rate has a mean cardiac output value of $Q = 90.7 \frac{ml}{s}$ and a total heart period of 1 s. Note that this flow is specified *forward* in the model, so the negative sign is imposed before the original waveform values. Then the *Pre-Solver* compute a *Fourier Series transformation* of the *.flow* file and a generic ***plug*** profile is chosen for the analytic velocity shape.

Blood is considered as a ***Newtonian incompressible*** fluid for all simulations. The wall of the blood vessels is assumed as ***rigid*** and ***no-slip condition*** was applied.

About the outlet boundary condition, in these preliminary simulations, it has been decided to adopt a lumped parameter model completely ***resistive.***

$$\begin{cases} R_{TOT} = R_{AORTA} = 1371.93 \ \frac{dynes \cdot s}{cm^5} \\ R_{CORONARY-TOT} = 24 \cdot R_{TOT} = 32926.27 \ \frac{dynes \cdot s}{cm^5} \end{cases}$$

Total coronary resistance value is split for each single branch in order to calculate their resistance values. This action is automatically computed only imposing the ***Murray's Law Coefficient*** [67]*, that in this work is chosen equal to 2.6* [81].

The flow solver parameters manually set, are:

- *Number of Timesteps = 1000*
- *Time Step Size = 0.001*
- *Number of Timesteps between Restarts = 100*
- *Step Construction = 5*
- *Residual Criteria = 0.0001*
- *Time Integration Rule = First Order*

2.5.2 Step 1

Different ***anisotropic radius-based*** meshes are simulated, where the mesh size on aorta is fixed at the value of *0.12*, while the mesh sizes prescribed on the coronaries are progressively decreasing in a dimension range between *0.029* and *0.013*.

N° MESH	***Number of ELEMENTS***	***Coronary arteries MESH SIZE***
1	1342869	0,029
2	1481605	0,027
3	1595930	0,025
4	1923802	0,022
5	2249797	0,02
6	3548384	0,015
7	4250400	0,014
Reference	5172702	0,013

Table 3: Step1, Meshes and their size.

Focusing on each coronary branch, the left (*LCA*) and right (*RCA*) coronary arteries are manually clipped from the entire models, using VMTK [65].

To evaluate the fittest mesh, a ***percentage difference analysis*** is performed, in which each branch mesh is compared to the reference mesh (the best mesh with the highest number of elements):

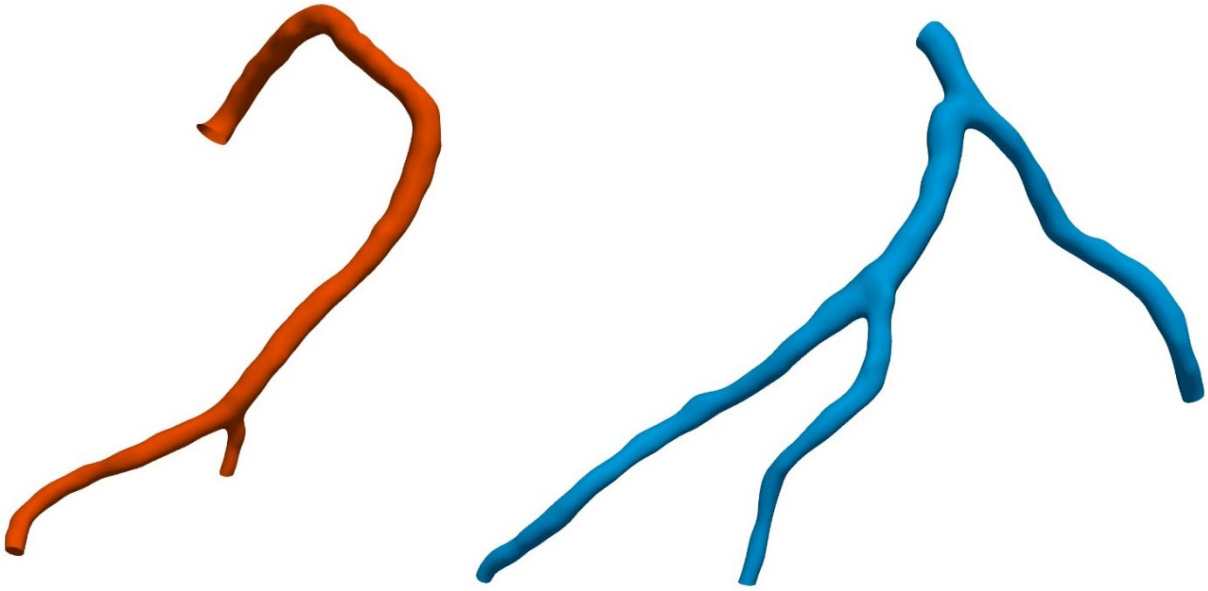

Figure 2-6: Right and Left coronary arteries clipped.

$$\Delta VALUE_{\%} = \frac{VALUE_{BestMesh} - VALUE_{Mesh_i}}{VALUE_{BestMesh}} \cdot 100$$

Then four of the main *hemodynamic parameters* (their mean values) are extracted from the steady simulations and their absolute value of the percentage differences are calculated and plotted. To understand which one of the seven meshes is more appropriate, a ***threshold*** is defined for each of these parameters, as shown in the following table:

Analyzed results	***Threshold***
FLOW RATE	*1%*
WSS	*1%*
WALL PRESSURE	*1%*
VELOCITY MAGNITUDE	*1%*

Table 4: Step1, Thresholds.

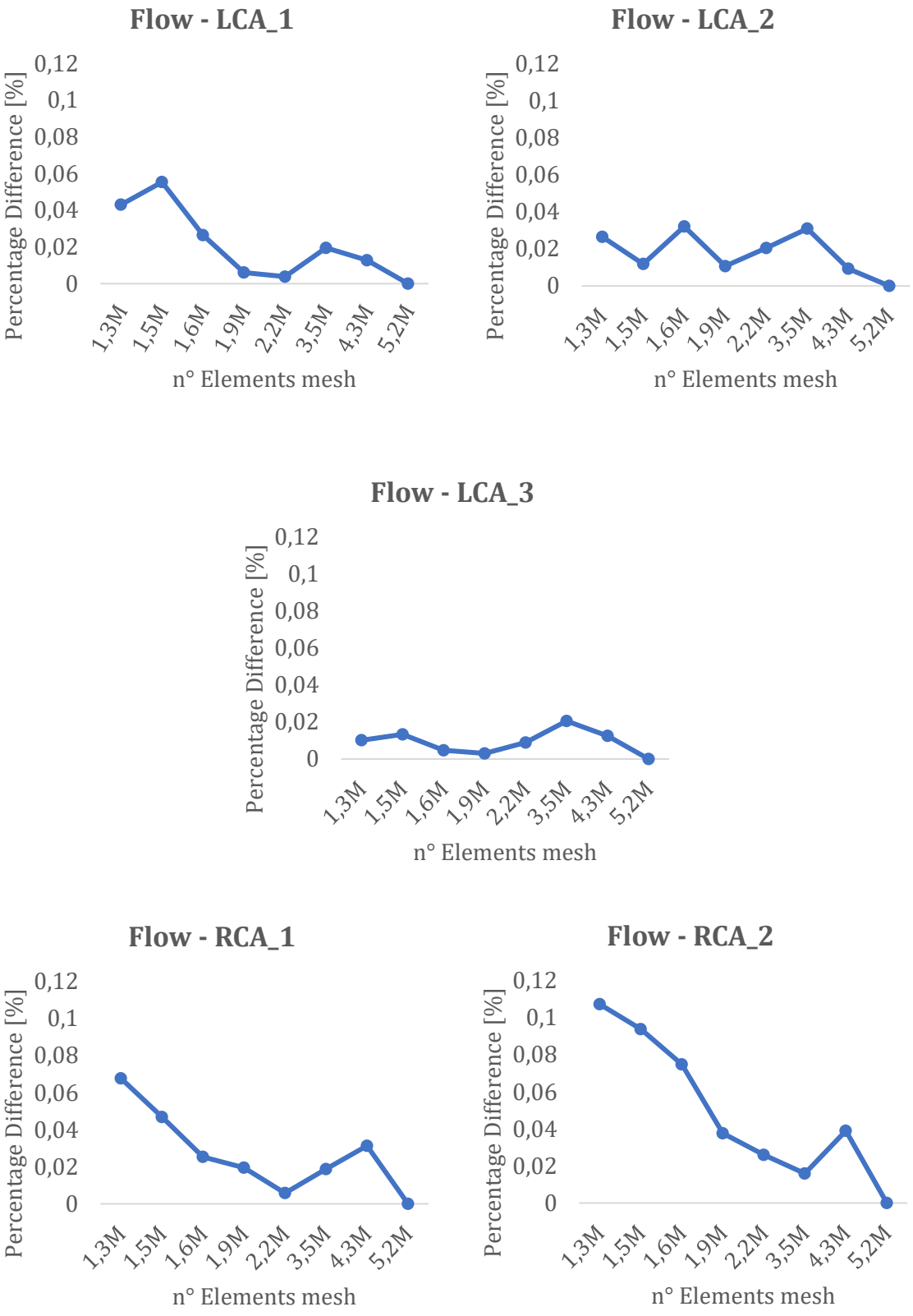

Figure 2-7: Flow percentage differences on coronary arteries.

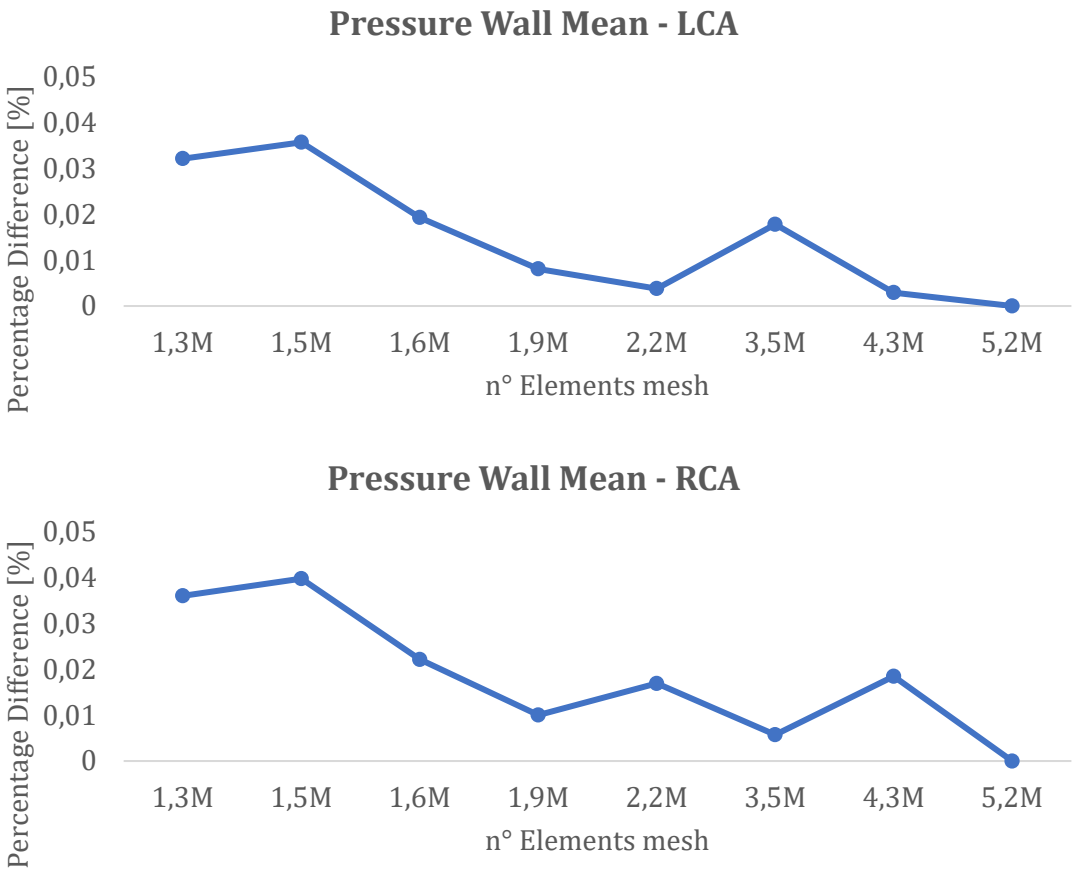

Figure 2-8: Pressure percentage differences on coronary arteries.

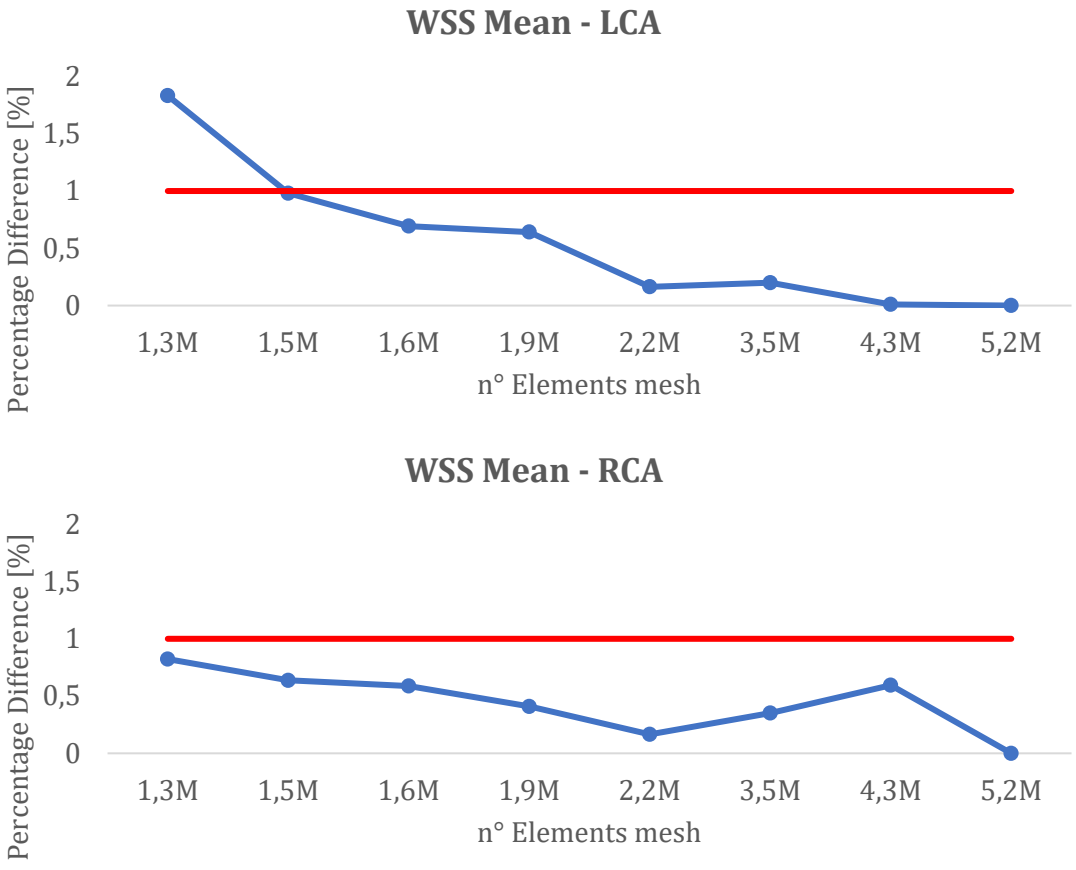

Figure 2-9: WSS percentage differences on coronary arteries.

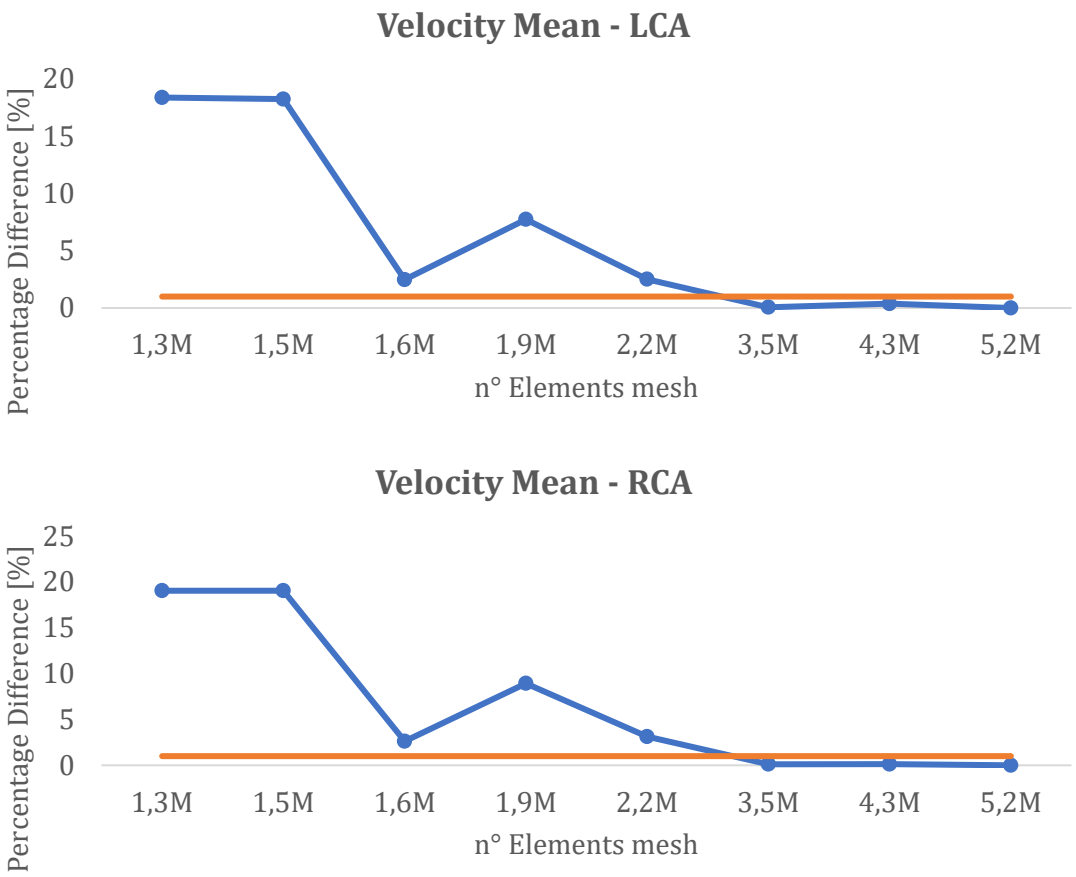

Figure 2-10: Velocity magnitude percentage differences on coronary arteries.

After this first step, results can be resumed:

- About *flow*: it is possible to observe that all meshes in exam are widely under the error of 1%, so they are hypothetically all acceptable.
- About wall *shear stress*: in the RCA cases all meshes are below the threshold, while in the LCA cases the first mesh adequate is that of 1.6 million.
- About *pressure wall*: in this parameter all meshes satisfy the chosen gold standard.
- About *velocity*: the smallest mesh is 3.5 million, both in LCA and RCA branches.

In coronary arteries, thresholds imposed are very low, so high accuracy is ensured. The ***3,5 million* mesh** is the best resulting optimization that ensures the requests previously mentioned. This mesh shows a coronary mesh size of **0*.015*** and an aorta mesh size of ***0.12***.

2.5.3 Step 2

At this point, a new group of **anisotropic radius-based** meshes are simulated in the same steady conditions of the previous step. The difference is that this time, the optimization is focused on the mesh size on aorta section, so the fixed size is that on the coronary arteries at *0.025*, while decreasing mesh sizes are prescribed on aorta, in a range between *0.12* and *0.07*.

N° MESH	***N° ELEMENTS***	***Aorta MESH SIZE***
1	1595930	0,12
2	2222019	0,1
3	2790253	0,09
4	3634264	0,08
Reference	5143522	0,07

Table 5: Step2, Meshes and their size.

Focusing only on the aorta section, using VMTK, aorta is manually clipped from the entire models. After that all the same percentage difference analysis are performed and plotted, in the same way and about the identical hemodynamic parameters described for the step 1, but changing thresholds, as shown in the following table:

Analyzed results	***Threshold***
FLOW	*5%*
WSS	*10%*
PRESSURE WALL	*5%*
VELOCITY MAGNITUDE	*5%*

Table 6: Step2, Thresholds.

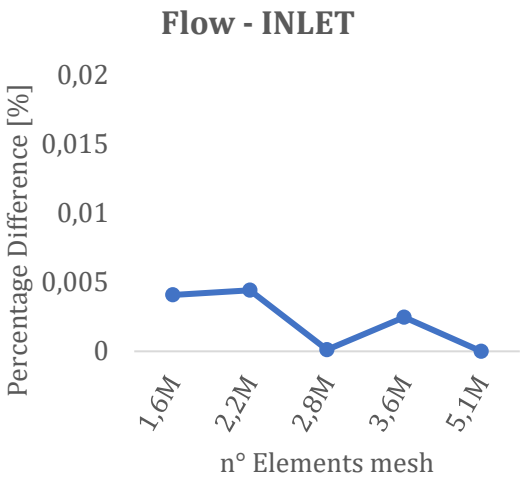
Flow - INLET
Percentage Difference [%]
0,02
0,015
0,01
0,005
0
1,6M
2,2M
2,8M
3,6M
5,1M
n° Elements mesh

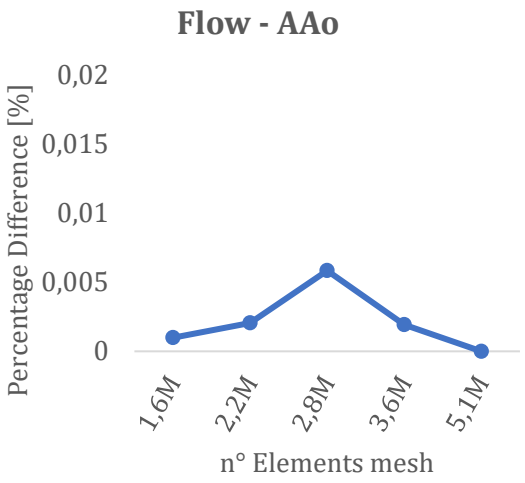
Flow - AAo
Percentage Difference [%]
0,02
0,015
0,01
0,005
0
1,6M
2,2M
2,8M
3,6M
5,1M
n° Elements mesh

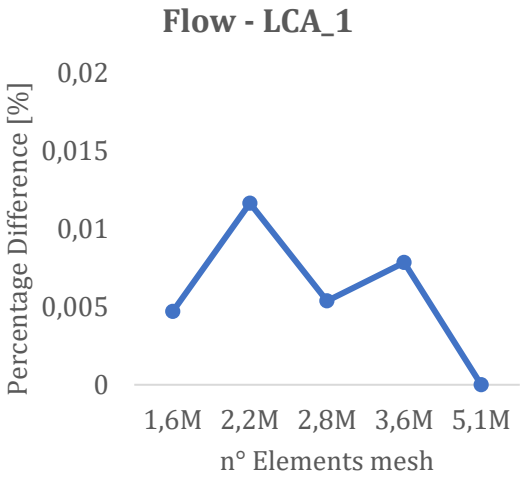
Flow - LCA_1
Percentage Difference [%]
0,02
0,015
0,01
0,005
0
1,6M
2,2M
2,8M
3,6M
5,1M
n° Elements mesh

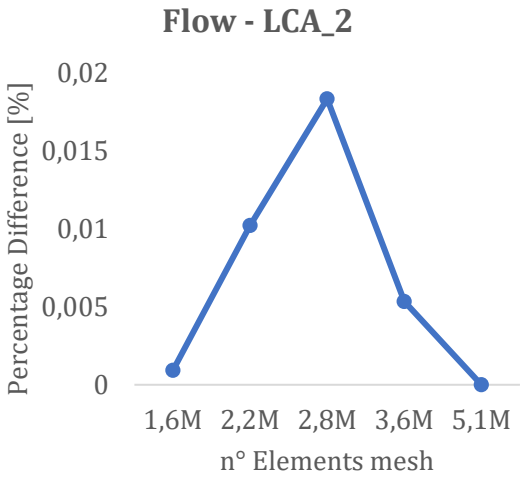
Flow - LCA_2
Percentage Difference [%]
0,02
0,015
0,01
0,005
0
1,6M
2,2M
2,8M
3,6M
5,1M
n° Elements mesh

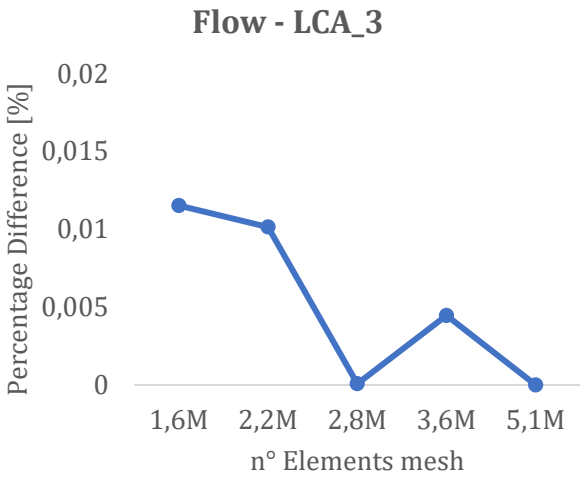
Flow - LCA_3
Percentage Difference [%]
0,02
0,015
0,01
0,005
0
1,6M
2,2M
2,8M
3,6M
5,1M
n° Elements mesh

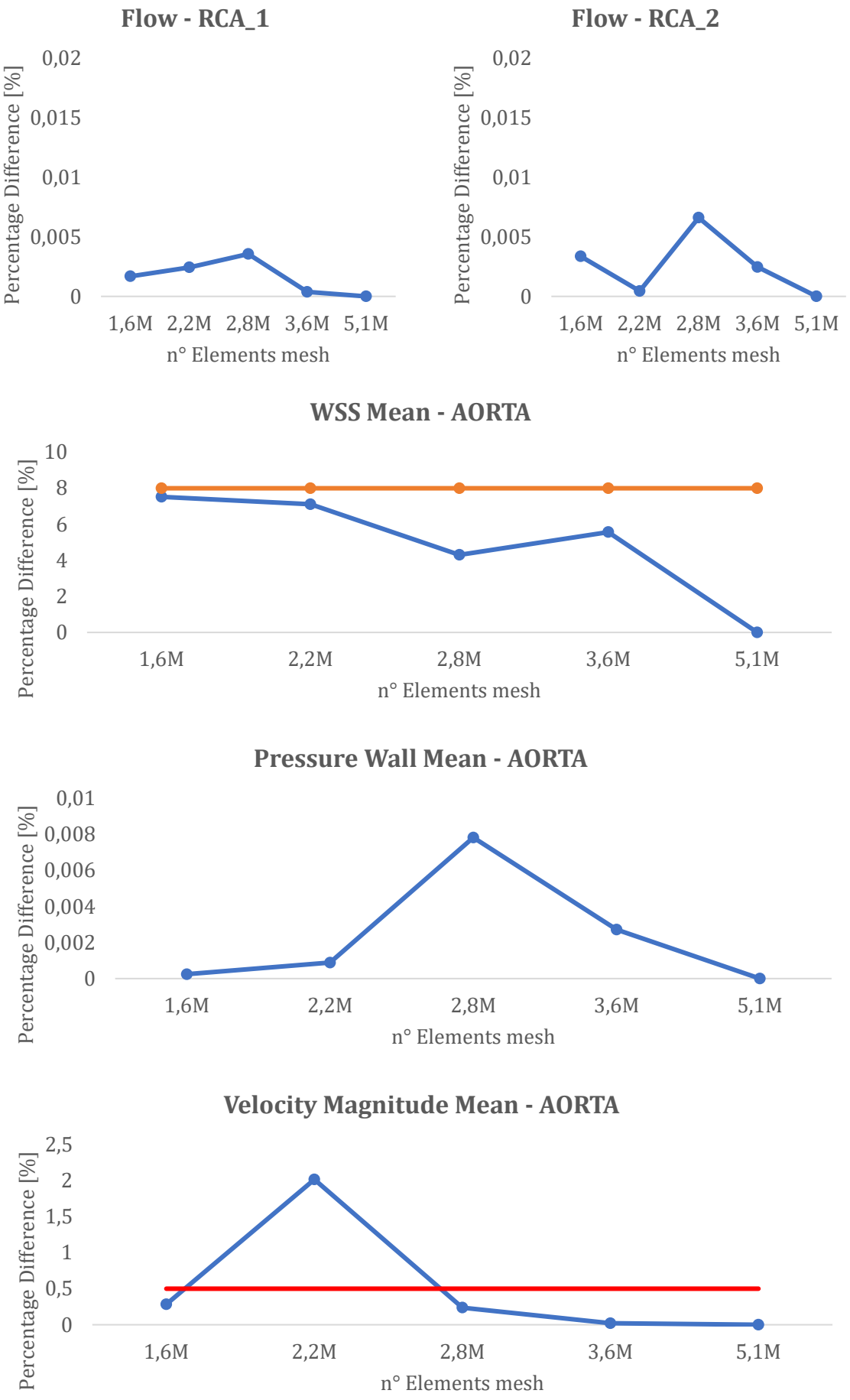

Figure 2-11: Flow percentage differences on all caps; WSS, Pressure and Velocity percentage differences on aorta section.

After the second step, now the resulting sensitivities can be schematic resume in this way:

- About *flow*: all meshes in question show the value of 0.07 as maximum percentage error and it is easily under the threshold of 1%, so they are all acceptable.
- About *wall shear stress*: all meshes are adequate.
- About *pressure wall*: in this parameter all meshes satisfy the chosen gold standard.
- About *velocity*: the smallest mesh is 1.6 million.

After the second optimization, the mesh of ***1.6 million*** of elements result to be the best, so an aorta mesh size of ***0.12*** results proper.

Remembering that the maximum number of elements has been set at around 5 million, a careful observation has led us to add further consideration to what has already been done.

The thesis aim is focused on the study of the hemodynamic of the coronary arteries, so in terms of sensitivity, we are interested in obtaining better accuracy on branches rather than on aorta. Obviously, aorta phenomena are insignificant if they do not directly affect coronaries. This justifies having chosen the thresholds equal to 1% in all coronary quantities, while, in aorta section, we want to choose a mesh with an elements number around 4M. For this reason, we decide to accept as aorta mesh size the value of **0.12** (although it shows higher percentage differences), but a denser grid of **0.015** on coronaries. Therefore, the nest mesh has a total number of elements of ***4323793*** and thus a better quality of the results.

STATISTICS

Number of Nodes	727869
Number of Elements	4323793
Number of Edge	227679
Number of Faces	151786

Table 7: Best mesh statistics.

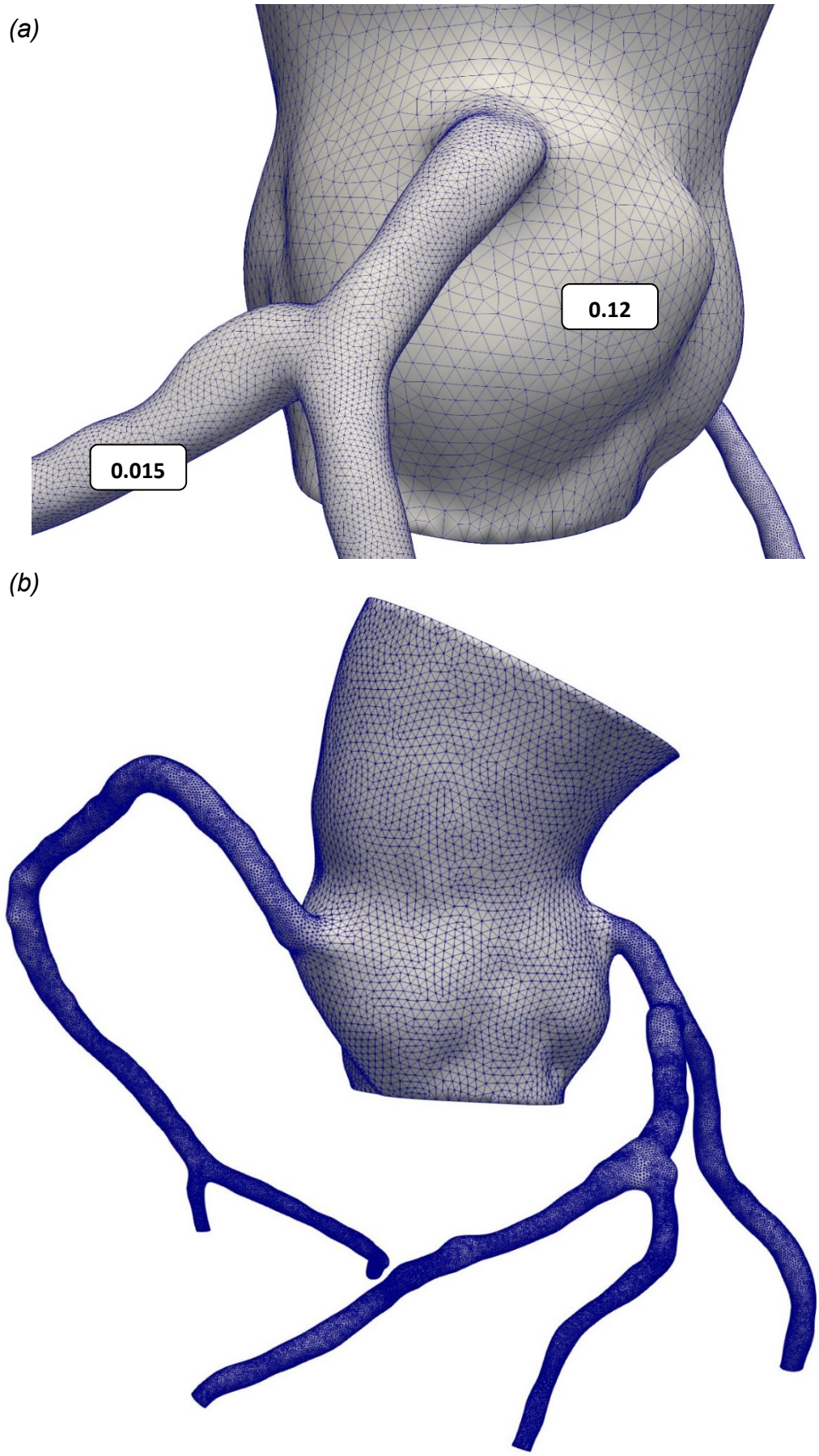

Figure 2-12: (a) zoom on the 4M mesh; (b) overview on the complete 4M mesh.

3. BAV 3D VELOCITY PROFILES

3.1 DATA REFERENCES

Physiologically, the aortic valve has *tri-leaflet* (***TAV***), but people birth with ***Bicuspid aortic valve*** (***BAV***) anomaly presents only *two flaps* of which one of these is the result of a fusion (with a prevalence of *1%* to *2%* in the developed world) [60,62].

Three different phenotypes groups can be classified in order of frequency [57]:

- ***Type I*** = fusion between left and right coronary leaflets (***LR-BAV***)
- ***Type II*** = fusion between right and non-coronary leaflets (***RN-BAV***)
- ***Type III*** = fusion between left and non-coronary leaflets (***NL-BAV***)

Several studies evidence the morphologic patterns role in the hemodynamic and flow changes outing from valve. Obviously, these modifies are strongly associated to different impacts on the development of consequently pathologies.

A wide literature has concentrated its interest about the effect of this disease on aortic branch (especially ascending aorta and its arc aortic). This thesis wants to change the point of view and observes experimentally the same pathologic problem on coronary arteries.

Computational approaches (*PC-MRI, echocardiography, particle-image velocimetry*) on patients allowed to measure and determinate flow and velocity field through each valve type.

Cao et al. designed 3D *valve-aorta* geometry models [61] and then *3D fluid-structure interaction* (*FSI*) simulation performed on them, obtaining qualitatively accurate ***velocity*** patterns [63].

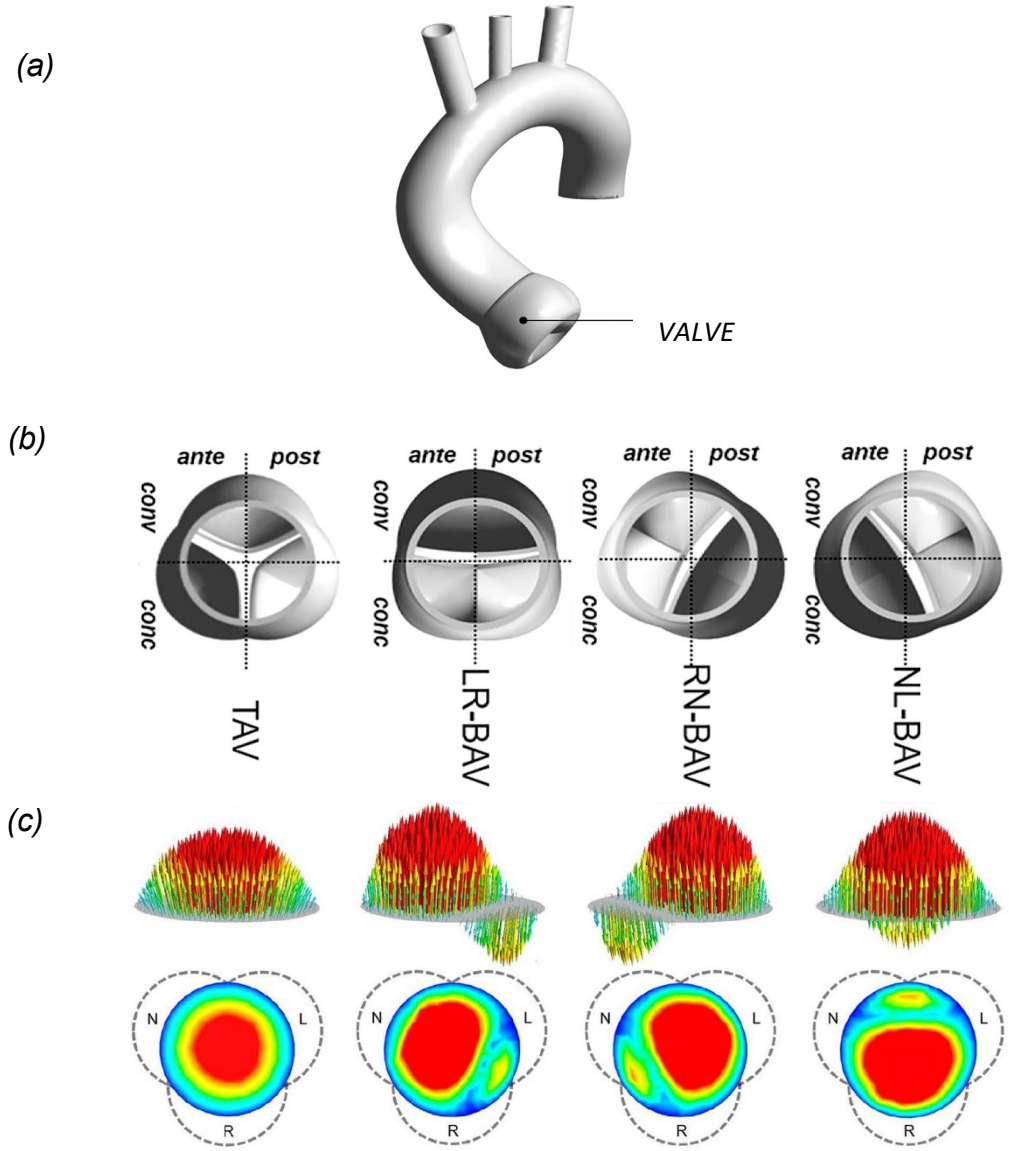

Figure 3-1: (a) valve-aorta model [61]*; (b) TAV and BAV model* [61]*; (c) TAV and BAV velocity profile and surface contour* [63].

As shown in the previous contour images, the inlet surface evidences a side where the velocity is forward, and the other side where is backward. This characteristic is associated to valve opening and closing movement during the cardiac cycle and it can be classified based on the minimal cross-sectional area of the valve orifice at peak systole, called ***Geometric Orifice Area*** (***GOA***) [72]. From *Cao et al*, the *GOA* at the systolic peak for each model are [72]:

- *TAV GOA = 3.7 cm^2*
- *BAV GOA = 2.3 cm^2*

while the *GOA* at the diastole phase show a progressive reduction [72]:

- *TAV GOA = 22% decrease*
- *BAV GOA = 54% decrease*

Note that in our work, we decided to adopt as correct values to subdivide the inlet surface and differentiate *TAV* condition from *BAV* condition, only the GOA numbers at peak systole. Following these indications, it is easy to calculate that, the ***forward area*** *of BAV* ($\boldsymbol{A^{+}_{BAV}}$) is around *62%* of the inlet surface area and the remaining *38%* is the *BAV* ***backward area*** ($\boldsymbol{A^{-}_{BAV}}$). Clearly, the forward area is the area of the leaflet not fused, so it is adequately oriented in each BAV type.

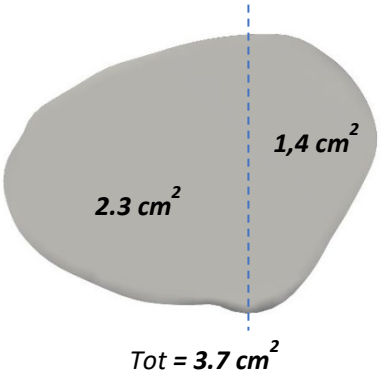

Figure 3-2: Inlet surface (LR-BAV case) subdivision, forward area and backward area.

About the ***flow rate***, *Barker et al.* in their work, using *4D Flow MRI* acquisitions, extracted these following waveform quantifications for *TAV* and *BAV* conditions [73]:

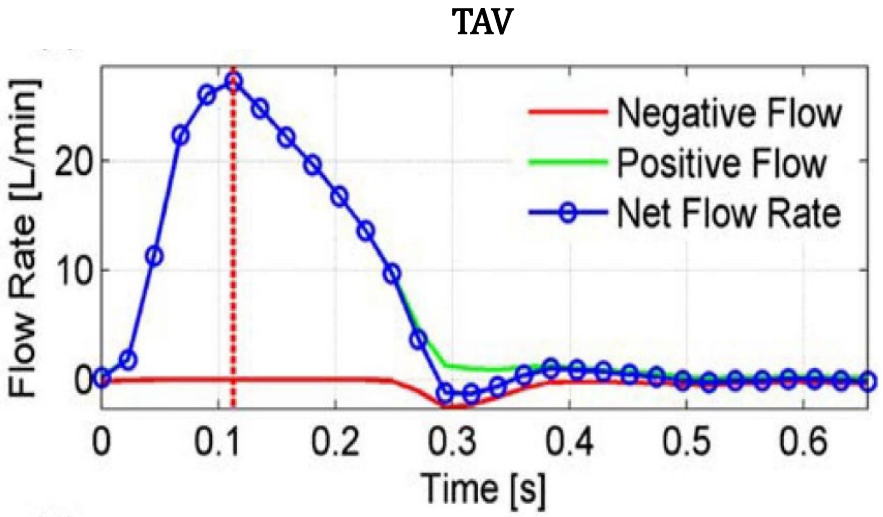

Figure 3-3: TAV flow rate waveform [73].

BAV

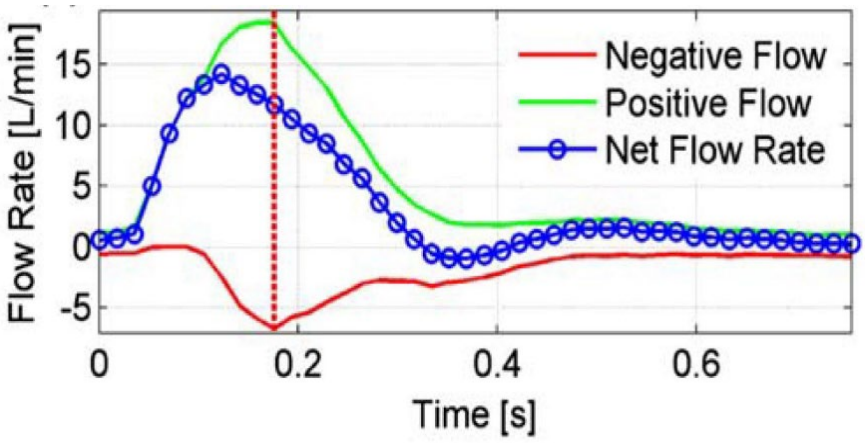

Figure 3-4: TAV and BAV flow rate waveform [73].

3.2 THROUGH-PLANE VELOCITY

Cao et al. results inspired the miming processing of the velocity profiles in this work tying to reproduce the typical velocity profiles of a patient affected by BAV, considering both the forward and backward profiles [63].

3.2.1 Formulation

The *TAV* case is imitated associating it to a parabolic ***Poiseuille*** profile with the peak on the centre point and a progressive decrease until zero, moving towards the boundary of the surface.

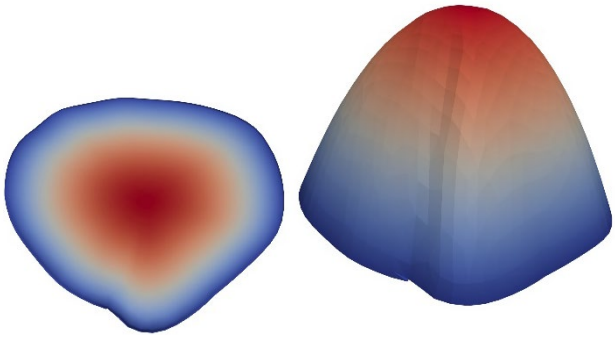

Figure 3-5: TAV Poiseuille profile.

Observing *BAV* cases, note that the positive and negative velocity distributions show a parabolic shape, similar to classic *Poiseuille* profile (TAV case), but with an important eccentric displacement of the maximum peak towards the respective sinus. To model this velocity behaviour, the following formulation of the ***Generalized Poiseuille*** *(through-plane) velocity profile* was implemented using an ad-hoc *Python* script:

$$v_{tp}(r,\theta) = \left\{ \boldsymbol{a} \cdot \left[1 - \left(\frac{r}{R(\vartheta)} \right)^{\boldsymbol{K}} \right] + \boldsymbol{b} \cdot \left[\left(\frac{r}{R(\vartheta)} \right)^{3} - \frac{r}{R(\vartheta)} \right] \cdot \cos(\vartheta + \boldsymbol{\alpha}) \right\}$$

Every single parameter has an important meaning and each change implies significant shape modifications:

- **a** increment is correlated to an forward surface area increase, at the expense of the backward surface which area decrease.
- **b** is related to the backward surface area increment or decrement.
- **k** is the parameter that set the curve smoothing, to obtain a profile more or less parabolic and restrained.
- $\boldsymbol{\alpha}$ is included between 0 and 360, it adjusts the angular orientation to rotate the profile in the affected sinus

For this reason, in this formulation ***parameter optimization*** is the key to replicate the correct profile.

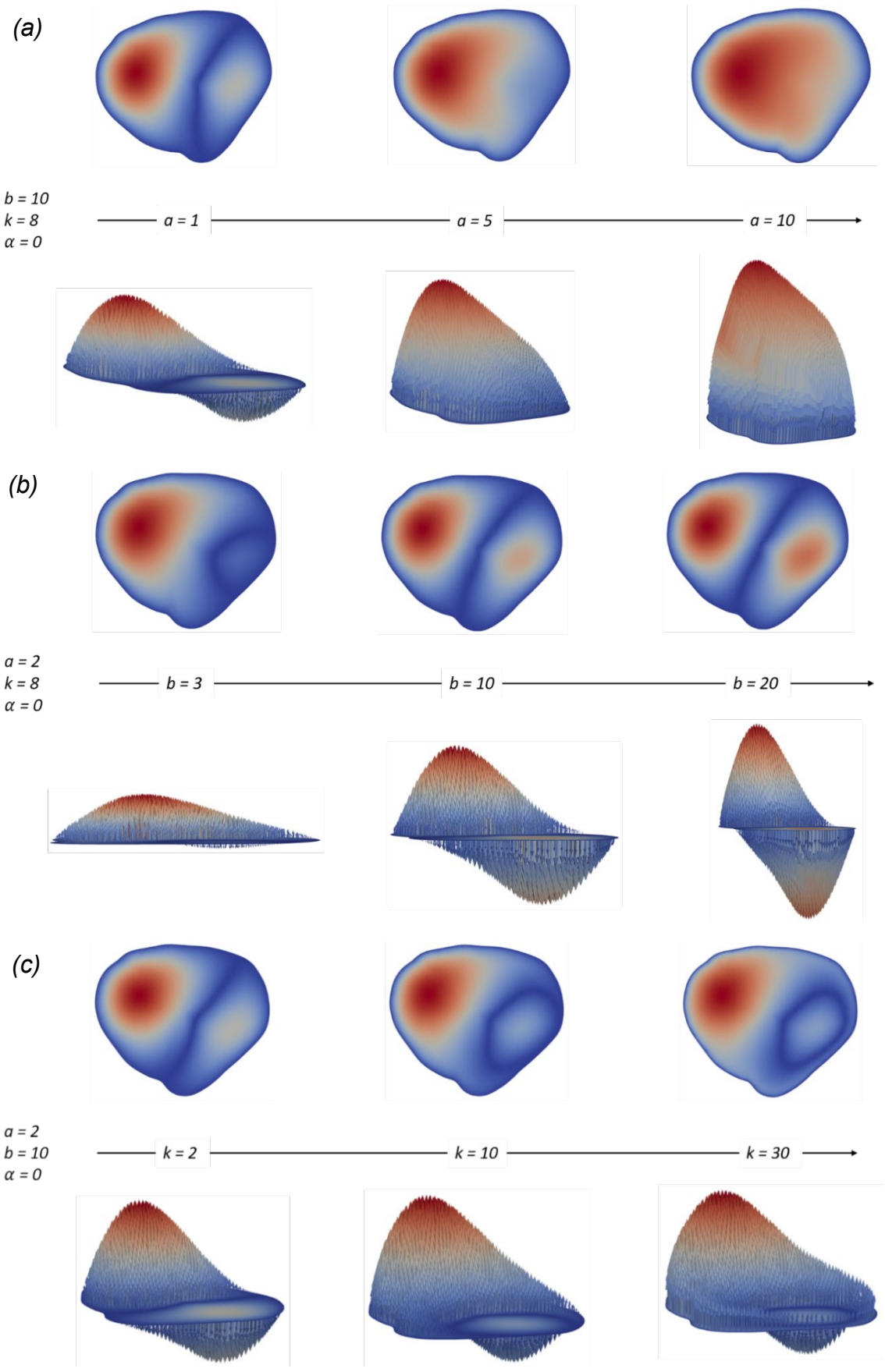

Figure 3-6: (a) effect of a parameter; (b) effect of b parameter; (c) effect of k parameter.

3.2.2 Parameter Optimization Algorithm

The analysis is performed focusing on the ***basic criterion*** to obtain the correct area subdivision. According to *Cao et al.* paper, we want to ensure that:

$$A_{BAV}^{-} = \mathbf{38}\% \text{ of } A_{TAV}$$

The algorithm is implemented in *Python* and an automatic optimization of all parameters of the formula would be the best desirable level, but in this work, we decided to manually set almost all parameters (after accurate valuations) and perform an iterative improvement of a single ***variable parameter***. After initial observations, an enough wide ***range*** *from* ***0*** *to* ***50*** is set for the variable parameter with a ***fixed size step*** of ***0,5***

FIXED PARAMETER	***VARIABLE PARAMETER***
a	b
k	Range = 0 : 50
α	Size step = 0.5

Now, the script iteratively computes the value of the area determinate by the current variable parameter set: $(\boldsymbol{A_{BAV}^{-}})_{\boldsymbol{CALCULATED}} = \boldsymbol{A_{BAV}^{-}}(\boldsymbol{b_i})$

Then the ***percentage difference*** is calculated. A threshold of **10%** is imposed to consider the b value in exam reliable. If this control phase is verified, the value is saved in a new array, called "**new_b**".

$$\frac{A_{BAV}^{-} - (A_{BAV}^{-})_{CALCULATED}}{(A_{BAV}^{-})_{WANTED}} * 100 < 10\%$$

When the range is at the end, a new cycle begins, taking the new array elements as values of variable parameter. The new range has the maximum value and the minimum value of new_b array as extremes and the new *size step* is calculated as: $\frac{\max(new_b) - \min(new_b)}{100}$. The operations are iteratively repeated, in the same way as cycle 1, the only variaton is about the *control threshold*, which is imposed to **1%** to perform a refiner discretization. Values, which over pass the control statement, are saved in a support array and at the end of iterations the value related to the ***lowest error percentage*** is confirmed as the ***best optimization*** of the variable parameter.

The following workflow resume schematically the algorithm process:

- **CYCLE 1:**

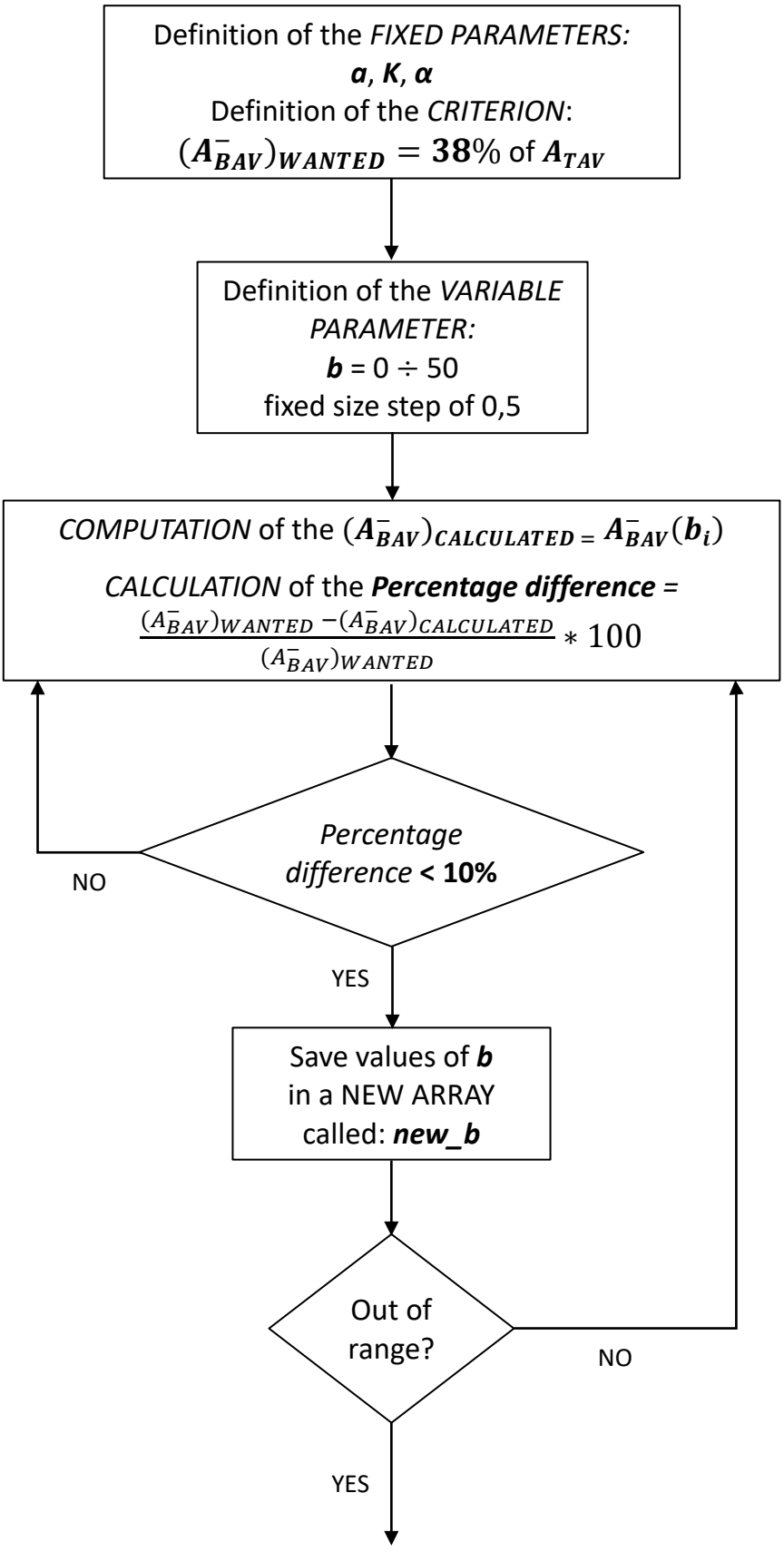

- **CYCLE 2:**

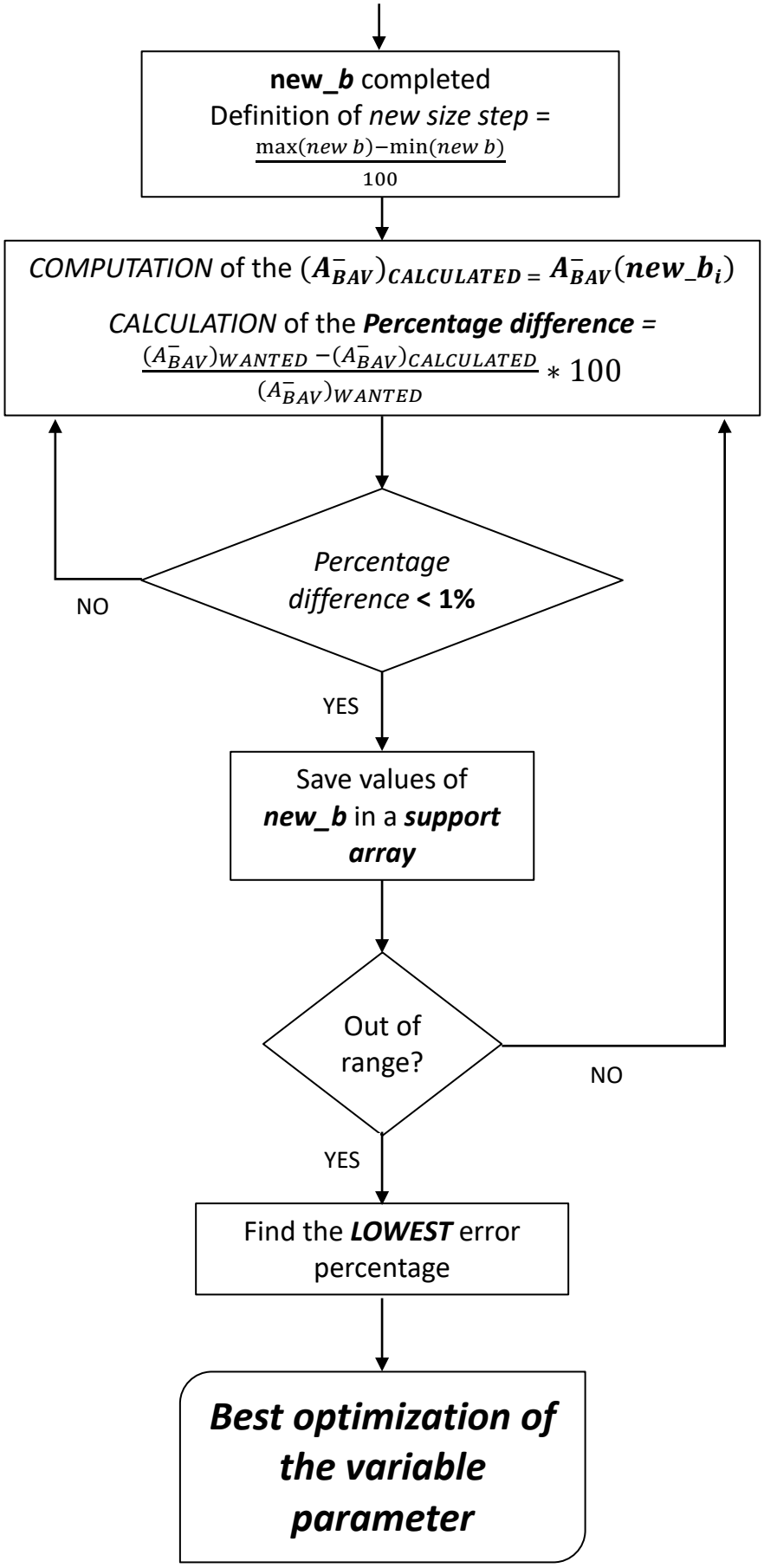
new_b completed
Definition of *new size step* = $\frac{\max(new\ b)-\min(new\ b)}{100}$
COMPUTATION of the $(\bar{A}_{BAV})_{CALCULATED} = \bar{A}_{BAV}(new\_b_i)$
CALCULATION of the ***Percentage difference*** = $\frac{(\bar{A}_{BAV})_{WANTED} - (\bar{A}_{BAV})_{CALCULATED}}{(\bar{A}_{BAV})_{WANTED}} * 100$
Percentage difference **< 1%**
NO
YES
Save values of ***new_b*** in a ***support array***
Out of range?
NO
YES
Find the ***LOWEST*** error percentage
Best optimization of the variable parameter

3.2.3 Waveform Modulation

After profiles generation and parameters optimization, we fundamentally have the right shapes but mathematically wrong because they don't yet reflect the real physiological BAV conditions. We decided to digitalized *Barker et al. flow rates* [73], we extracted the numerical sample values and then we performed an interpolation with a Fourier series, to pass from a discrete to a continue and analytical time depending waveform:

$$f(t) = a_0 + \sum_{n=1}^{N} [a_n \cdot \cos(2\pi nt) + b_n \cdot \sin(2\pi nt)]$$

- a_0 = mean values of discrete flow rate
- a_n and b_n are the Fourier coefficients
- N = the number of coefficients that we use to reconstruct the waveform.

BAV positive and *negative* flow waveforms were reconstructed using a *N = 8* and *N = 9* respectively, while the *net* flow is obtained as difference between the previous two. Then all curves were scaled in $\frac{ml}{s}$. Same processing was done on *positive*, *negative* and *net TAV* flow rate.

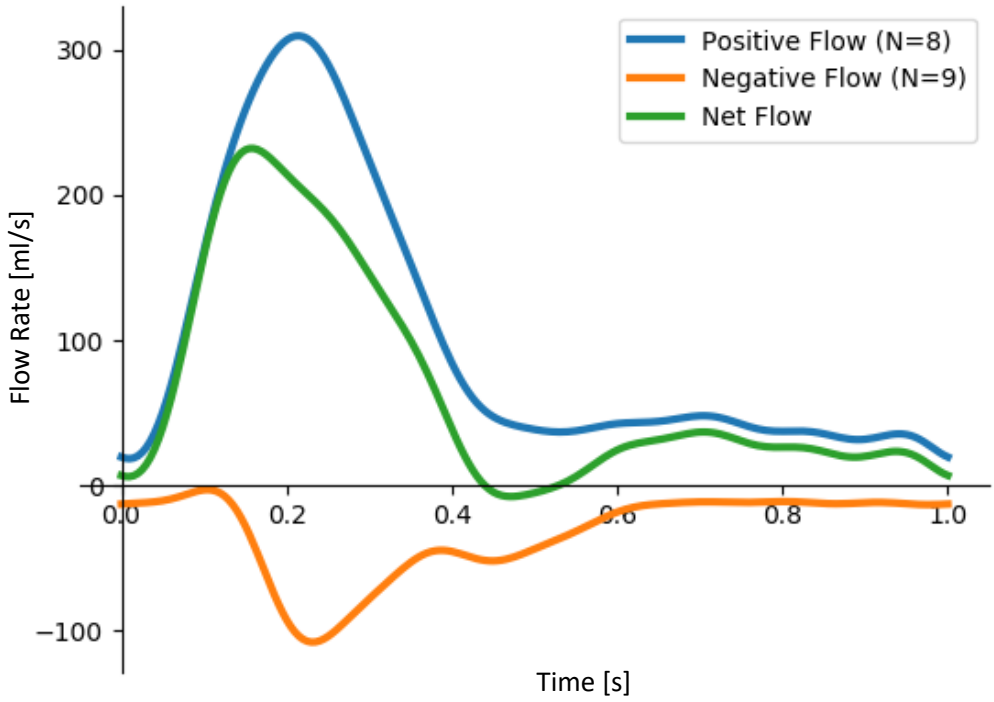

Figure 3-7: Fourier Reconstruction and Scaling Barker et al. Flow Rate waveform [73].

In this work, we decided to only take the ***net flow rates*** as reference.

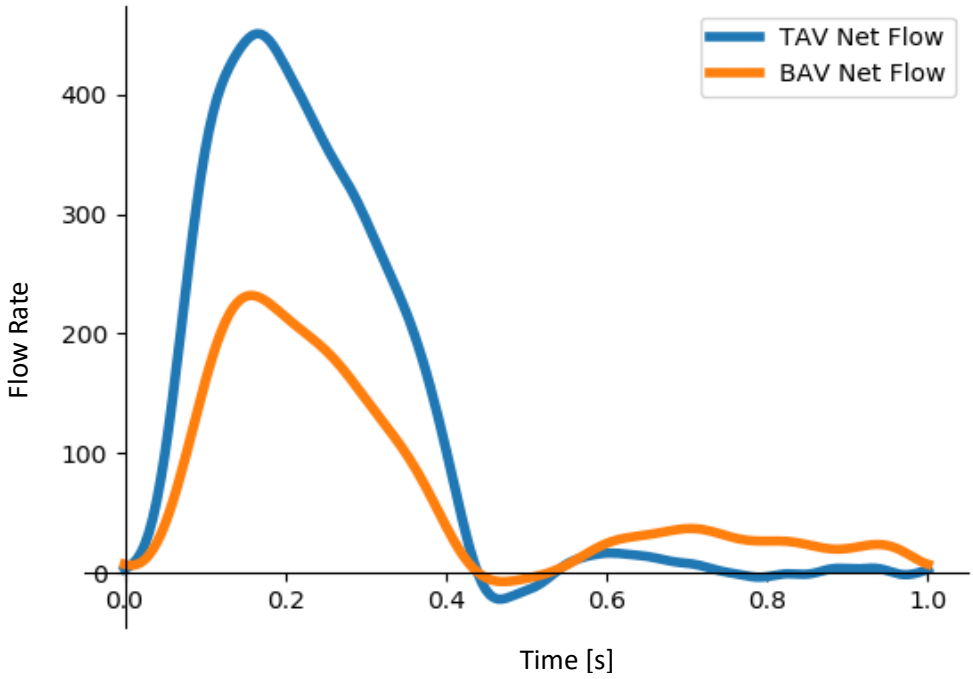

Figure 3-8: TAV and BAV Net flow rate.

In order to make the study uniform focusing the dependency of the results only on velocity shape and so improve following comparisons and considerations. Programing a *Python* script, ***same TAV waveform*** is imposed in all cases and the BAV has been adequately modulated so as to obtain the ***same Reynolds number*** in both shapes.

The *Reynolds numbers* are calculated respectively as:

$$Reynolds_{\ TAV} = \frac{\rho}{\mu} \cdot \overline{velocity_{TAV}} \cdot D_{h-TAV}$$

$$Reynolds_{\ BAV} = \frac{\rho}{\mu} \cdot \overline{velocity_{BAV}} \cdot D_{h-BAV}$$

where *density* and *viscosity* are all the same:

- $\rho = 1.06\ \frac{g}{cm^3}$
- $\mu = 0.04\ poise$

Velocity [cm/s] and *characteristic length [cm]* are calculated as:

$$velocity_{\ TAV} = \frac{flow_{\ TAV}}{Area_{\ TAV}} \qquad velocity_{\ BAV} = \frac{flow_{\ BAV}}{Area_{\ BAV}}$$

$$D_{\ h-TAV} = \frac{Area_{\ TAV}}{perimeter_{\ TAV}} \cdot 4 \qquad D_{\ h-BAV} = \frac{Area_{\ BAV}}{perimeter_{\ BAV}} \cdot 4$$

Now, we have all parameters to compute the mean value of BAV velocity imposing the hypothesis of have $\boldsymbol{Reynolds}_{\boldsymbol{TAV}} = \boldsymbol{Reynolds}_{\boldsymbol{BAV}}$:

$$\overline{velocity\ (Re)_{BAV}} = \frac{D_{\ h-TAV}}{D_{\ h-BAV}} \cdot \overline{velocity_{TAV}}$$

The last step is to scale the flow rate with Reynolds, which will be used to scale the velocity profile.

$$Flow_{\ BAV(Re)} = velocity(Re)_{\ BAV} \cdot Area_{\ BAV}$$

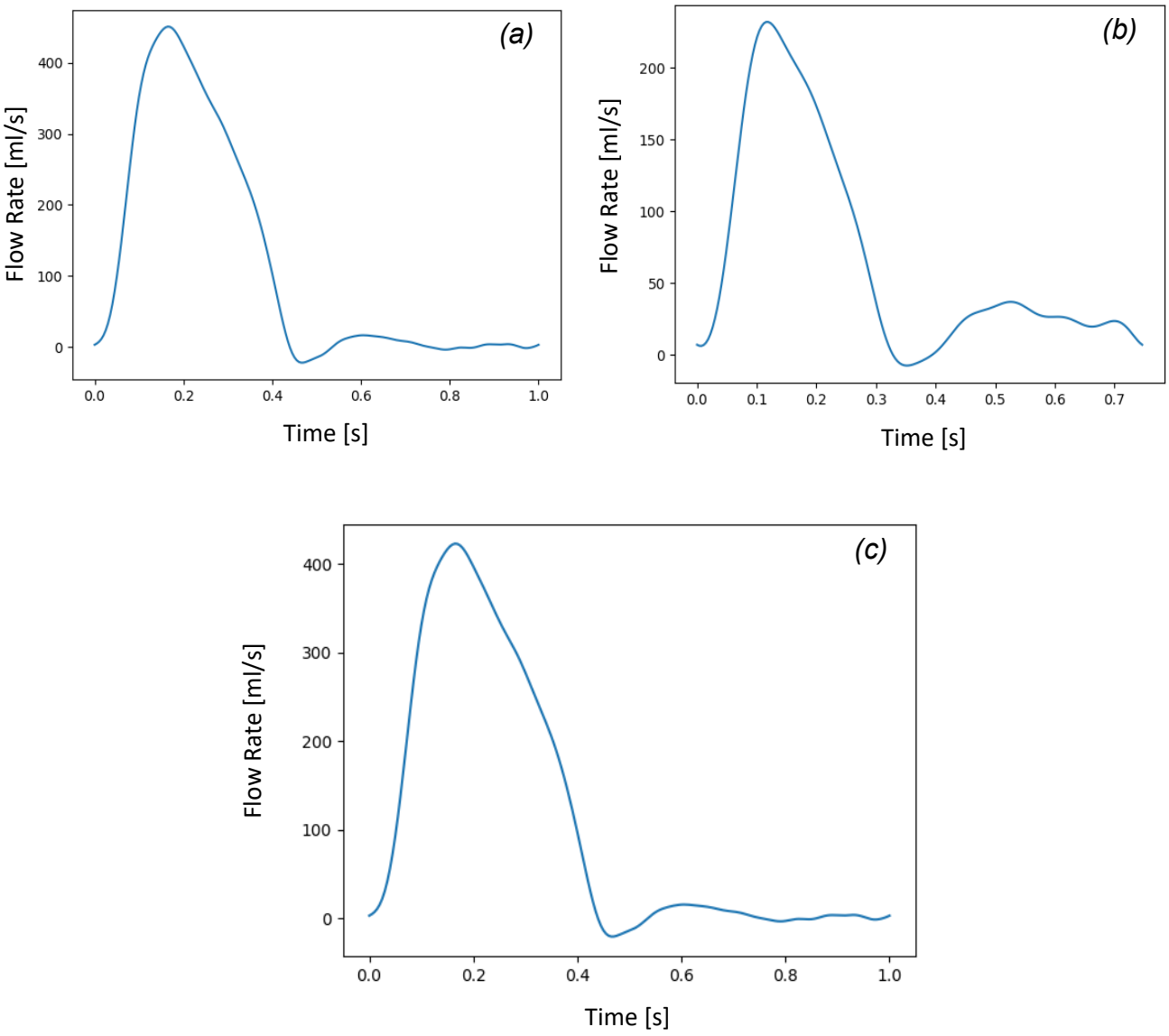

Figure 3-9: (a) TAV flow rate with Reynolds = 1406.11; (b) BAV flow rate with Reynolds = 866.39; (c) Wave form TAV scaled with Reynols BAV.

Before to compute the actual modified velocities, we need to pay more attention to the initial conditions of study that determined the resulting velocity profile, used in our work as starting idea.

Cao et al. declare that their 3D reconstruction if obtain evaluating the hemodynamic velocity behavior at a level little upper than the sinus position. Therefore, at this stage where the mechanical effect, due to opening and closing valve movements, are negligible and the flow has already undergone changes. The flow reverses its direction by hitting against the aortic wall, thus creating a forward zone and a backward zone on inlet surface.

Now, we must consider that we are adapting a piece of Cao's work in our study and the general conditions are obviously different. Above all evaluating the position where velocity profiles are imposed, because our mimed shapes are set on our inlet surface, placed under the sinus bulges, where supposing an only forward and eccentric flow is more predictable.

In view of aforementioned reflections, we decided to perform two strategies about velocity profile modulation, which means mimic a first group of 3D shapes having only the forward profile and a second group of 3D shapes complete with forward and backward profiles. So that we can make a further comparison on the incidence of the presence or absence of backward flow.

3.2.3.1 Velocity Modulation

First strategy is to have a profile with ***only the forward flow***. We computed the velocity on each *i-th* point of the surface, as formulation of the *Generalized Poiseuille through-plane,* mentioned above. Then, those values have been normalized on their mean value and discriminating them according to their sign, we decide to assign ***0*** or the ***correct velocity value resized***, in order to have one of the two surfaces with the forward shape and the other without.

$$velocity(Re)_{BAV\_i} = \begin{cases} 0, & i < 0 \\ vel_{BOUNDARY}, & i = 0 \\ vel = \dfrac{v_{tp}}{\overline{v_{tp}}} \cdot \overline{velocity\ (Re)_{BAV}}, & i > 0 \end{cases}$$

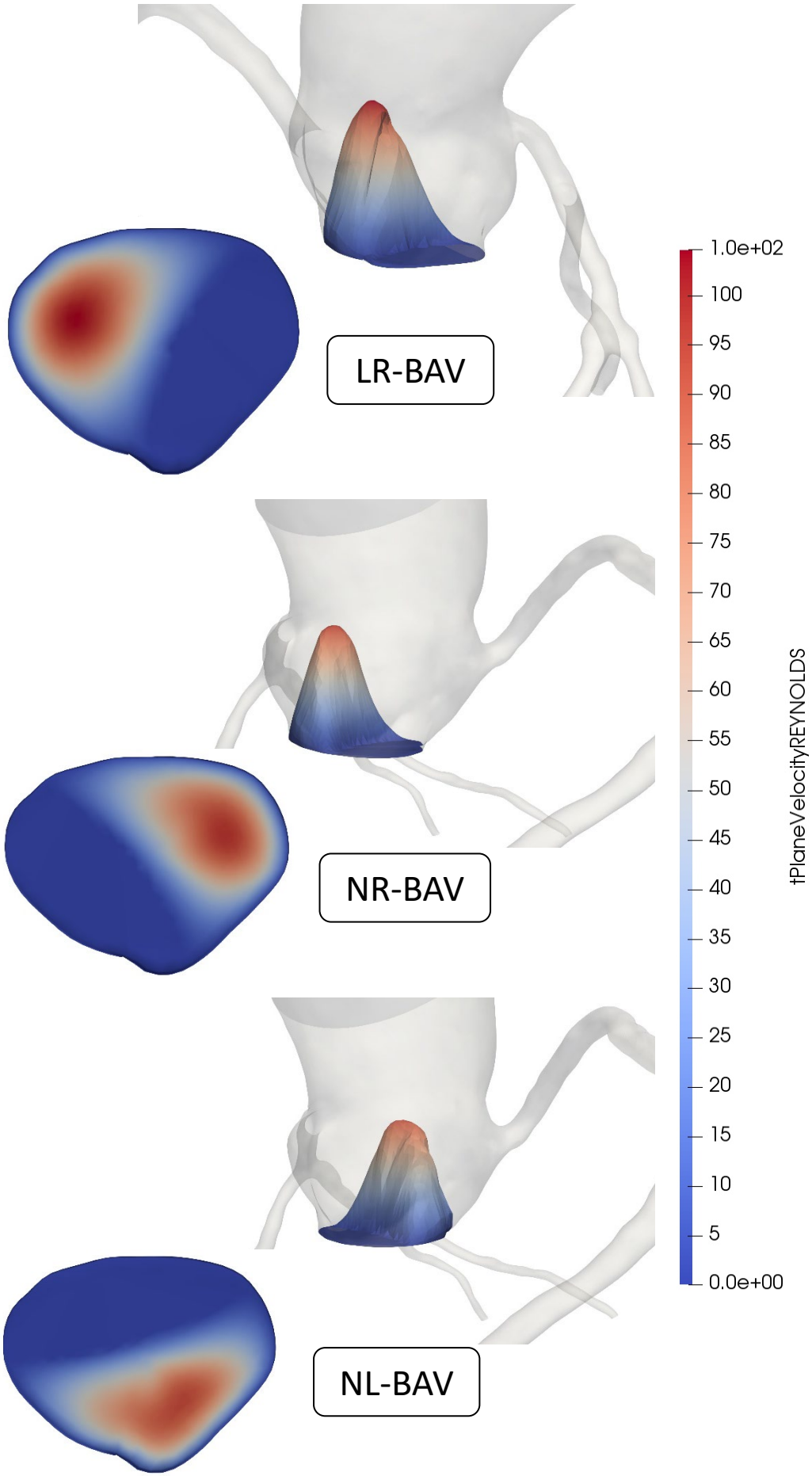

Figure 3-10: (a) NC-sinus velocity profile; (b) LEFT-sinus velocity profile; (c) RIGHT-sinus velocity profile.

3.3 STEADY-STATE CFD SIMULATIONS

To quantitatively evaluate the results and understand how this pathology influences coronary hemodynamics, appropriated ***steady flow simulations*** has been performed in *SimVascular,* one for the TAV case and three for the BAV cases.

It is important to remember that the same simulation setting must be done for each clinical study in question, because the results must be comparable to each other.

3.3.1 Boundary Conditions

TAV inlet boundary condition prescribed at the aorta face is set as a generic ***parabolic Poiseuille*** profile with an inflow waveform imposed by an ad hoc ***.flow*** file created in a previous moment. The flow rate has a mean cardiac output value of $\boldsymbol{Q = -115.16\ \frac{ml}{s}}$ (note the *negative sign* before the value due to underline that the flow is in forward direction to aorta) and a total heart period of 1 s. The SimVascular file, necessary to impose a correct steady inflow waveform in steady simulation, is written in the following format:

Time	***Flow Rate***
0.0	-115.16417705
1.0	-115.16417705

BAVs inlet boundary conditions are prescribed by a ***bct.dat*** file, that it has been replaced instead of the original before to run the simulation. The .dat file, in steady simulation, is written using the following format:

np	nl			
x1	y1	z1	nl	nn(x1)
Vx(x1)_1	vy(x1)_1	vz(x1)_1	t_1	
.	.	.	.	
.	.	.	.	
.	.	.	.	
vx(x1)_nl	vy(x1)_nl	vz(x1)_nl	t_nl	
.	.	.	.	
.	.	.	.	
.	.	.	.	
xnp	ynp	znp	nl	nn(xnp)
vx(xnp)_1	vy(xnp)_1	vz(xnp)_1	t_1	
.	.	.	.	
.	.	.	.	
.	.	.	.	
vx(xnp)_nl	vy(xnp)_nl	vz(xnp)_nl	t_nl	

- **np** = number of surface point (*spatial definition*)
- **nl** = point number of time instants for each position (*temporal definition*).
- **x, y, z** = *spatial coordinates* along x, y, and z-directions (for each np point on the surface)
- **nn** = *global node ID* (for each *np* point)
- **vx, vy, vz** = *velocity values* along x, y, and z-directions a time **t**.

"*Point Number*" and "*Fourier Modes*" values have to be set, in steady condition, to *2* and *1* respectively.

About the "***Basic Parameters***", we consider the blood as a ***Newtonian incompressible*** fluid for all simulations, so the parameters chosen are:

- Fluid *Density* (ρ_{blood}) $= 1.06\ \frac{g}{cm^3}$
- Fluid *Viscosity* (μ_{blood}) $= 0.04\ Poise$
- Initial *Pressure* $= 0.0\ \frac{dynes}{cm^2}$
- Initial *Velocities* $= 0.0001\ 0.0001\ 0.0001\ \frac{cm}{s}$

About the ***outlet boundary condition***, a lumped parameter model completely ***resistive*** has been adopted, so all outlet caps are set as "*Resistance*".

The ***average pressure*** is calculated adopting as reference a standard health patient, with systolic and diastolic blood pressure of *120 mmHg* and *80 mmHg* respectively ($1\ mmHg = 1333.2\ \frac{dynes}{cm^2}$).

$$P_{MEAN} = \frac{1}{3} \cdot P_{SYSTOLIC} + \frac{2}{3} \cdot P_{DIASTOLIC} = 93.33\ mmHg = \mathbf{124433.87}\ \boldsymbol{\frac{dynes}{cm^2}}$$

The ***total resistance***, which corresponds to aorta resistance, is calculated as the ratio between the mean pressure value and the volumetric flow rate:

$$R_{TOT} = R_{AORTA} = \frac{P_{MEAN}}{Q} = \mathbf{1080.49}\ \boldsymbol{\frac{dynes \cdot s}{cm^5}}$$

As already said about the coronary circulation, many studies have estimated that the portion of blood flowing through coronary arteries is around the *4-5%* of the aortic flow. This can be translated in terms of ***total coronary resistance*** as:

$$R_{CORONARY-TOT} = 24 \cdot R_{TOT} = 24 \cdot \frac{P_{MEAN}}{Q} = \mathbf{25931.79}\ \boldsymbol{\frac{dynes \cdot s}{cm^5}}$$

The automatic process of splitting and calculating of the coronary resistances is computed imposing the ***Murray's Law Coefficient.*** Murray theorizes a criterion that explain the relationship between the diameter of the daughter vessels and their respectively original vessels [74]. The equivalent resistance of each branch is mathematically estimated to be proportional to the flow through it, starting from the total coronary resistance and splitting it on the ratio of radius raised to an exponential value [67]:

$$\mathrm{R}_{\mathrm{CORONARY_i}} = \frac{\sum_j \sqrt{\mathrm{A}_j}^{\mathrm{x}}}{\sqrt{\mathrm{A}_j}^{\mathrm{x}}} \cdot \mathrm{R}_{\mathrm{CORONARY-TOT}}$$

There are many discussions in literature about the most adequate power value, it is generally possible to say that this value ranges between 2 (in larger arteries) and 3 (in arterioles) [75]. In this simulation we decided to adopt the value **2.6**, which is the default value recommended by SimVascular references [74]. The resulting resistances associated to each coronary branch outlet are:

Coronary Outlet	*Resistance*
LCA_1	229163
LCA_2	238458
LCA_3	67934
RCA_1	204600
RCA_2	96175.6

Table 8: Resistences of outlet BCs.

The wall of the blood vessels is modelled assuming the ***no-slip condition*** and ***rigid wall***, so the last boundary condition to set is the "*Wall Properties*" as *Rigid*.

3.3.2 Solver Parameters

SimVascular flow solver gives the possibility to modify many parameters. Below, are only the essential ones to be set manually, while the other advanced options remain unchanged.

- *Number of Timesteps = 500*
- *Time Step Size = 0.002*
- *Number of Timesteps between Restarts = 10*
- *Step Construction = 5*
- *Residual Criteria = 0.0001*
- *Time Integration Rule = First Order*

4. HEAMODYNAMICS DESCRIPTORS

After a CFD simulation, a huge amount of data, which contain all the phenomena that take place in the model, are extractable during the post-processing. For this reason, a lot of hemodynamic descriptors has been proposed over the years, to look for synthesizing the mechanics information. It clear that aggravated flow events lead to abnormal biological events that can evolve into changes in the function and health of vessels. These indicators have been introduced to put in relation cause and effect. They are intended to reduce the complexity of four-dimensional fluid field and to help to perform a quantitative hemodynamic analysis on the wall surface or in the bulk flow [76].

In this work the *hemodynamic quantities* and *hemodynamic descriptors* used to analyze results are:

- ***Flow***
- ***Pressure***
- ***Velocity***
- ***Vorticity***
- ***WSS***
- ***LNH***
- ***Helicity Descriptors***

4.1 WSS

In hemodynamic field, the fluid forces acting on the vessels wall play a key role in inhibition or promoting process of pathological event [76]. Several studies suggest how a shear flow with indeterminate path influence the vessel tissue to response with abnormal signal transduction, gene expression, unfavorable structure changes and nonstandard function [84,85].

The ***Wall Shear Stress*** (***WSS***) is probably the main and the most used descriptor over years. For Newtonian fluid, the Wall Shear Stress is given by the formulation:

$$\tau_w = \mu \cdot \left(\frac{\partial u}{\partial y}\right)_{y=0}$$

Where μ is the dynamic viscosity, u is the velocity parallel to the wall and y is the distance to the wall.

The WSS is a vector whose magnitude is equal to the viscous stress on the surface and whose direction is the direction of the viscous stress acting on the surface [79]. It was demonstrated that is fundamental to ensure the normal circulation and that a its variations are always associated to a local disturbed flow. In details, vessel districts showing ***low*** and ***oscillating WSS*** with the resultant stagnation of blood may commonly be the first candidates to be influenced by the initial phenomena of CAD [32].

4.2 HELICITY AND LNH

Wall descriptors were the first to be widely used but forced us to reduce the analysis to 2D field. Recently, the need to consider the greater hemodynamic complexity of the flow and to expand the analysis to volume domain, has led to the introduction of bulk flow descriptors to evaluate the significant role played by complex helical / vortical schemes [5].

Helicity gives measure of alignment of velocity and vorticity and its value can be related to energy dissipation, because of its role in the transfer and Redistribution processes of energy through dissipative scales [5].

The ***density of kinetic helicity*** (***H_k***) is defined as the internal product between *velocity* (v) and *vorticity* (w):

$$w(s,t) = \nabla \times v(s,t)$$

$$H_k(s,t) = v(s,t) \cdot w(s,t)$$

A useful indicator of how velocity field is oriented with respect to the vorticity field is given by the local value of the cosine of the angle between the velocity and vorticity vectors, obtained through the ***local normalized helicity*** (***LNH***) [76]:

$$LNH = \frac{v(s,t) \cdot w(s,t)}{|v(s,t)| \cdot |w(s,t)|} = \cos \varphi(s,t)$$

LNH shows a high potentiality because it has a finite range between **1** and **-1**, the meaning is:

- $LNH = 0 \rightarrow H_k = 0 \rightarrow v \perp w$ (typical value associated with the Poiseuille flow)
- $LNH = 1 \rightarrow H_k = max \rightarrow v \parallel w$ (typical value associated with purely helical flow)
- $LNH = -1 \rightarrow H_k = min \rightarrow v \parallel w$ (opposite direction of rotation)

Note that *rotation versus* is established according to the model's point of view.

Figure 4-1: LNH visualization, angle between velocity and vorticity[5].

4.3 HELICITY DESCRIPTORS

Recently, some *helicity-based descriptors* have also been applied to characterize bulk flow according to a Eulerian approach [79]. Now, we present their formulation, considering in our constant field of study, without time integration and average over the period.

The descriptor $\mathbf{h_1}$ is the averaged *value of the helicity* in the volume of interest, normalized with respect to the volume itself [76].

- $h_1 = 0$: symmetric counter-rotating helical structures
- $h_1 \neq 0$: information about the predominant direction of rotation

$$h_1 = \frac{1}{V} \int_V H_k \; dV \; dt$$

The descriptor $\mathbf{h_2}$ is the *intensity of the helicity*, irrespective of direction. [76].

$$h_2 = \frac{1}{V} \int_V |\, H_k| \; dV \; dt$$

The descriptor $\mathbf{h_3}$ describes the *major direction of rotation* [76].

- $h_3 = -1$: only left-handed helical structures
- $h_3 = 1$: only right-handed helical structures

$$h_3 = \frac{h_1}{h_2}$$

The descriptor $\mathbf{h_4}$ describes the *balance* between counter-rotating structures, neglecting what is the major direction of rotation [76].

$$h_4 = |h_3| = \frac{|h_1|}{h_2}$$

5. RESULTS and DISCUSSION

The simulations were performed on complete model, but the resulting data were interpolated for each point onto the same mesh without flow extensions. A specific *Python* script was run to extract results and then display them using *Excel* and *ParaView*.

5.1 FLOW AND PRESSURE

Flows are extracted from *SimVascular* and each output value is normalized respect to the input value*:*

step	***LCA_1***	***LCA_2***	***LCA_3***	***RCA_1***	***RCA_2***
TAV	0,432%	0,417%	1,47%	0,484%	1,02%
BAV-NC	0,432%	0,417%	1,47%	0,485%	1,02%
BAV-Left	0,432%	0,417%	1,47%	0,484%	1,02%
BAV-Right	0,432%	0,417%	1,47%	0,484%	1,02%

Table 9: Normalized flows on coronary outlets.

We calculate a relative measure of percentage of flow coming out from branches. Obtaining these values, a percentage difference analysis is performed and, having the same condition at the output boundary, resulting values are all 0. They suggest that there are ***no flow differences*** between BAVs and TAV cases. Thus, the same percentage of inlet flow, jet into the coronary arteries.

Pressure is analyzed plotting two histograms relative to LCA and RCA individually and then the histogram relative to total model (Figure 5-1). Then percentage differences are calculated and displayed as bar graph (Figure 5-2).

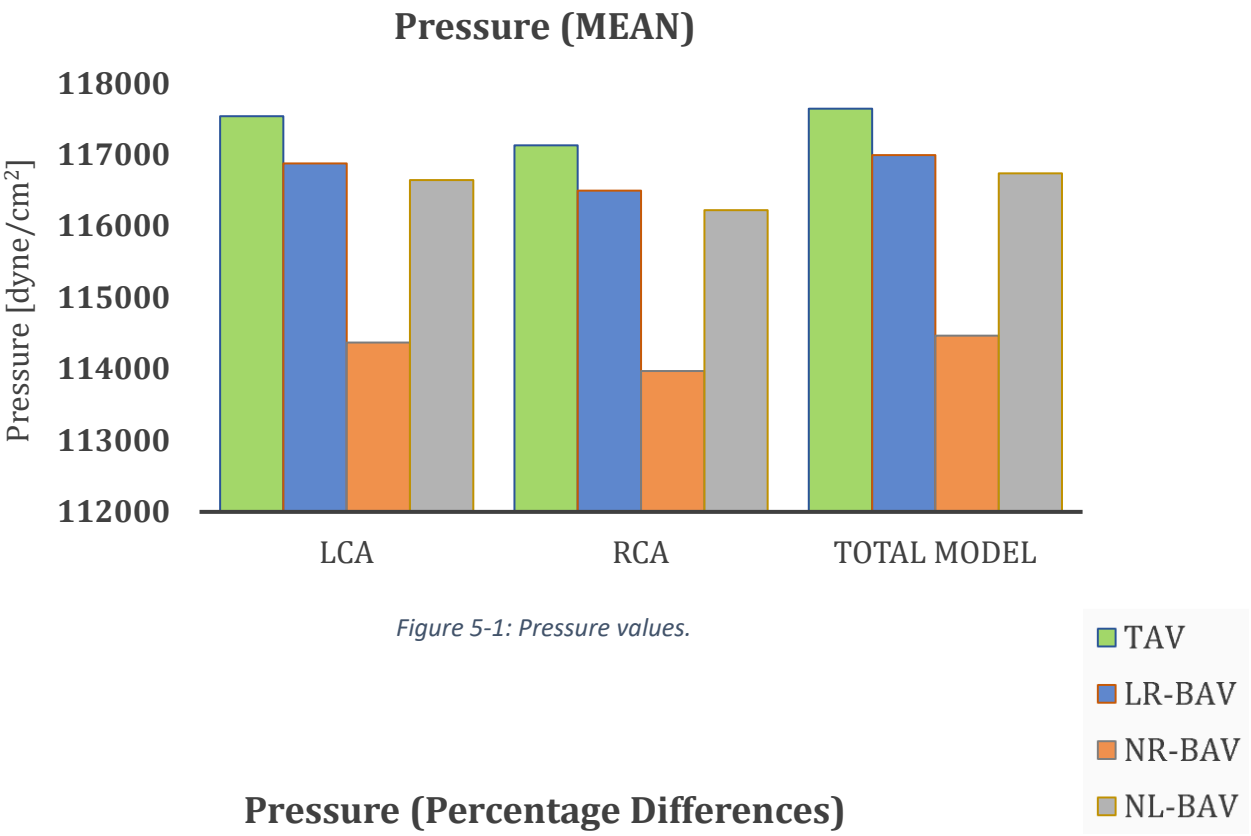

Figure 5-1: Pressure values.

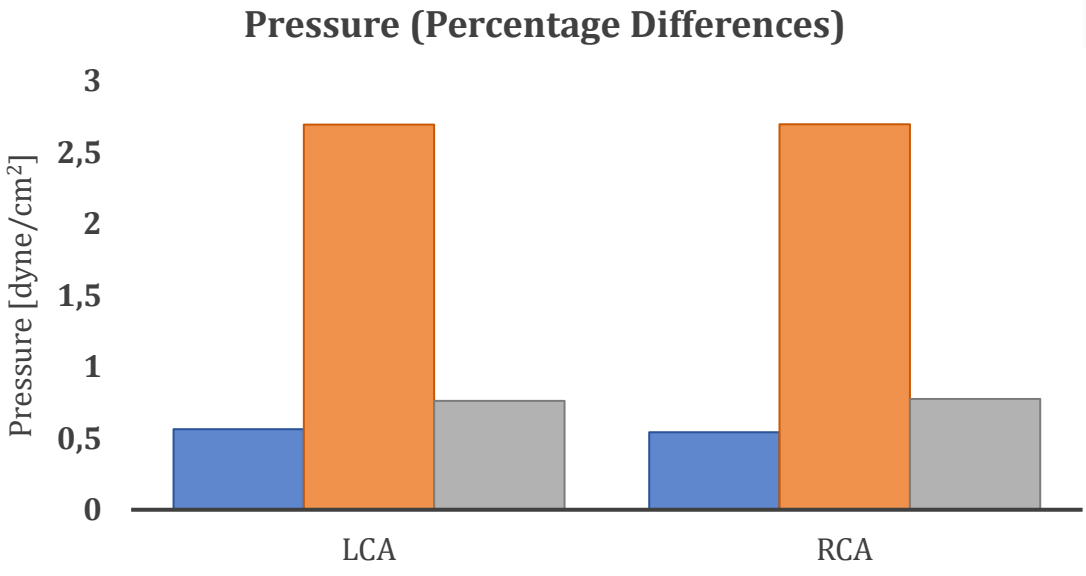

Figure 5-1: Mean of the percentage difference of pressures.

5.2 WSS

Surface averaged values of ***wall shear stress*** was extracted, and they are plotted in the bar diagram in Figure 5-3, where LCA, RCA and total model are compared for each different valve configuration. After that, percentage differences are computed both in term of surface averaged value and in term of punctual values, results are reported as histogram (Figure5-7) and colormaps (Figure5-4, 5-5, 5-6). Colormaps allow to see the spatial distribution of the wall descriptors, highlighting zones where differences are greater.

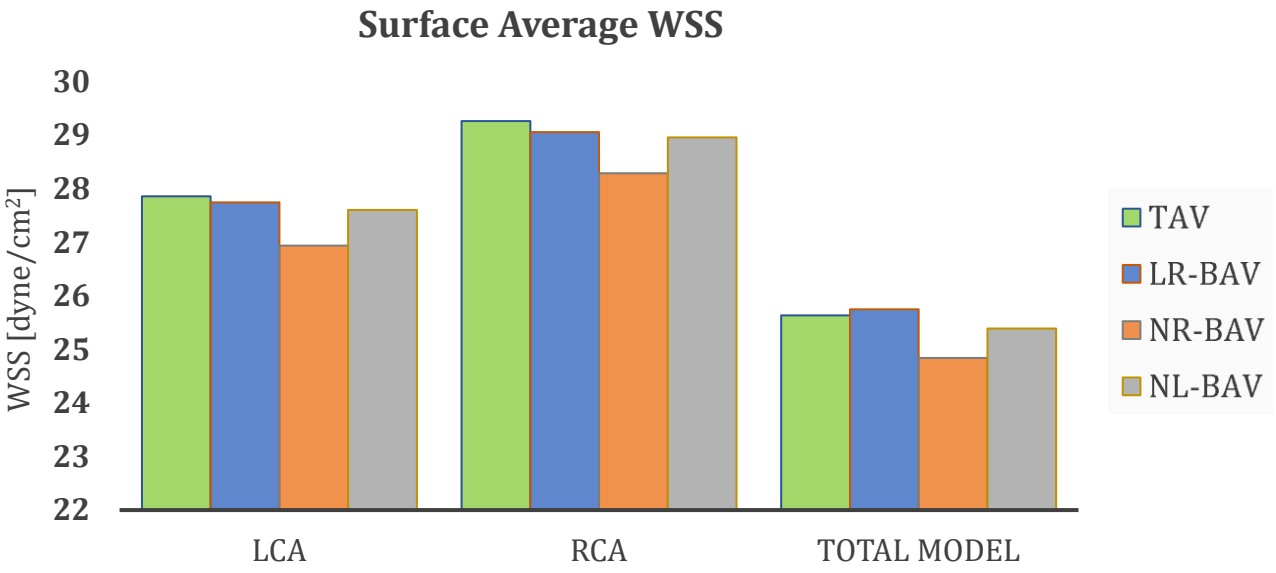

Figure 5-2: WSS mean values.

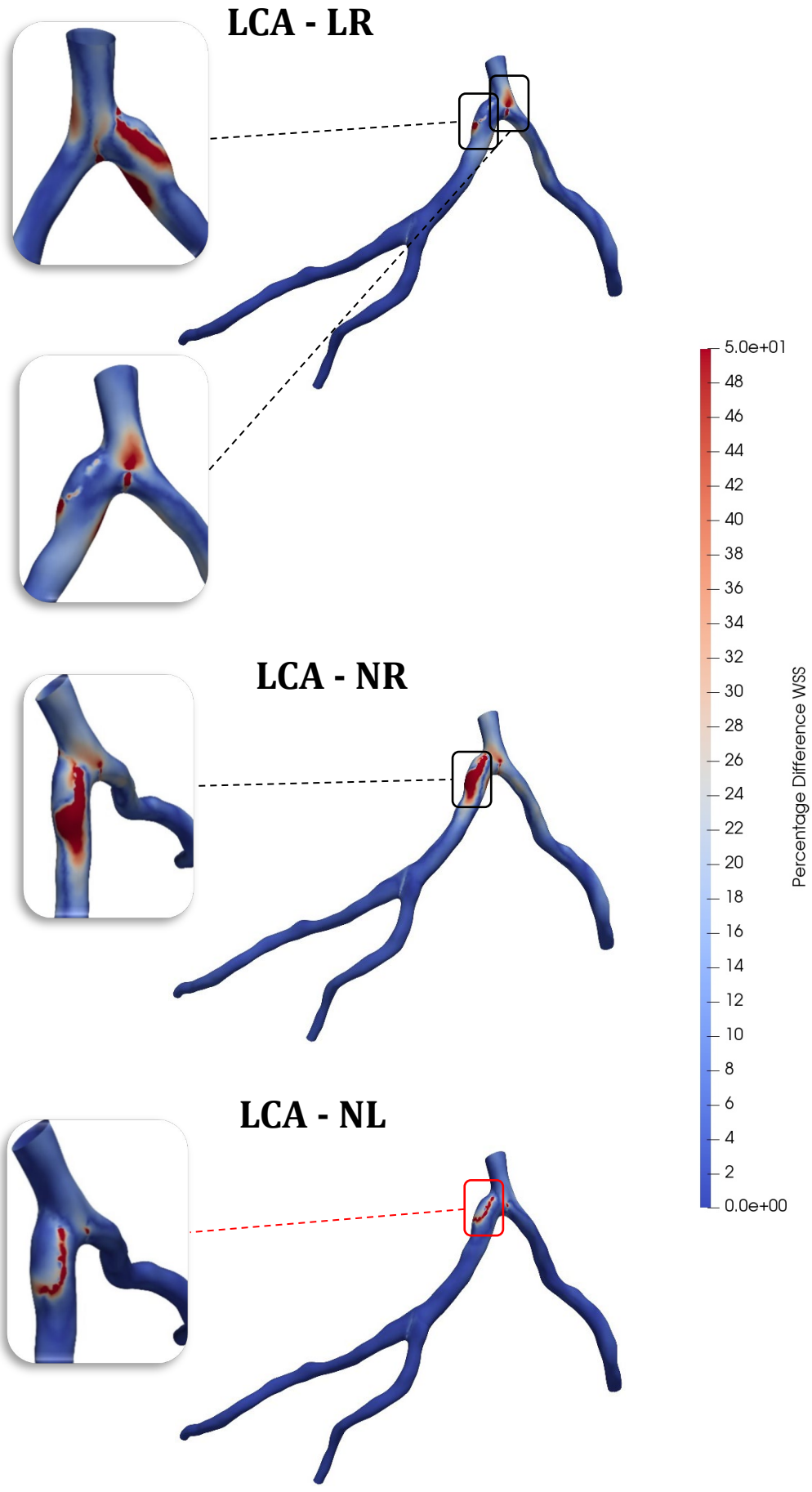

Figure 5-3: Colormaps of WSS percentage differences on left coronary arteries.

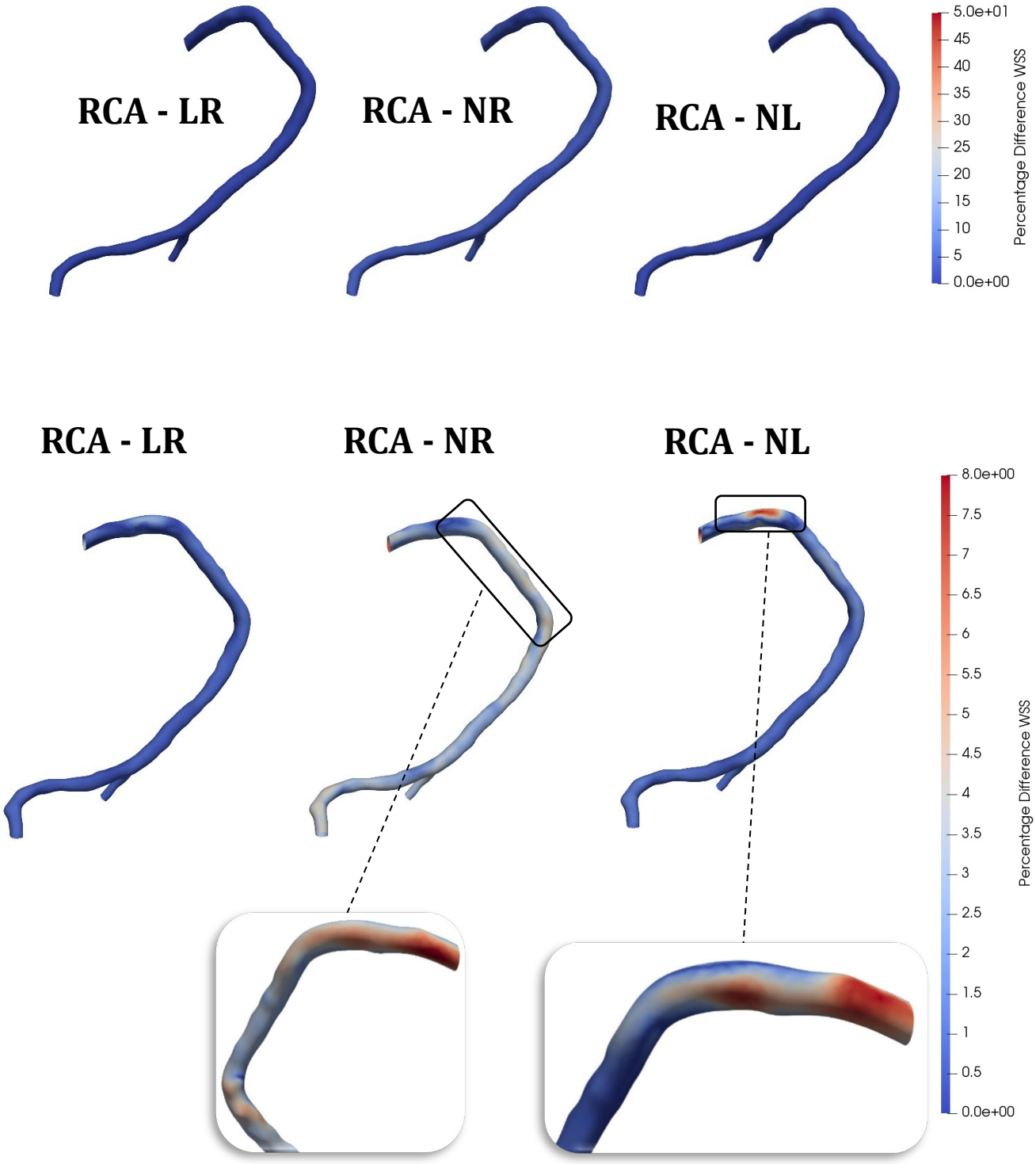

Figure 5-4: Colormaps of WSS percentage differences on right coronary arteries.

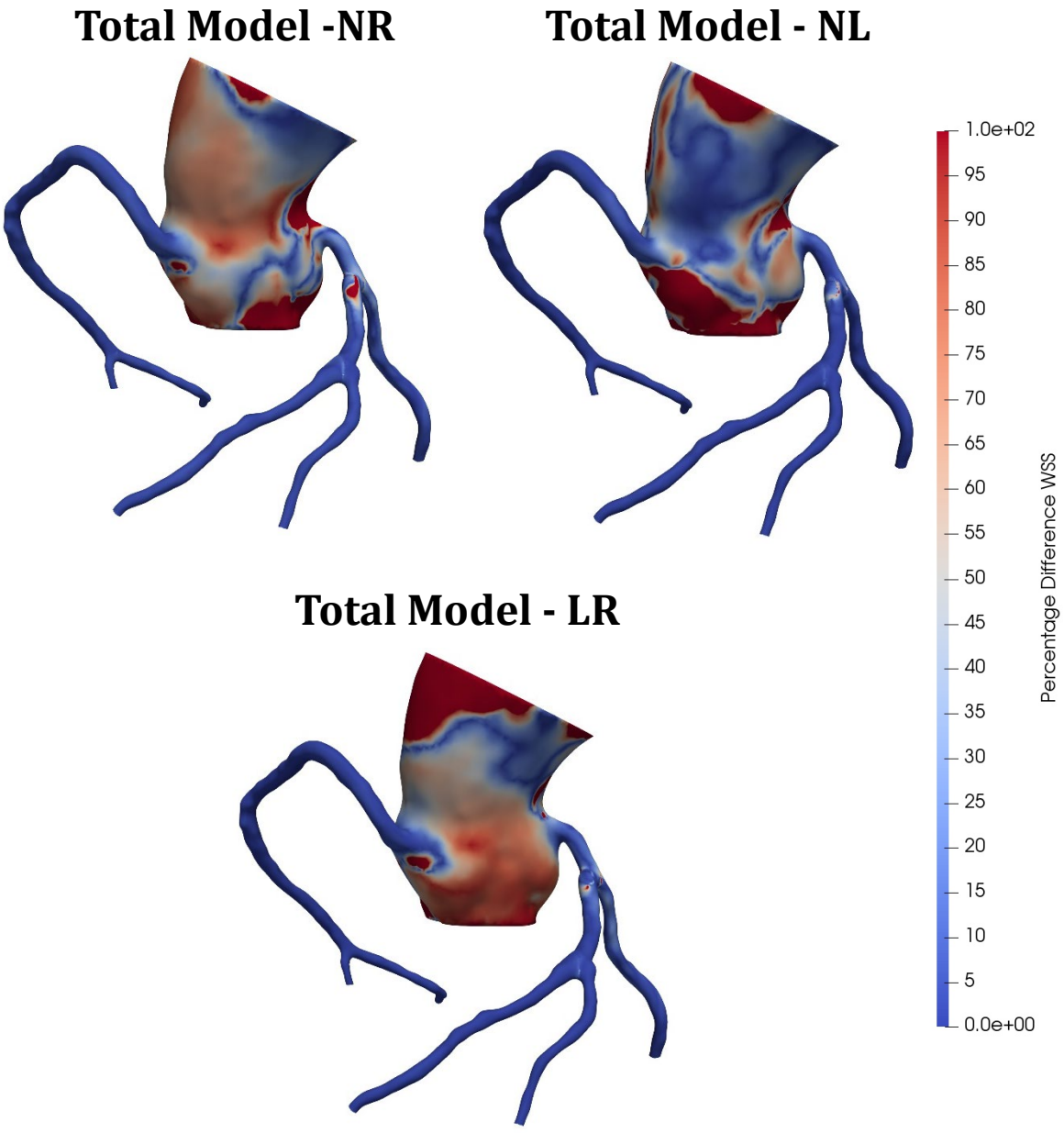

Figure 5-5: Colormaps of WSS percentage differences on total model.

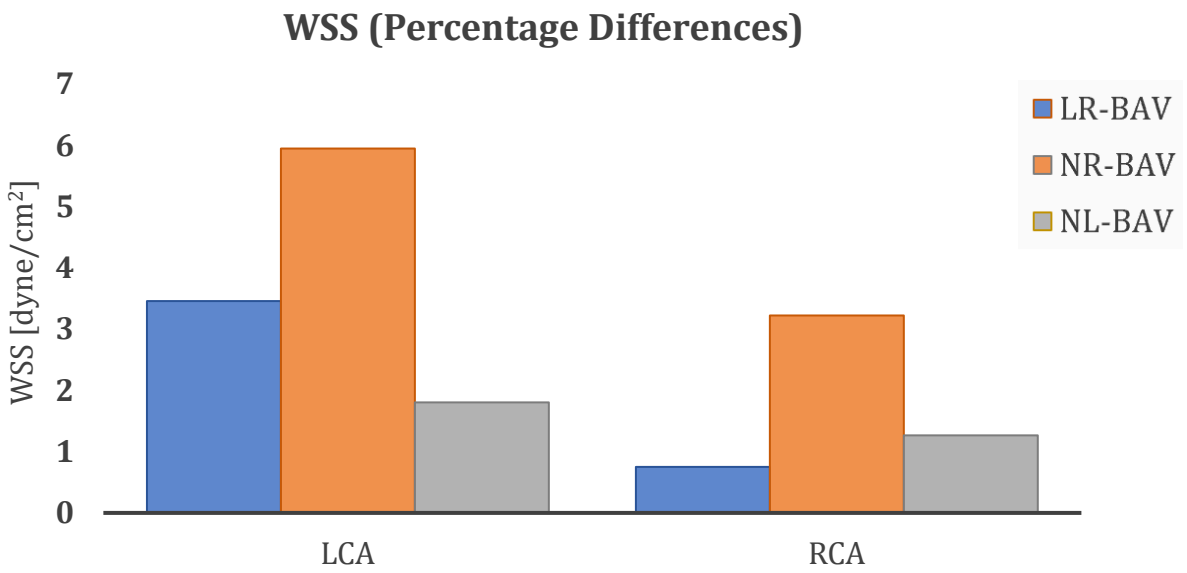

Figure 5-6: WSS percentage differences on coronary arteries.

These results indicate, as predictable, that the total model has the highest percentage differences (Figure 5-6). We note that the most stressed areas change consequently to the peak orientation of the imposed velocity profile. This zones generally are over the ostium and the crowning of the sinus. *LR-BAV* condition shows the highest difference (*26,7%*). About percentage differences in coronary arteries, we can affirm that: in RCA, percentage differences were found low in the whole model, so is possible to assert that WSS is almost equal to physiological reference case, and a maximum mean difference of 3,5% was found for the *NR-BAV* configuration; on the contrary, in LCA, WSS alterations were found focused in specific region, in correspondence of the bifurcation between left anterior descending and left circumflex coronary arteries with focal differences over 50%. Despite this global mean values remain still low with a maximum of 6% difference for the *NR-BAV* configuration (Figure 5-7). Furthermore, they ensure that coronary arteries do not undergo excessive modifications of WSS.

5.3 VELOCITY

Velocity mean values and relative percentage differences were computed and obtained values is reported in Figure 5-8. In addition to bar charts, streamlines and iso-surfaces corresponding to the ninetieth percentile (7% for LCA and 2% for RCA) were highlighted with adequate thresholds to improve the qualitative study about the areas with the highest differences.

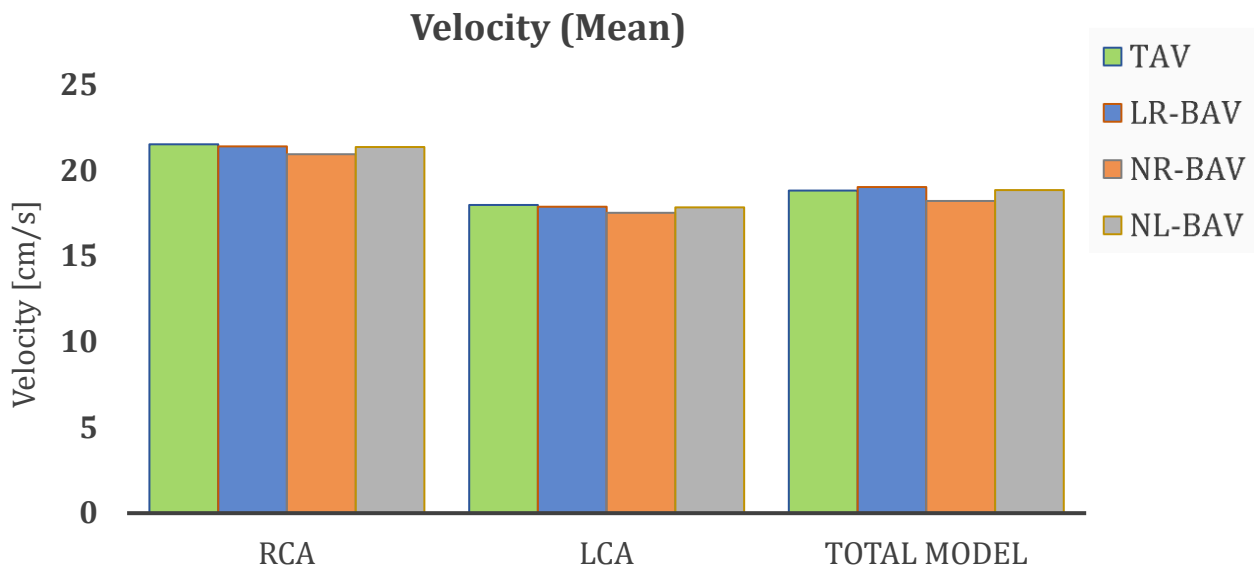

Figure 5-7: Velocity mean values.

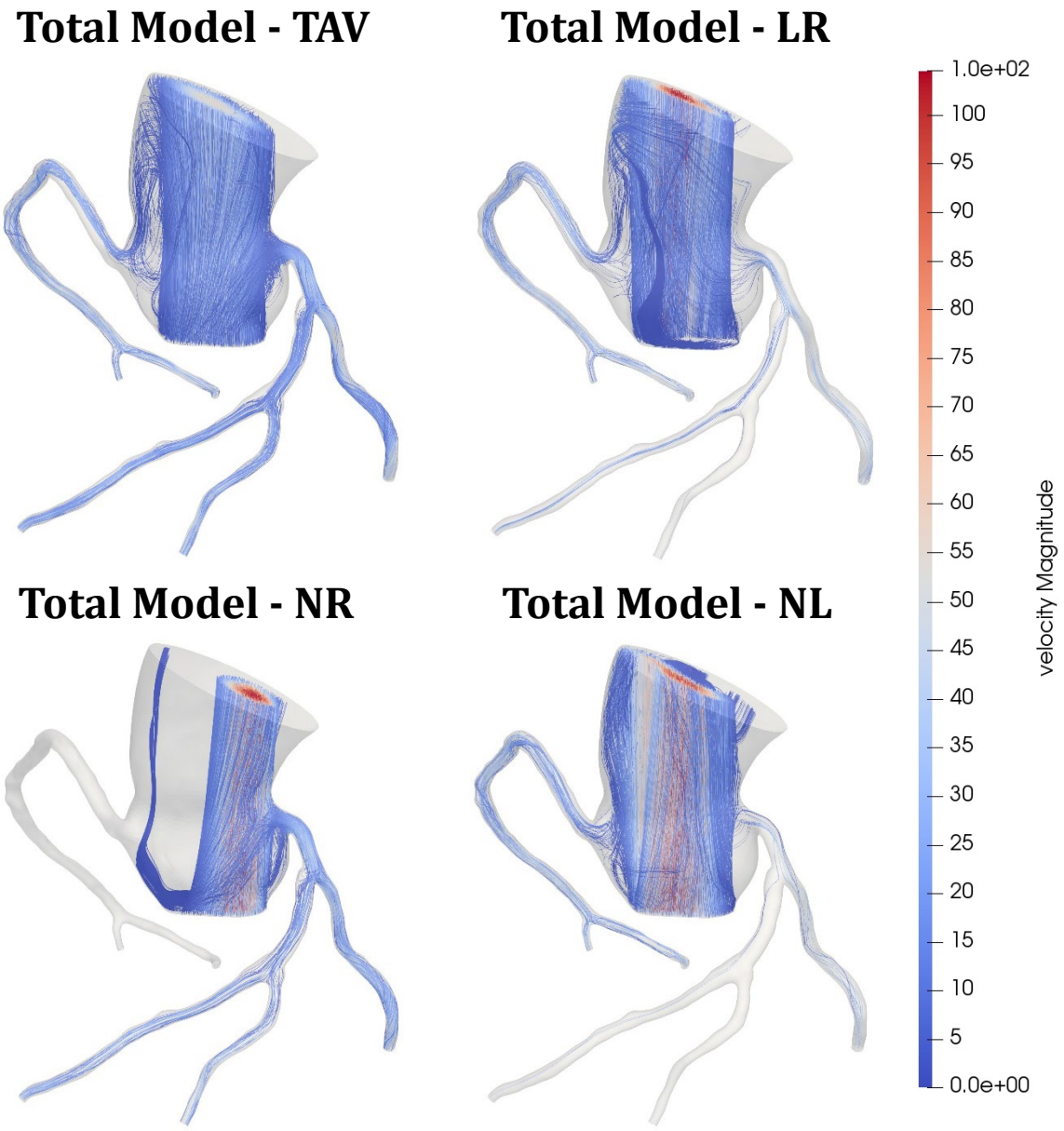

Figure 5-8: Velocity streamlines into total model.

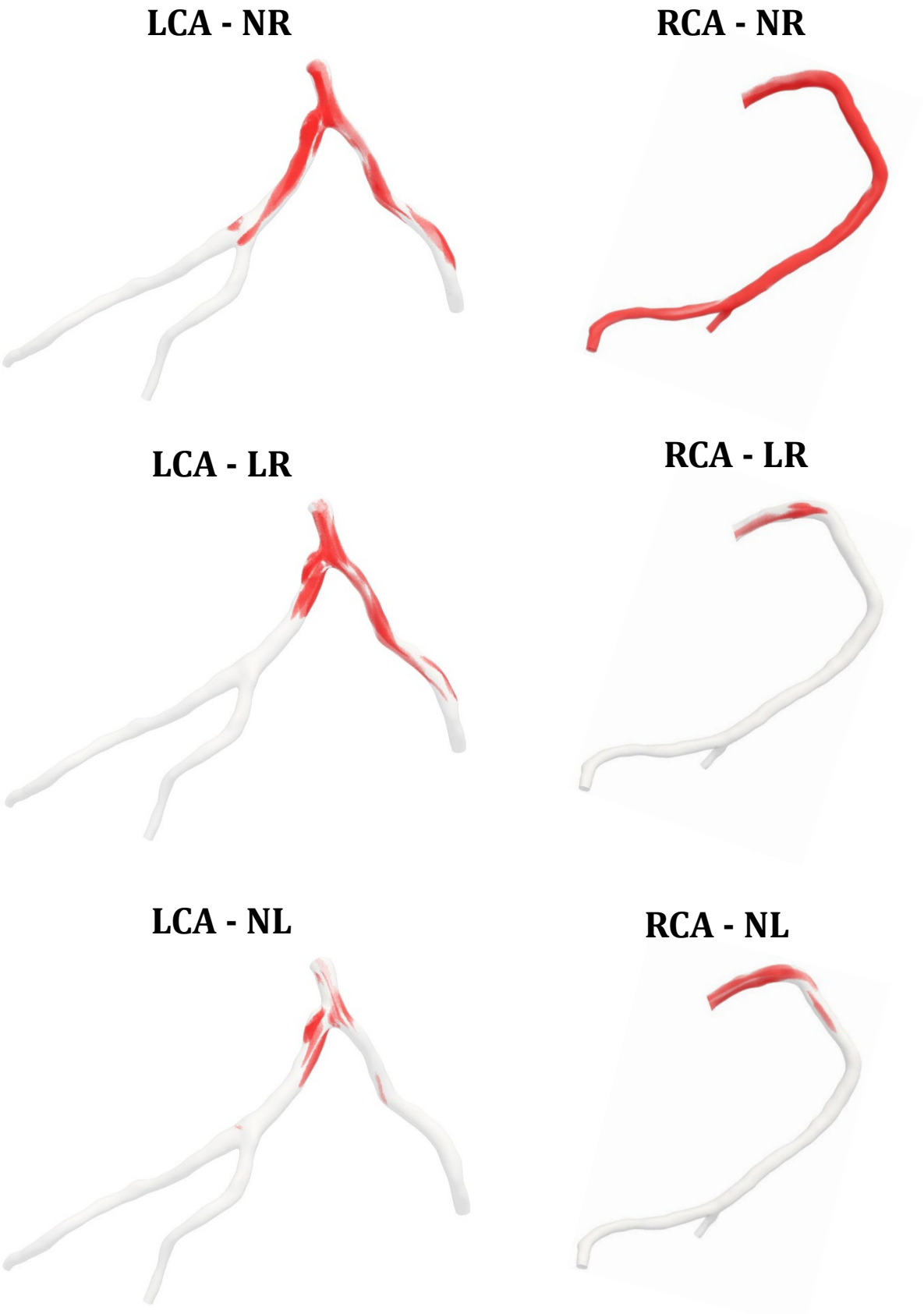

Figure 5-9: Velocity iso-surfaces (90th percentile) on left and right branches.

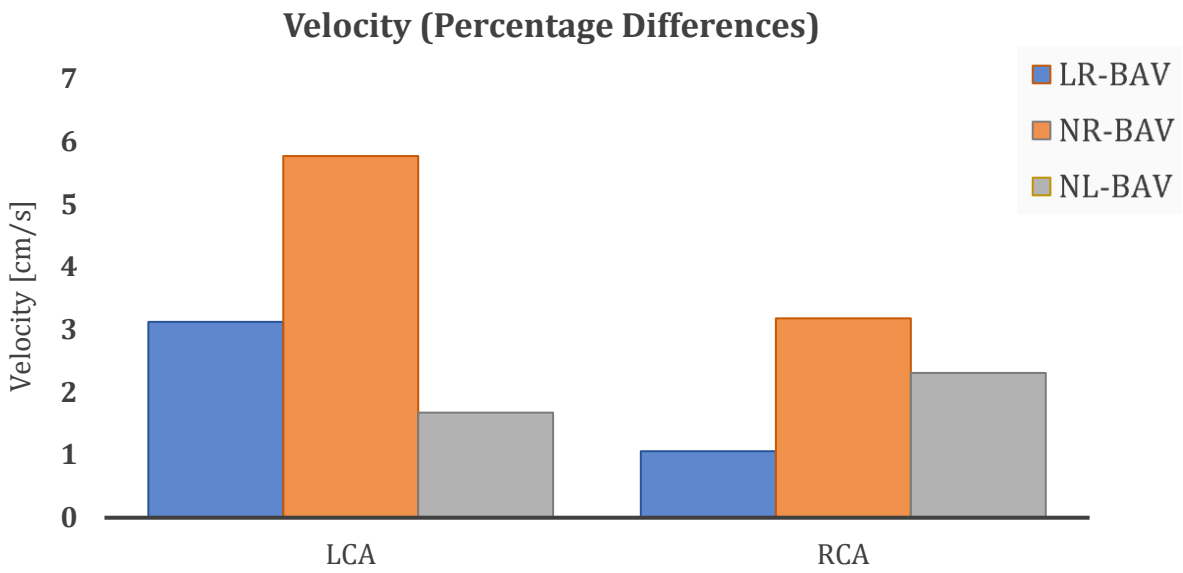

Figure 5-10: Velocity percentage differences on coronary arteries.

In this study we prescribe specific velocity profiles at inlet surface, three defined eccentric morphologies and one parabolic. Therefore, we expect that the different orientation of shapes influences each coronary in a different way. These results seem to confirm our expectations, because when the forward peak of velocity is eccentric toward a specific sinus, the velocity values in the coronaries, arising from that sinus, have higher different respect to the physiologic-like orientation. In coronary arteries, low values of percentage differences were found, in particular, less than *6%* in LCA for *NR-BAV* configuration and less than *3,5%* in RCA for *NR-BAV* configuration (Figure 5-11). From a qualitative point of view, iso-surfaces are useful to identify the regions more sensible to hemodynamic changes, diverging from the physiological case (Figure 5-10). Sites most influenced are the bifurcation zone and ostia. However, we can sustain that velocity behavior is approximately physiologic in both coronary arteries.

5.4 LNH AND HELICITY INDEXES

About helical blood flow patterns, they are examined and characterized in term of ***LNH*** and four ***helicity indexes***, investigating their mean values and their percentage differences. Bar charts and iso-surfaces are used to show results. Ninetieth percentile is equal to 43 for LCA and 10 for RCA models.

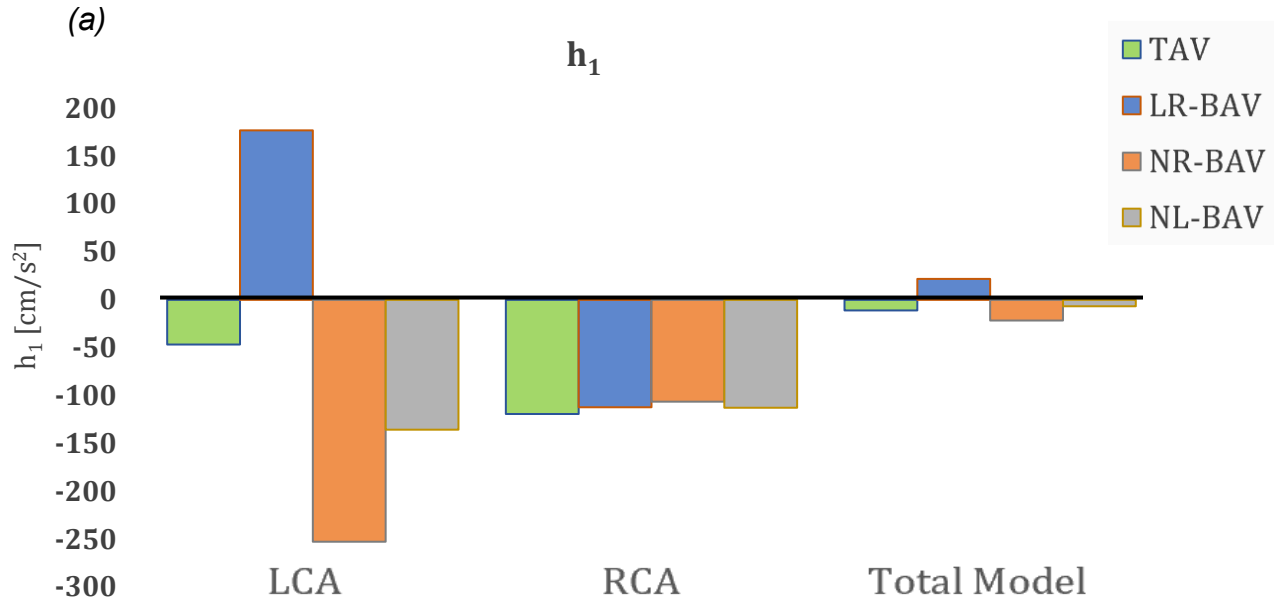

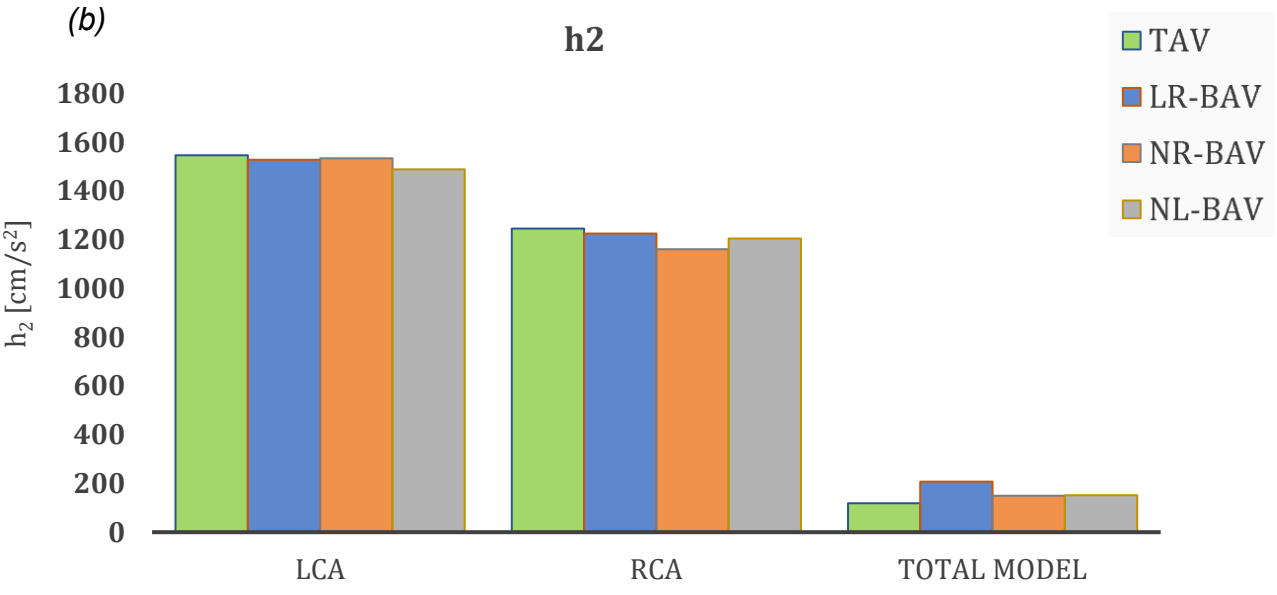

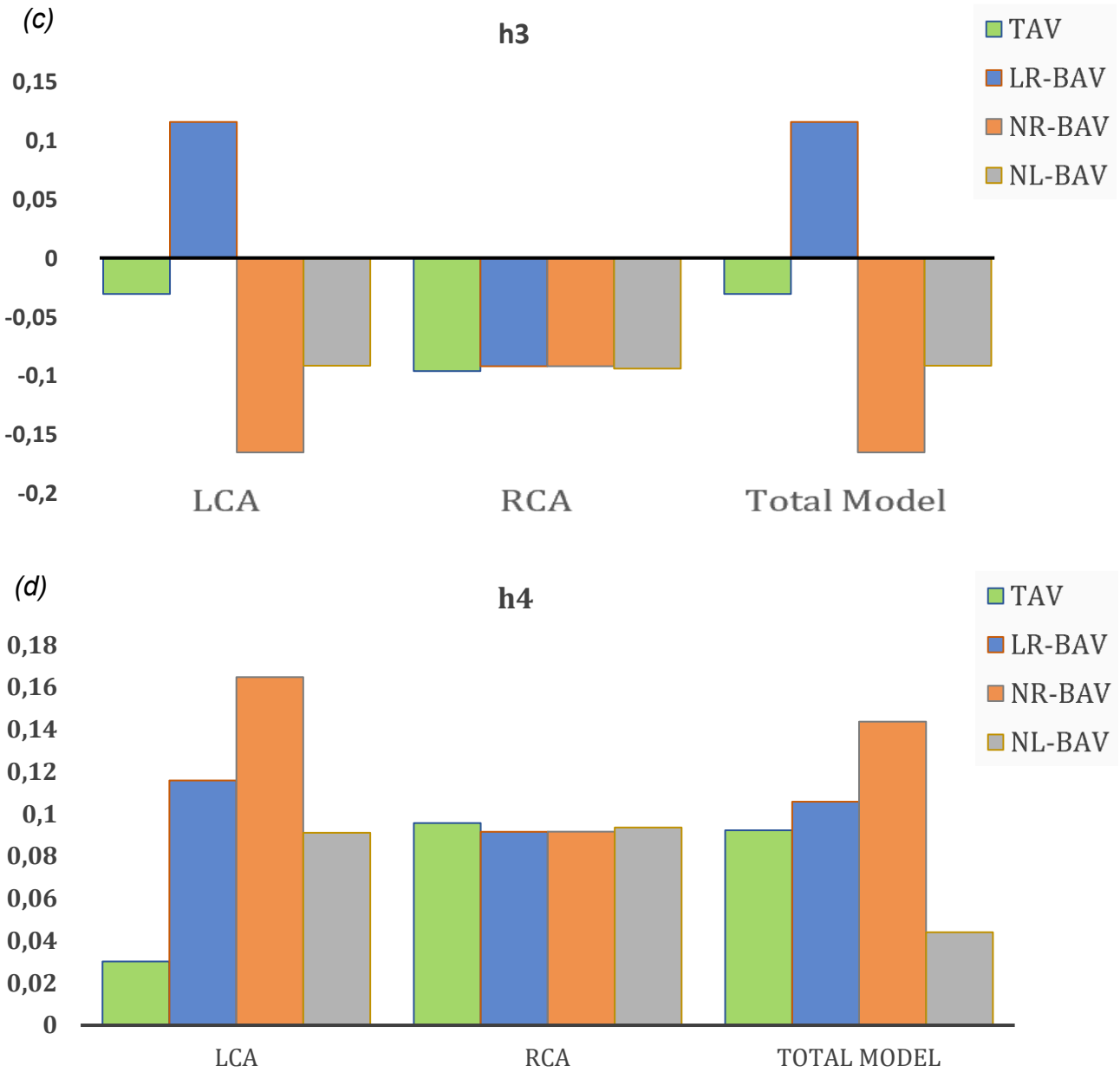

Figure 5-11: Helicity and helicity indexes mean values.

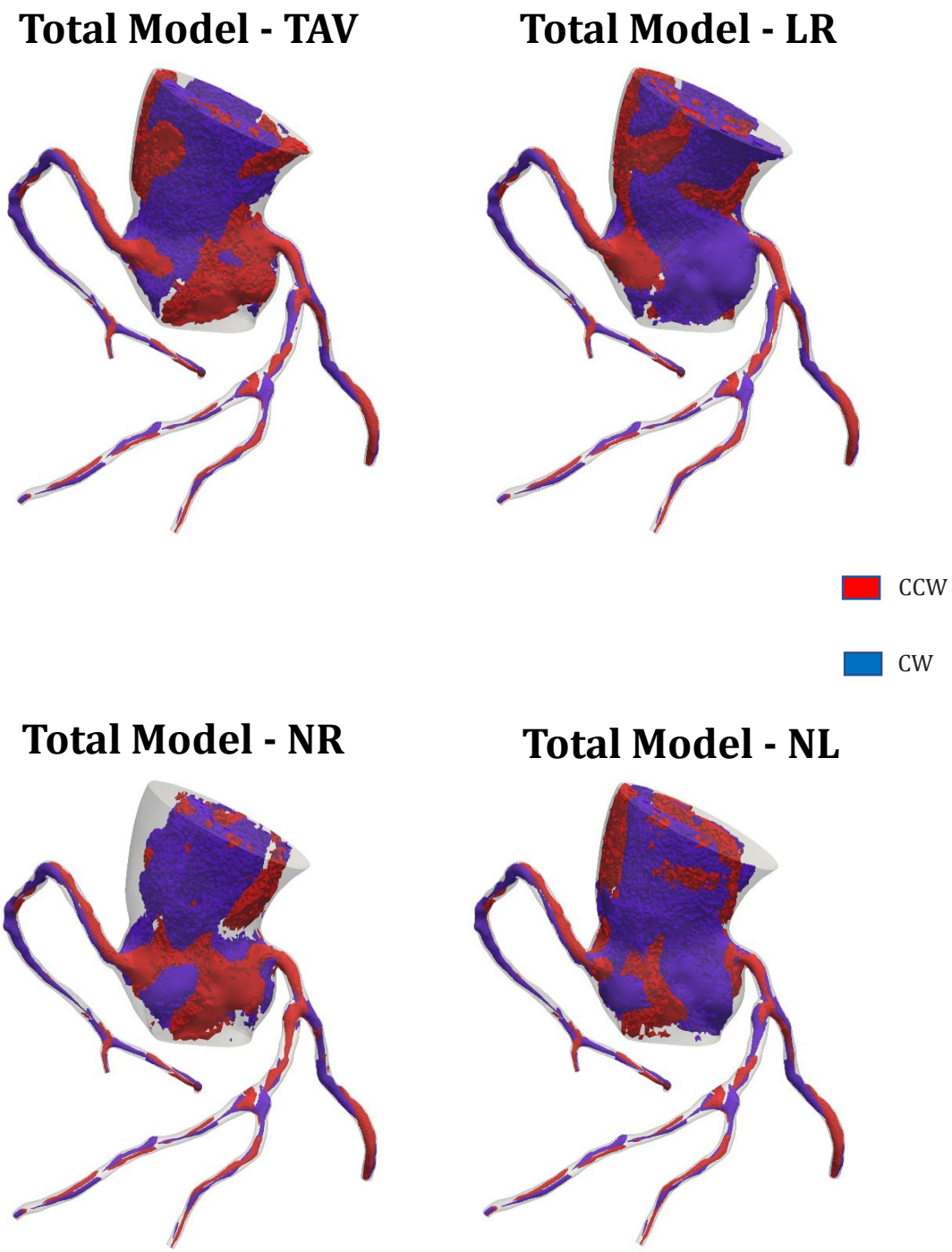

Figure 5-12: LNH and orientation of fluid structures on total model.

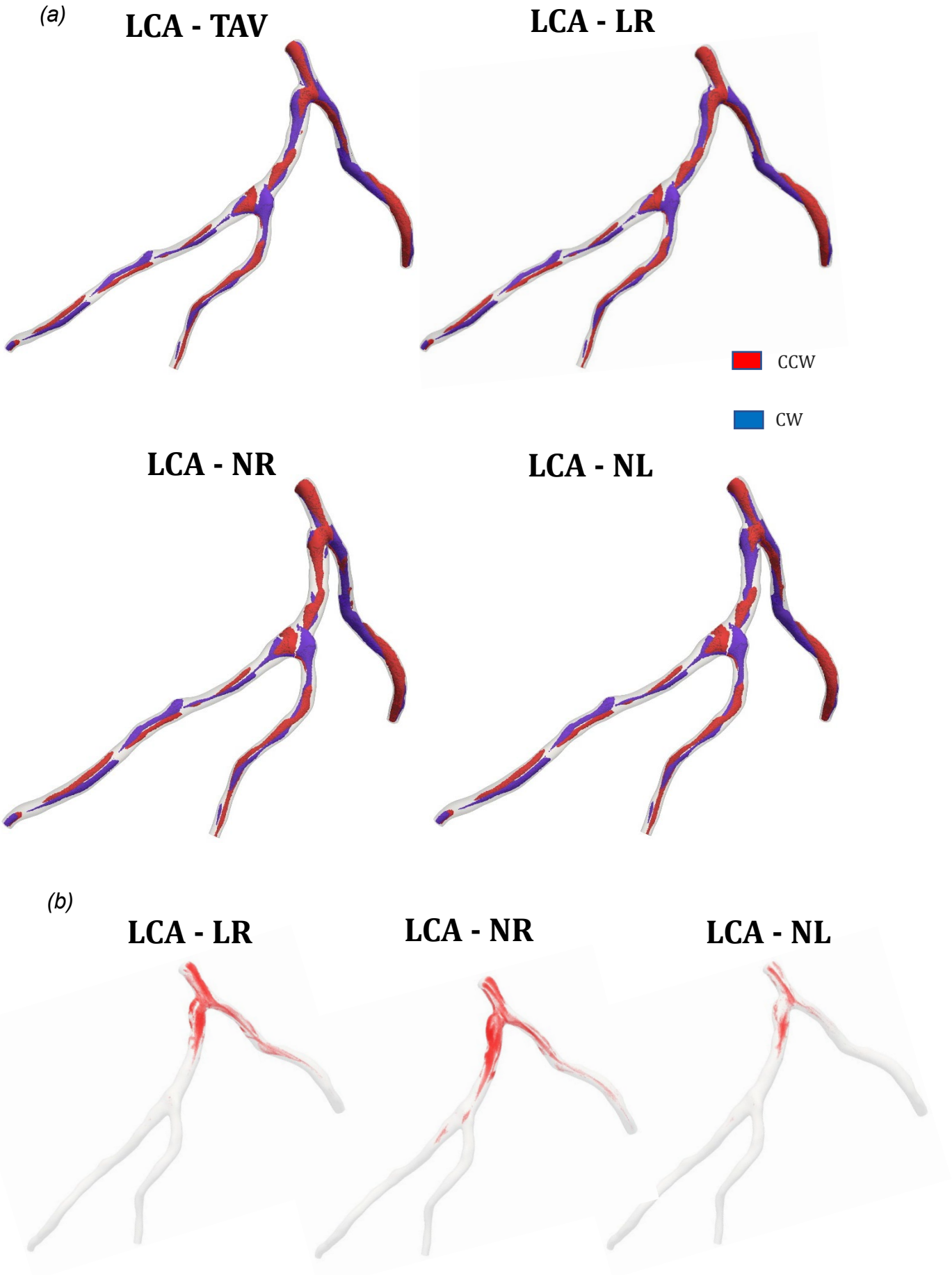

Figure 5-13: a) LNH and orientation on left artery; b) Visualization of LNH iso-surface (90th percentile) on left coronary artery.

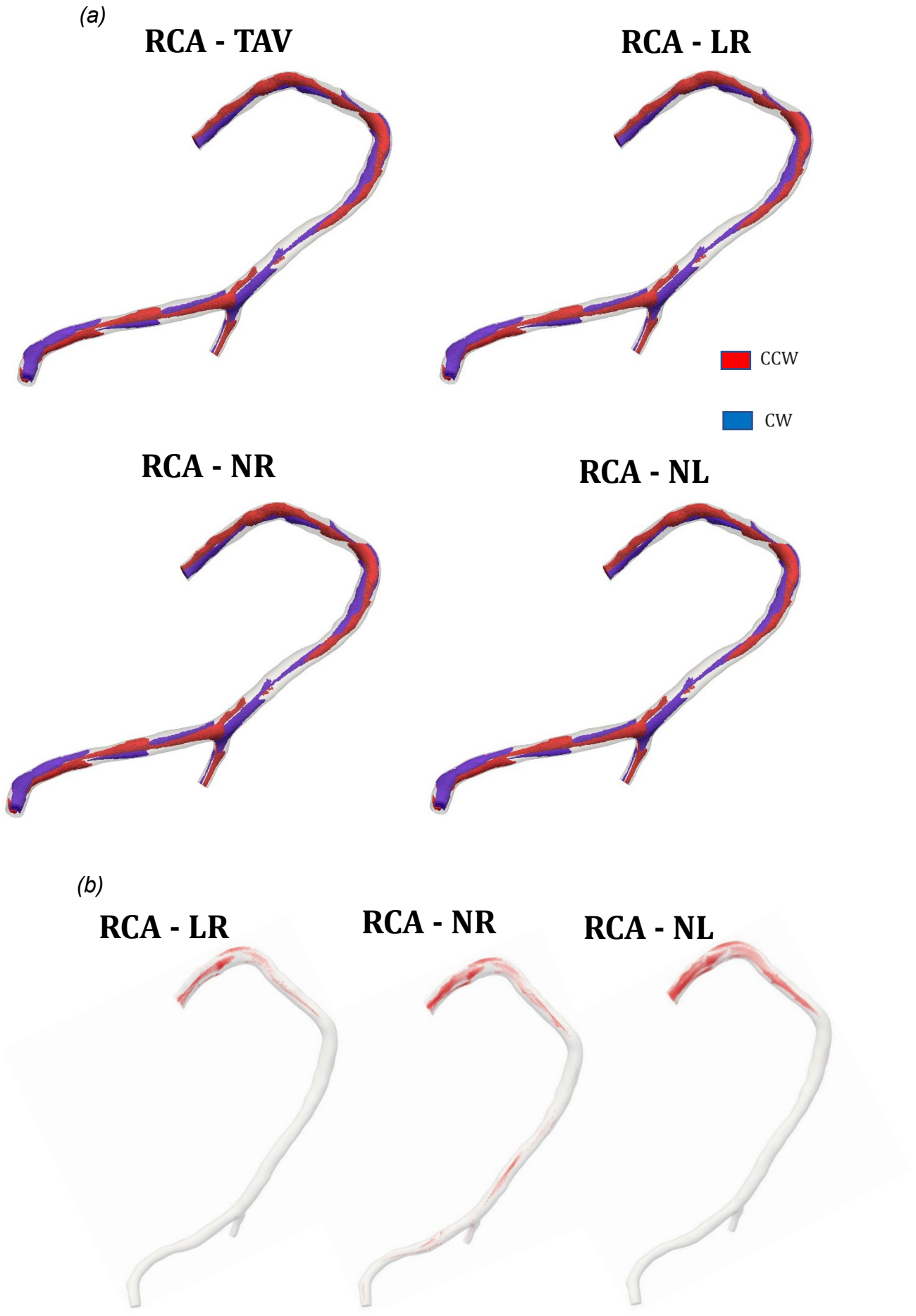

Figure 5-14: a) LNH and orientation on right artery; b) Visualization of LNH iso-surface (90th percentile) on right coronary artery.

(a)

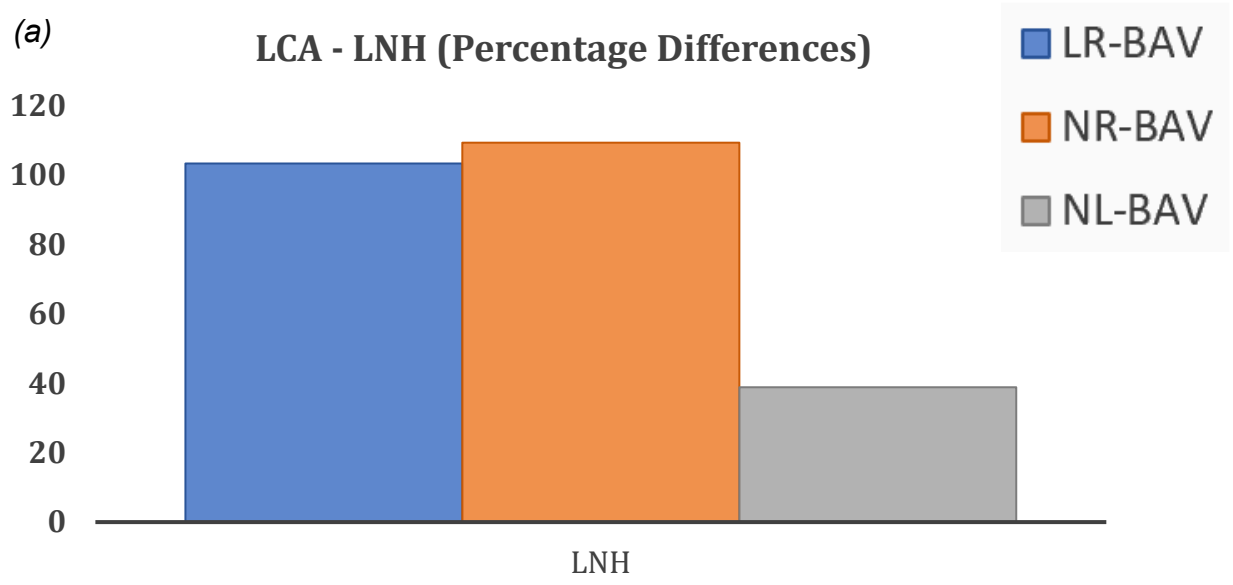
LCA - LNH (Percentage Differences)
LR-BAV
NR-BAV
NL-BAV
120
100
80
60
40
20
0
LNH

(b)

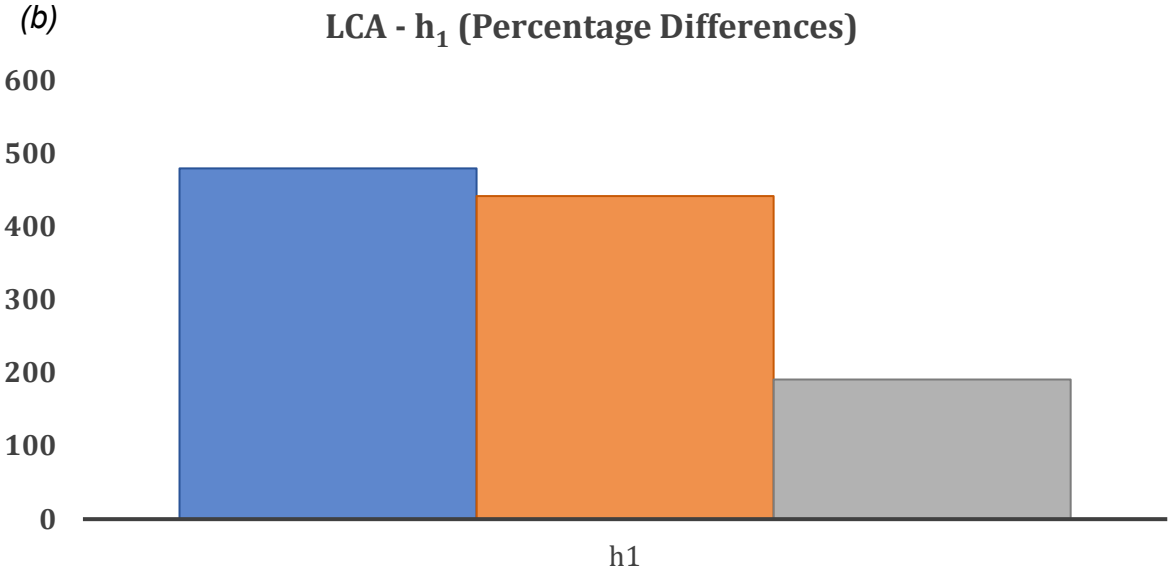
LCA - h1 (Percentage Differences)
600
500
400
300
200
100
0
h1

(c)

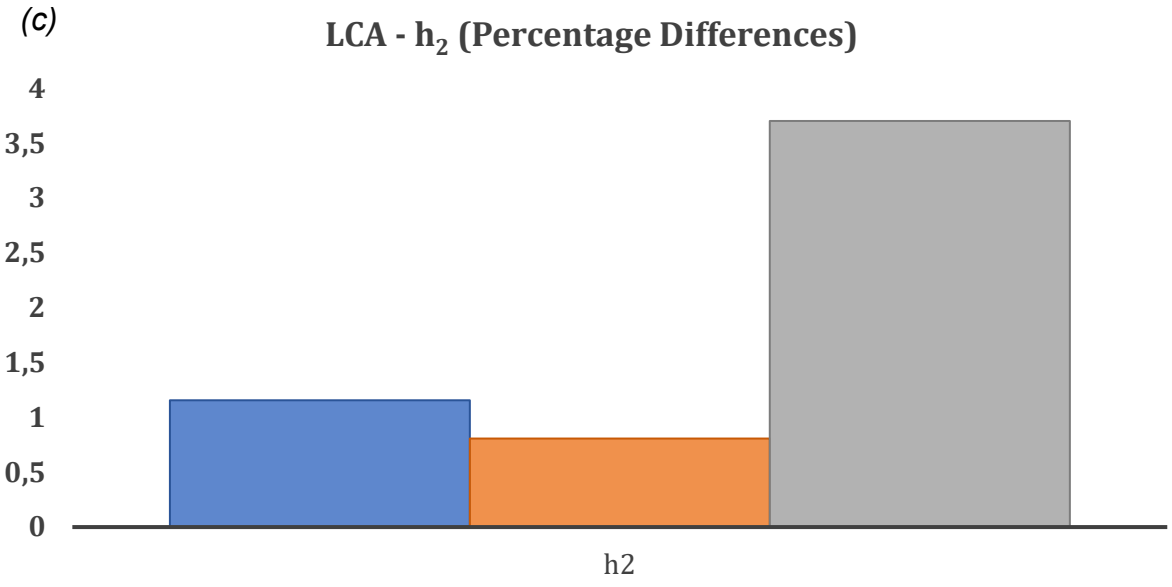
LCA - h2 (Percentage Differences)
4
3,5
3
2,5
2
1,5
1
0,5
0
h2

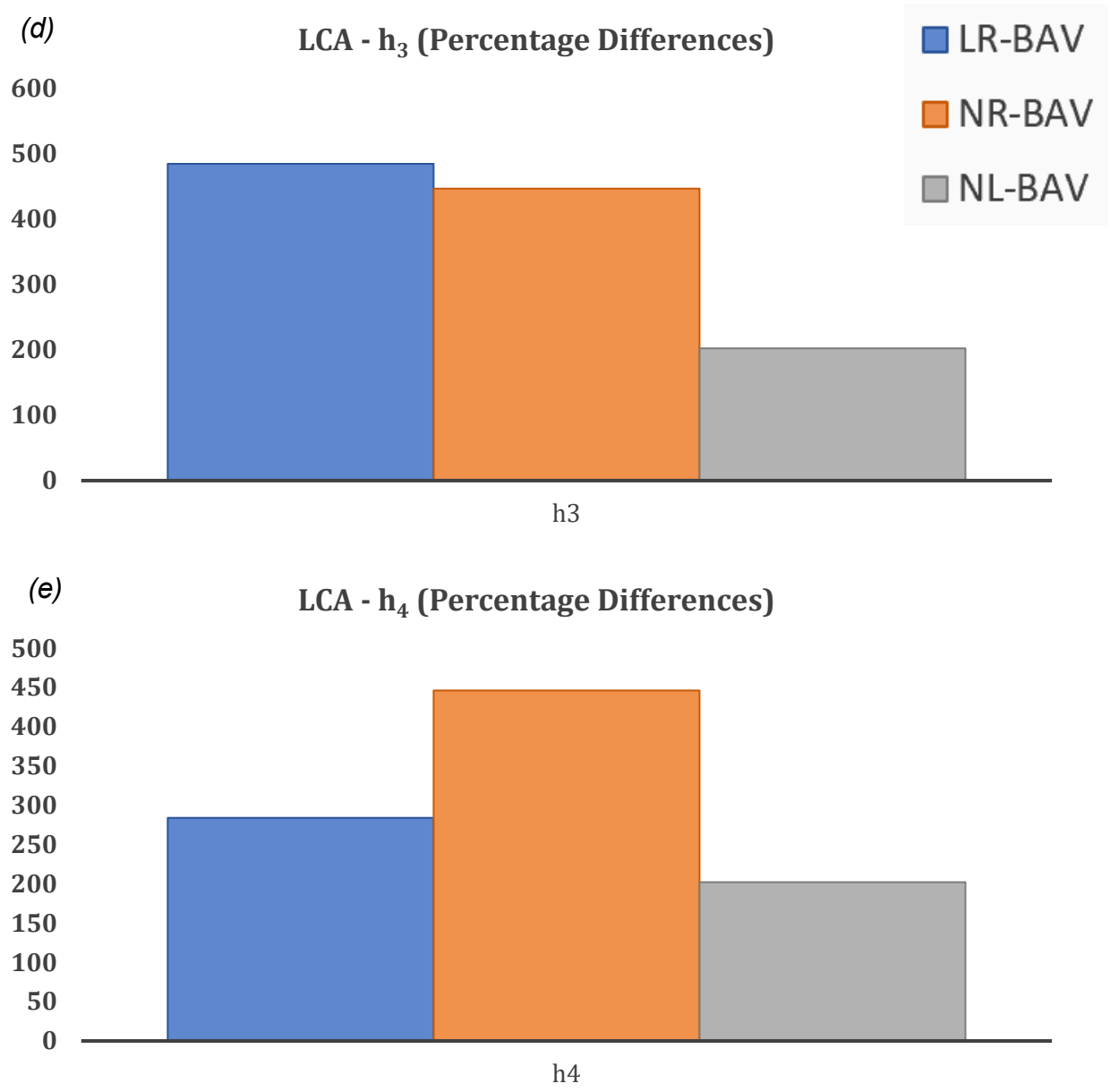

Figure 5-15: Helicity descriptors percentage differences on left coronary arteries.

(a)

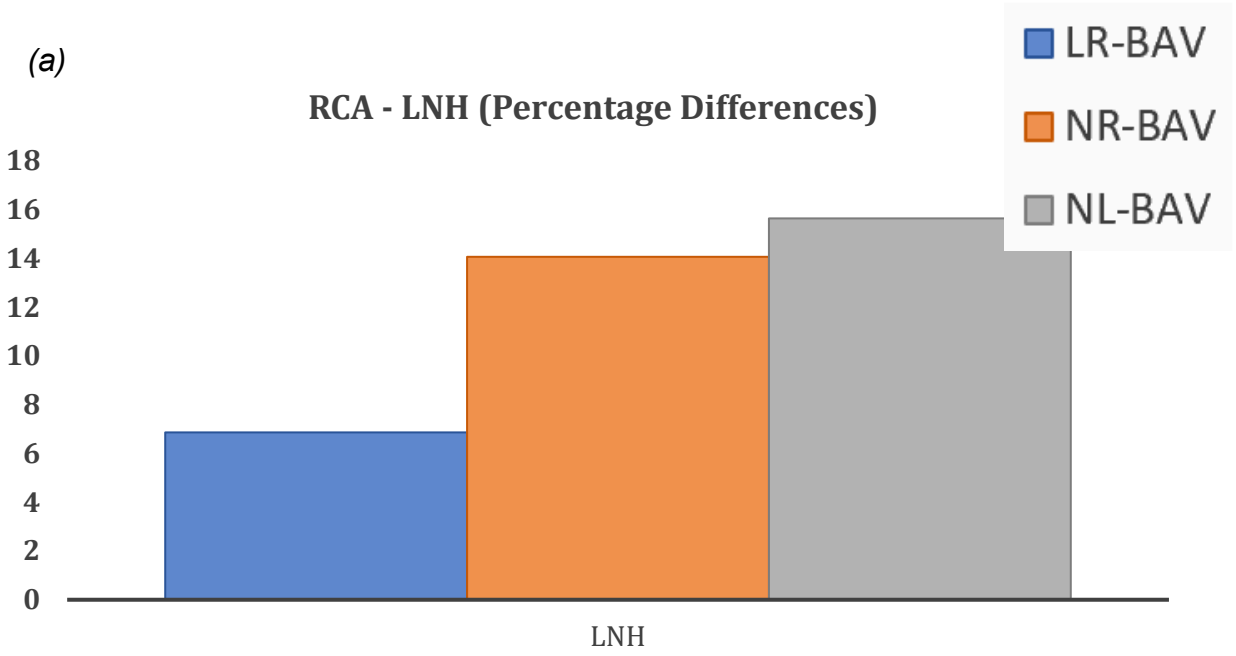
RCA - LNH (Percentage Differences)
LR-BAV
NR-BAV
NL-BAV
18
16
14
12
10
8
6
4
2
0
LNH

(b)

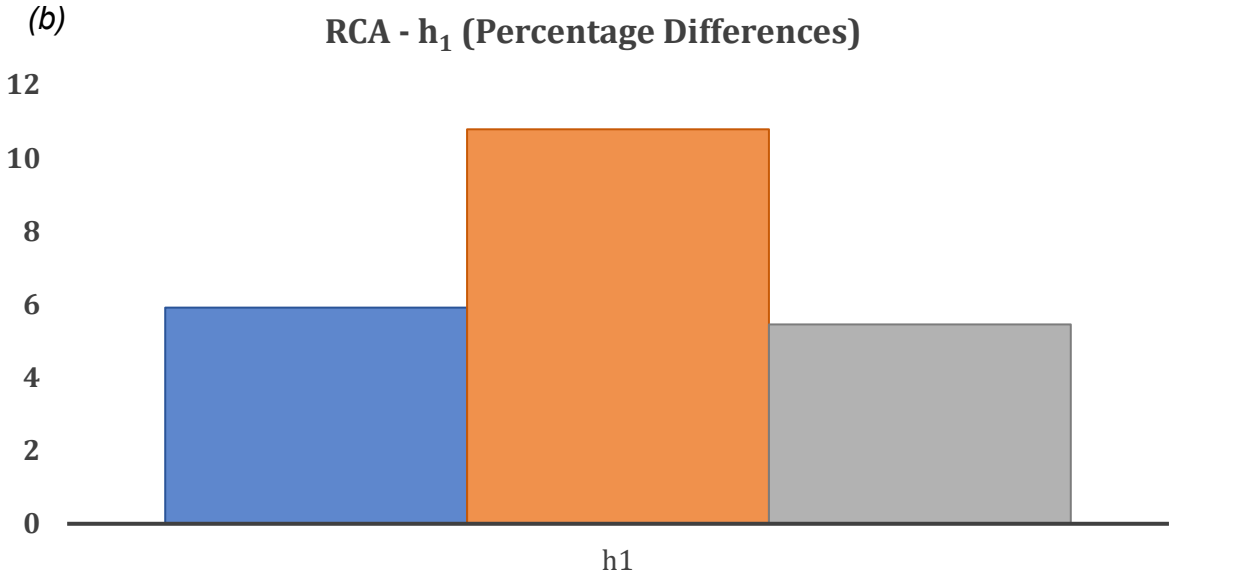
RCA - h1 (Percentage Differences)
12
10
8
6
4
2
0
h1

(c)

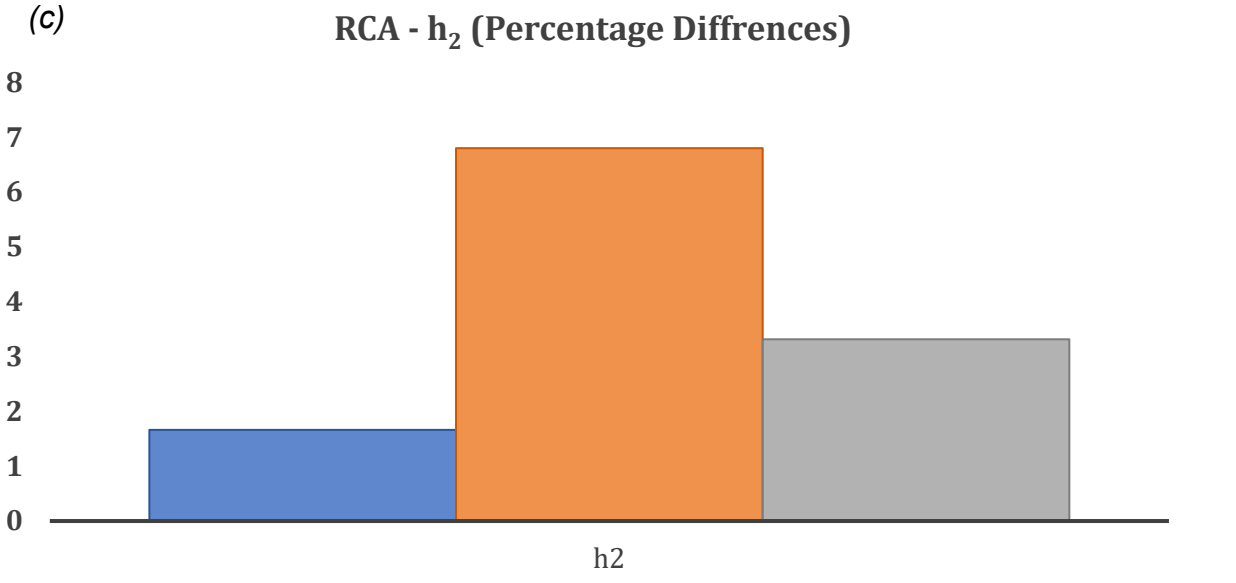
RCA - h2 (Percentage Diffrences)
8
7
6
5
4
3
2
1
0
h2

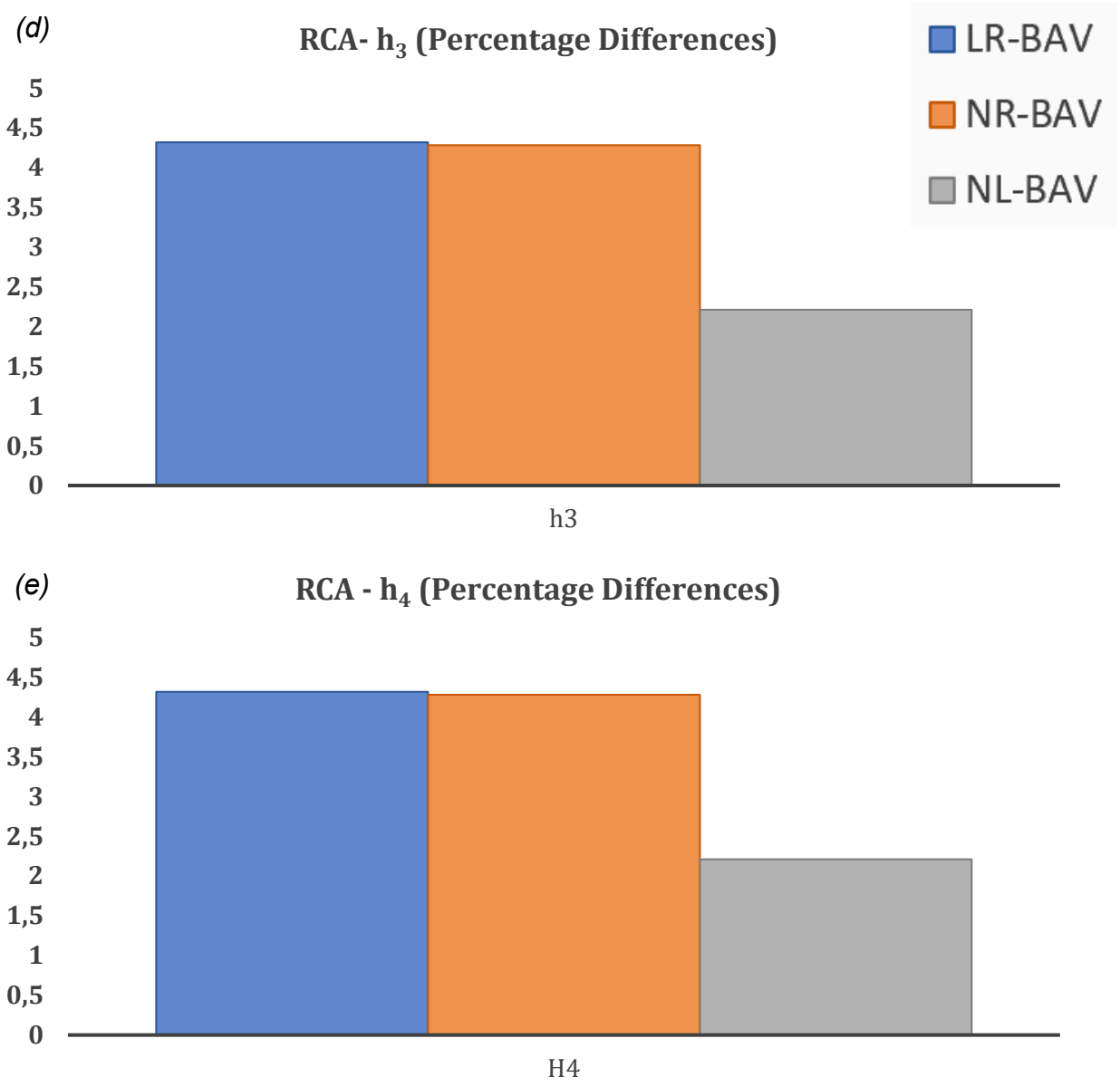

Figure 5-16: Helicity descriptors percentage differences on right coronary arteries.

LNH and helicity indexes are computed to evaluate distribution and intensity of the bulk fluid structures. The physiologic case, we note tata the fluid structures are arranged as left-handed. Qualitatively from LNH visualizations we note evident differences in the aorta sections where some structures can invert their orientation (Figure 5-13), while observing coronary arteries, seem that same left-handed helical structures are mostly respect in all BAV cases excepted for the *LR-BAV* configuration (Figure5-14 and Figure 5-15). This consideration is confirmed by the h1 and h3 quantity that indicates a prevalence toward physiological direction, although there are high percentage differences in terms of absolute value (Figure5-16b,d and Figure 5-17b,d). The h2 quantity show that helicity intensity does

not too distant from the physiological case, especially in coronary districts, less than 4% in LCA for NR-BAV configuration and less than 7% in RCA for NL-BAV (Figure5-16c and Figure 5-17c). We desire that helicity is not highly alter, in order to ensure and respect the physiologic-like movements of helical structure to ensure low loss of energy and to avoid abnormal flow behavior within these delicate vascular regions. An overview about outcomes, suggest that RCA helical flow is not too disturbed, while LCA percentage differences are very high in all BAV cases.

6. CONCLUSIONS

Aim of this master thesis work was to evaluate if BAV-like three-dimensional velocity profiles could affect hemodynamics in coronary arteries.

Our hemodynamic study was performed on a complete model of aorta and coronary branches, reconstructed from clinical images acquired with a CT scan. Model was accurately meshed to create a grid which guarantees a compromise between accuracy and excessive computational time. For this reason, a mesh independence analysis was performed with a particular attention on the refinement of coronary arteries. BAV-like profiles were reconstructed and then modulated in order to mimic the main features of this pathology. After CFD steady-state simulations, data post-processing was particularly focused on left and right coronary arteries.

Furthermore, results in term of wall and bulk quantities were extracted from BAV-like conditions and compared with results extracted from physiological-like (Poiseuille-Hagen velocity profile) condition. All hemodynamics quantities were investigated both in term of mean, maximum and minimum values and percentage differences.

Based on outcomes, it is possible to assert that the flow, imposed at the inlet surface, is distributed equally in term of percentage into coronary outlets. This depends on the same lumped parameter model assigned as outlet boundary conditions.

Wall shear stress main differences are located on the aorta walls, over the LCA bifurcation and in the early part of RCA ostium. Considering coronary arteries, *NR-BAV* is the valve morphology with the highest differences. Overall, we must to underline that WSS percentage difference are low on average, with a maximum of 6% difference for the *NR-BAV* configuration.

Regarding velocity, according to the shape of imposed velocity profile, we note that each coronary branch is influenced in a different way. TAV-like configuration is generated as parabolic profile using Poiseuille equation, so its velocity has a central peak. The forward peak of BAV velocity is eccentric toward a specific sinus, so the velocity values in the coronary, rising from that sinus, have higher different respect to the physiologic-like orientation. Our results suggest that velocity behavior is almost physiologic in both

coronary arteries. This affirmation is supported by low percentage differences, in particular, less than *6%* in LCA for *NR-BAV* configuration and less than *3,5%* in RCA for *NR-BAV* configuration. Instead, higher predictable differences are present in the bulk of aorta section, just above the inlet surface where BAV-like profiles are prescribed.

Regarding, the analysis of helical blood flow patterns, LNH and helicity indexes were computed to evaluate distribution and intensity of helical fluid structures. Qualitative studies show that the physiologic case has a prevalence of left-handed helical structures in all sections and same orientations seem to be respected in all BAV-like cases, except for the *LR-BAV* configuration. Combining findings information from all helical flow descriptors, we note that RCA helical flow are not too distant from the physiologic case (LNH around 16%, h1 around 10%, h2 about 7%, h3 and h4 around 4,5%), but on contrary LCA percentage differences are very high in all BAV cases (LNH around 110%, h2 is 0%, h1, h3 and h4 around 450%).

In conclusion, it is important to underline that these observations are preliminary results, so we cannot conclude whether the coronary circulation is severely disturbed by BAV eccentric velocity profile or not. We must considerer that there are numerous aspects to improve for the future. Just some example can be: (1) miming of the three-dimensional shape of velocity profile (maybe more patient-specific); (2) better optimization of equation parameters with more complex algorithms, such as genetics algorithm; (3) mesh with higher accuracy; (4) more specific boundary conditions and CFD unsteady simulations which allow to study effects of BAVs during the cardiac cycle; (5) FSI simulations, to be able to simulate also mechanical behaviour of valves . These could be a good starting point to understand which quantities need to be further investigated to understand the role of this pathology on coronary arteries hemodynamic.

7. APPENDIX

7.1 ProfileParameter.py

```
# -*- coding: utf-8 -*-
"""
Created on Wed Sep 19 18:49:15 2018
Aorta inlet flow conditions: peak-systolic 3D inlet velocity profiles based on
the percentage values taken from Literature # [K. Cao, P. Sucosky 2016]
@author: Gabriele Birritta
"""

# some imports
import math
from math import isclose
import numpy as np
import vtk
from vtk.util.numpy_support import vtk_to_numpy
from vmtk import vmtkscripts

# Functions definition
def WritePolyData(input,filename):
# Write PolyData file (*.vtp)
  writer = vtk.vtkXMLPolyDataWriter()
  writer.SetInputData(input)
  writer.SetFileName(filename)
  writer.Write()

def ReadPolyData(filename):
# Read PolyData file (*.vtp)
  reader = vtk.vtkXMLPolyDataReader()
  reader.SetFileName(filename)
  reader.Update()
```

```
  return reader.GetOutput()


def computeCenterPoints(pointCoordinates):
# compute geometric center from points coordinates
    cx = np.mean(pointCoordinates[:,0])
    cy = np.mean(pointCoordinates[:,1])
    cz = np.mean(pointCoordinates[:,2])
    c = np.array([cx,cy,cz])
    return c


def computeBoundaryCoordinates(surface):
# extract boundary points coordinates from vtkpolydata surface
    FeatureEdges = vtk.vtkFeatureEdges()
    FeatureEdges.SetInputData(surface)
    FeatureEdges.BoundaryEdgesOn()
    FeatureEdges.FeatureEdgesOff()
    FeatureEdges.NonManifoldEdgesOff()
    FeatureEdges.ManifoldEdgesOff()
    FeatureEdges.Update()
    BC = FeatureEdges.GetOutput()
    return BC


def computeNormalVersor(surface):
# compute normal versor for each node of vtkpolydata surface
# output: numpy array
    normalsFilter = vtk.vtkPolyDataNormals()
    normalsFilter.SetInputData(surface)
    normalsFilter.SetAutoOrientNormals(1)
    normalsFilter.SetConsistency(1)
    normalsFilter.SplittingOff()
    normalsFilter.Update()
    normalSurface = normalsFilter.GetOutput()
    normalArray = normalSurface.GetPointData().GetArray('Normals')
```

```
    un = vtk_to_numpy(normalArray)
    N = int(np.size(un[:,0]))
    for i in range(0,N):
      if un[i,2]<0:
        un = -un
    return un


def computeRadialVersor(coordinates,center):
# compute radial versor for each node given points and center coordinates
    N = int(np.size(coordinates[:,0]))
    r_xyz = np.zeros([N,3])
    ur = np.zeros([N,3])
    for i in range(0,N):
      r_xyz[i,:] = coordinates[i,:]-center
     r_coordinates[i]=np.sqrt(np.power(coordinates[i,0]-center[0],2)+np.power(coordinates[i,1]-
center[1],2)+np.power(coordinates[i,2]-center[2],2))
    for i in range(0,N):
      ur[i,:] = r_xyz[i,:]/r_coordinates[i]
    return ur


def computeAngularVersor(un,ur):
# compute angular coordinate as cross product of normal and radial versors
    N = int(np.size(un[:,0]))
    utheta = np.zeros([N,3])
    for i in range(0,N):
        utheta[i,:] = np.cross(un[i,:],ur[i,:])
    return utheta


def computeTheta(coordinates,center):
# compute theta coordinate from points and center coordinates
    coordinates_x = coordinates[:,0] - center[0]
    coordinates_y = coordinates[:,1] - center[1]
    theta = np.arctan2(coordinates_y,coordinates_x)
    return theta
```

```
def computeRadialCoordinates(coordinates,center):
# compute radial coordinate from point and center coordinates
    N = int(np.size(coordinates[:,0]))
    r_coordinates = np.zeros(N)
    for i in range(0,N):
        r_coordinates[i]=np.sqrt(np.power(coordinates[i,0]-center[0],2)+np.power(coordinates[i,1]-
center[1],2)+np.power(coordinates[i,2]-center[2],2))
    return r_coordinates


def computeVariableRadius(surfaceTheta, boundaryTheta, r_boundary):
# variable Radius definition:
    N = int(np.size(surfaceTheta))
    Radius = np.zeros(N)
    for i in range(0,N):
        a = np.abs(boundaryTheta - surfaceTheta[i])
        b = np.where(a==np.min(a))[0][0]
        Radius[i] = r_boundary[b]
    return Radius


# Profile function definitions:
def findNewCenter(inletCoordinates,targetRadius,tolerance,targetTheta):
# find a virtual center for eccentric velocity profile generation
# tolerance depend on mesh size
    r_coordinates = computeRadialCoordinates(inletCoordinates,inletCenter)
    pointsRadius = np.where((r_coordinates<=targetRadius+tolerance) &
(r_coordinates>=targetRadius-tolerance))[0]
    distTheta = np.zeros(np.size(pointsRadius))
    for i in range(0,np.size(pointsRadius)):
        distTheta[i] = np.abs(inlet_theta[pointsRadius[i]]-targetTheta)
    thetaIndex = np.where(distTheta==np.min(distTheta))[0]
    pointIndex = pointsRadius[thetaIndex]
    newCenter = np.transpose(inletCoordinates[pointIndex,:])
    return newCenter
```

```
def computeCartesianCoordinates(v,u):
# Cartesian coordinates velocity using velocity and versors
# v is velocity magnitude; u is direction versors
   v_x = v*u[:,0]
   v_y = v*u[:,1]
   v_z = v*u[:,2]
   return(v_x,v_y,v_z)

def computeCenterPoints(pointCoordinates):
   cx = np.mean(pointCoordinates[:,0])
   cy = np.mean(pointCoordinates[:,1])
   cz = np.mean(pointCoordinates[:,2])
   c = np.array([cx,cy,cz])
   return c

### Loading inlet surface on which velocity profile has to be imposed
#inletSurface = ReadPolyData('inlet.vtp')
#inletSurface = ReadPolyData('inletRemeshed.vtp')

name = 'inletNoBL.vtp'
#inletSurface = ReadPolyData(name)
from SubDivisionFunction import SubDivisions
inletSurface = SubDivisions(name)

# Compute coordinates of surface, boundary and center
inletCoordinates = vtk_to_numpy(inletSurface.GetPoints().GetData())
VTKboundaryCoordinates = computeBoundaryCoordinates(inletSurface)
boundaryCoordinates = vtk_to_numpy(VTKboundaryCoordinates.GetPoints().GetData())
GlobalNodeID = vtk_to_numpy(inletSurface.GetPointData().GetArray('GlobalNodeID'))
inletCenter = computeCenterPoints(inletCoordinates)

# Arrays' size:
```

```
N_point = int(np.size(inletCoordinates[:,0]))

# Radial coordinate computation:
r_coordinates = computeRadialCoordinates(inletCoordinates,inletCenter) #surface
r_boundary = computeRadialCoordinates(boundaryCoordinates,inletCenter) #boundary

# Angular coordinates computation:
inlet_theta = computeTheta(inletCoordinates,inletCenter) #surface
boundary_theta = computeTheta(boundaryCoordinates,inletCenter) #boundary

# Variable radius computation:
Radius = computeVariableRadius(inlet_theta,boundary_theta, r_boundary) #Adaptive Radius

# Axial,Radial and Angular versors computation
un = computeNormalVersor(inletSurface)
ur = computeRadialVersor(inletCoordinates,inletCenter)
utheta = computeAngularVersor(un,ur)

################################################################################
################################################################################

### CALCULATE SURFACE PERCENTAGE BAV/TAV
## Values taken from Literature # [K. Cao, P. Sucosky 2016]

# Area surface TAV
TAV_goa = 3.7 #cm^2
# Area surface BAV
BAV_goa = 2.3 #cm^2

# Percentage Inflow and Backflow
BAV_percInfl = (BAV_goa/TAV_goa)*100 #%
BAV_percBackfl = 100-BAV_percInfl
```

```
### GENERALIZED POISEUILLE PROFILE

# Sinus orientation

alphaNoCor = 0

alphaLeftCor = (np.pi*3)/4

alphaRightCor = -(np.pi*3)/4


# b definition

bNoCor = 9.82

bLeftCor = 8.40

bRightCor = 7.46


# Definition of parameters

aecc = 1

Kecc = 5

alfa = alphaNoCor

becc = bNoCor


vax_r = np.zeros(N_point)


# Implementation of the formula

for i in range(0,N_point):

   vax_r[i] = (aecc*(1-
np.power((r_coordinates[i]/Radius[i]),Kecc))+becc*(np.power((r_coordinates[i]/Radius[i]),3)-
(r_coordinates[i]/Radius[i]))*np.cos(inlet_theta[i]+alfa))


vaxg_X = vax_r*un[:,0]

vaxg_Y = vax_r*un[:,1]

vaxg_Z = vax_r*un[:,2]


# Definition of the points on the Backflow surface (they are negative <0)

surfaceBack_indx = []

boundary_indx = []


for i in range(0,N_point):
```

```
    if vax_r[i] < 0:
        surfaceBack_indx.append(i)
    if vax_r[i] == 0:
        boundary_indx.append(i)

surfaceBack_indx = np.array(surfaceBack_indx)
boundary_indx = np.array(boundary_indx)

surface_indx = np.arange(0,N_point)

# Definition of the points on the Inflow surface (positive points = all points - negative points)
surfaceIn_indx = np.array(list(set(surface_indx) - set(surfaceBack_indx) - set(boundary_indx)))

# Visualization Surface Inflow
surf1_coordinates = np.zeros((N_point,3))
surf1_points = np.zeros((len(surfaceIn_indx),3))

for i in range (0,N_point):
    for j in range(0,len(surfaceIn_indx)):
        if i == surfaceIn_indx[j]:
            surf1_coordinates[i,:] = inletCoordinates[i,:]
        surf1_points[j,:] = inletCoordinates[surfaceIn_indx[j],:]

# Visualization Surface Backflow
surf2_coordinates = np.zeros((N_point,3))
surf2_points = np.zeros((len(surfaceBack_indx),3))

for i in range (0,N_point):
    for j in range(0,len(surfaceBack_indx)):
        if i == surfaceBack_indx[j]:
            surf2_coordinates[i,:] = inletCoordinates[i,:]
        surf2_points[j,:] = inletCoordinates[surfaceBack_indx[j],:]
```

```
### CALCULATE AREA OF BACKFLOW and INFLOW SURFACES
import numpy as np
import scipy.spatial
import pylab

def heron(a,b,c):
    s = (a + b + c) / 2
    area = (s*(s-a) * (s-b)*(s-c)) ** 0.5
    return area

def distance3d(x1,y1,z1,x2,y2,z2):
    a=(x1-x2)**2+(y1-y2)**2 + (z1-z2)**2
    d= a ** 0.5
    return d

def areatriangle3d(x1,y1,z1,x2,y2,z2,x3,y3,z3):
    a=distance3d(x1,y1,z1,x2,y2,z2)
    b=distance3d(x2,y2,z2,x3,y3,z3)
    c=distance3d(x3,y3,z3,x1,y1,z1)
    A = heron(a,b,c)
    return A

# Find the ID associated to each element(cell)
GlobalElementID = vtk_to_numpy(inletSurface.GetCellData().GetArray('GlobalElementID'))

N_cells = inletSurface.GetNumberOfCells()

a = np.zeros([N_cells])
b = np.zeros([N_cells])
c = np.zeros([N_cells])
AreaToTBack = []
AreaToTIn = []
```

```
# Identification if the cell points are in inflow or backflow area
# 1 cell(triangular) --> 3 vertices points
for i in range(0,N_cells):
    cellPointIds = inletSurface.GetCell(i).GetPointIds()
    a[i] = cellPointIds.GetId(0)
    b[i] = cellPointIds.GetId(1)
    c[i] = cellPointIds.GetId(2)

for i in range(0,N_cells):
    pointBack = 0
    if (vax_r[int(a[i])] < 0):
        pointBack = pointBack + 1
    if (vax_r[int(b[i])] < 0):
        pointBack = pointBack + 1
    if (vax_r[int(c[i])] < 0):
        pointBack = pointBack + 1
    if pointBack >= 2:

      p1 = inletCoordinates[int(a[i]),:]
      p2 = inletCoordinates[int(b[i]),:]
      p3 = inletCoordinates[int(c[i]),:]

      AreaBack = areatriangle3d(p1[0], p1[1], p1[2], p2[0], p2[1], p2[2], p3[0], p3[1], p3[2])
      AreaToTBack.append(AreaBack)
    else:
      p1 = inletCoordinates[int(a[i]),:]
      p2 = inletCoordinates[int(b[i]),:]
      p3 = inletCoordinates[int(c[i]),:]

      AreaIn = areatriangle3d(p1[0], p1[1], p1[2], p2[0], p2[1], p2[2], p3[0], p3[1], p3[2])
      AreaToTIn.append(AreaIn)
```

```
# Real Area BAV and TAV
AreaToT_BAVbackflow = np.sum(np.array(AreaToTBack))
AreaToT_BAVinflow = np.sum(np.array(AreaToTIn))
AreaToT_TAV = AreaToT_BAVinflow + AreaToT_BAVbackflow

# Ideal Area BAV Backflow, used to check the correct value
AreaBAV_check = (AreaToT_TAV*BAV_percBackfl)/100

# Verification, calculating the percentage error
error_perc = (abs(AreaBAV_check-AreaToT_BAVbackflow)/AreaBAV_check)*100
error_perc_round = round(error_perc,2)
print (error_perc_round)

################################################################################
################################################################################

# Surface1 vector to vtk
info1 = vtk.vtkDoubleArray()
info1.SetNumberOfComponents(3)
info1.SetNumberOfTuples(N_point)
info1.FillComponent(0,0.)
info1.SetName('surface_INflow')
for i in range(0,N_point):
   info1.SetTuple3(i,surf1_coordinates[i,0],surf1_coordinates[i,1],surf1_coordinates[i,2])

# Surface2 vector to vtk
info2 = vtk.vtkDoubleArray()
info2.SetNumberOfComponents(3)
info2.SetNumberOfTuples(N_point)
info2.FillComponent(0,0.)
info2.SetName('surface_BACKflow')
for i in range(0,N_point):
   info2.SetTuple3(i,surf2_coordinates[i,0],surf2_coordinates[i,1],surf2_coordinates[i,2])
```

```
# Add array to surface
inletSurface.GetPointData().AddArray(info1)
inletSurface.GetPointData().AddArray(info2)

# Save new surface
WritePolyData(inletSurface,'ProfilesNC_noBL(step2).vtp')
#WritePolyData(inletSurface,'ProfilesLEFT_noBL(step2).vtp')
#WritePolyData(inletSurface,'ProfilesRIGHT_noBL(step2).vtp')

print('\nMESSAGE: Inlet - Inflow and Bakflow - Surface DONE.')

################################################################################
################################################################################

### EXTRAPOLATION WAVE FORM DATA
ExcelNameIN = 'flowRate2.xlsx'
SheetNameIN = 'BAV - Positive'
ExcelNameBACK = 'flowRate2.xlsx'
SheetNameBACK = 'BAV - Negative'
ExcelNameTAV = 'flowRate2.xlsx'
SheetNameTAV = 'TAV - Net'

AreaIN = AreaToT_BAVinflow #CAp info INflow surface
AreaBACK = AreaToT_BAVbackflow #CAp info BACKflow surface
AreaTAV = AreaToT_TAV #CAp info TAV surface

Nin = 8
Nback = 9
Ntav = 18

# Calculate the Fourier series
from FourierSeriesFunction import FourierSeries
```

```
t_fourier, x_flowIN, x_PulseVelocityIN = FourierSeries(ExcelNameIN, SheetNameIN, AreaIN, Nin)

t_fourier, x_flowBACK, x_PulseVelocityBACK = FourierSeries(ExcelNameBACK, SheetNameBACK, AreaBACK, Nback)

t_fourier, x_flowTAV, x_PulseVelocityTAV = FourierSeries(ExcelNameTAV, SheetNameTAV, AreaTAV, Ntav)


x_flowNET = x_flowIN + x_flowBACK

x_PulseVelocityNET = (x_flowNET/AreaIN)*(np.power(10,3)/60)

N_time = len(t_fourier)

#############################################################################################

#############################################################################################


from PerimeterCalculationFunction2 import PerimeterCalculation


nameBAV = 'ProfilesNC_noBL(step2).vtp'

#nameBAV = 'ProfilesLEFT_noBL(step2).vtp'

#nameBAV = 'ProfilesRIGHT_noBL(step2).vtp'


perimeterTAV, perimeterBAV = PerimeterCalculation('TAV.vtp', nameBAV)


#############################################################################################

#############################################################################################


### CALCULATE HYDRAULIC DIAMETER TAV

D_hTAV = (AreaToT_TAV/perimeterTAV)*4


### CALCULATE REYNOLDS TAV

ro = 1.06 #density [g/cm^3]

mu = 0.04 #viscosity [poise]


ReynoldsTAV = (ro/mu)*(np.mean(x_PulseVelocityTAV))*D_hTAV
```

```
################################################################################

### CALCULATE HYDRAULIC DIAMETER BAV
D_hBAV = (AreaToT_BAVinflow/perimeterBAV)*4

### CALCULATE REYNOLDS BAV
ro = 1.06 #density [g/cm^3]
mu = 0.04 #viscosity [poise]

ReynoldsBAV = (ro/mu)*(np.mean(x_PulseVelocityNET))*D_hBAV

################################################################################
################################################################################

# REYNOLDS SCALING
v_scalRe = (D_hTAV/D_hBAV)*(np.mean(x_PulseVelocityTAV))

################################################################################
################################################################################

# MODULATION INFLOW AND BACKFLOW WAVEFORM
# Barker et al. 2010 values from literature to scale the correct Inflow velocity profile
vax_rIN = vax_r[surfaceIn_indx]
vax_rINmean = np.mean(vax_rIN)
BAV_inflowMean = (5.335513004/AreaToT_BAVinflow)*(np.power(10,3)/60) #cm/s
vax_rIN_mod = (vax_rIN/vax_rINmean)*BAV_inflowMean

# Scaled Reynold
vax_rIN_modRe = (vax_rIN/vax_rINmean)*v_scalRe

# Barker et al. 2010 values from literature to scale the correct Backflow velocity profile
vax_rBACK = vax_r[surfaceBack_indx]
vax_rBACKmean = np.mean(vax_rBACK)
```

```
BAV_BackflowMean = -(2.360855239/AreaToT_BAVbackflow)*(np.power(10,3)/60) #cm/s
vax_rBACK_mod = (vax_rBACK/vax_rBACKmean)*BAV_BackflowMean

# Scaled ZeroBACK
vax_rBACK_modZero = 0*vax_rBACK_mod

# Scaled Reynold
vax_rBACK_modRe = 0

vax_r_mod = np.zeros(N_point)
vax_r_modZero = np.zeros(N_point)
vax_r_modRe = np.zeros(N_point)

for j in range(0, len(surfaceIn_indx)):
    pos = surfaceIn_indx[j]
    vax_r_mod[pos] = vax_rIN_mod[j]
    vax_r_modZero[pos] = vax_rIN_mod[j]
    vax_r_modRe[pos] = vax_rIN_modRe[j]

for j in range(0, len(surfaceBack_indx)):
    pos = surfaceBack_indx[j]
    vax_r_mod[pos] = vax_rBACK_mod[j]
    vax_r_modZero[pos] = vax_rBACK_modZero[j]
    vax_r_modRe[pos] = vax_rBACK_modRe

vaxg_Xm = vax_r_mod*un[:,0]
vaxg_Ym = vax_r_mod*un[:,1]
vaxg_Zm = vax_r_mod*un[:,2]

vaxg_XmZero = vax_r_modZero*un[:,0]
vaxg_YmZero = vax_r_modZero*un[:,1]
vaxg_ZmZero = vax_r_modZero*un[:,2]
```

```
vaxg_XmRe = vax_r_modRe*un[:,0]
vaxg_YmRe = vax_r_modRe*un[:,1]
vaxg_ZmRe = vax_r_modRe*un[:,2]

################################################################################
################################################################################

# Trought-plane velocity Scaled vector to vtk
tPlaneVelocityArrayScaled = vtk.vtkDoubleArray()
tPlaneVelocityArrayScaled.SetNumberOfComponents(3)
tPlaneVelocityArrayScaled.SetNumberOfTuples(N_point)
tPlaneVelocityArrayScaled.FillComponent(0,0.)
tPlaneVelocityArrayScaled.SetName('tPlaneVelocity Scaled cm/s')
for i in range(0,N_point):
   tPlaneVelocityArrayScaled.SetTuple3(i,vaxg_Xm[i],vaxg_Ym[i],vaxg_Zm[i])

# Trought-plane velocity vector to vtk
tPlaneVelocityArrayScaledZero = vtk.vtkDoubleArray()
tPlaneVelocityArrayScaledZero.SetNumberOfComponents(3)
tPlaneVelocityArrayScaledZero.SetNumberOfTuples(N_point)
tPlaneVelocityArrayScaledZero.FillComponent(0,0.)
tPlaneVelocityArrayScaledZero.SetName('tPlaneVelocity Scaled ZERO cm/s')
for i in range(0,N_point):
   tPlaneVelocityArrayScaledZero.SetTuple3(i,vaxg_XmZero[i],vaxg_YmZero[i],vaxg_ZmZero[i])

# Trought-plane velocity vector to vtk
tPlaneVelocityArrayScaledRe = vtk.vtkDoubleArray()
tPlaneVelocityArrayScaledRe.SetNumberOfComponents(3)
tPlaneVelocityArrayScaledRe.SetNumberOfTuples(N_point)
tPlaneVelocityArrayScaledRe.FillComponent(0,0.)
tPlaneVelocityArrayScaledRe.SetName('tPlaneVelocity Scaled (REYNOLDS) cm/s')
for i in range(0,N_point):
   tPlaneVelocityArrayScaledRe.SetTuple3(i,vaxg_XmRe[i],vaxg_YmRe[i],vaxg_ZmRe[i])
```

```
##############################################################################
##############################################################################

# Add array to surface
inletSurface.GetPointData().AddArray(tPlaneVelocityArrayScaled)
inletSurface.GetPointData().AddArray(tPlaneVelocityArrayScaledZero)
inletSurface.GetPointData().AddArray(tPlaneVelocityArrayScaledRe)

# Save new surface
WritePolyData(inletSurface,'NC_steady.vtp')
#WritePolyData(inletSurface,'LEFT_steady.vtp')
#WritePolyData(inletSurface,'RIGHT_steady.vtp')

print('\nMESSAGE: Inlet - Inflow and Bakflow - Velocity Profiles DONE.')
```

7.2 ProfileSteadyDAT.py

```
# -*- coding: utf-8 -*-
"""
Created on Mon Jul  9 18:43:31 2018
@author: Gabriele Birritta
"""
# some imports
import numpy as np
import vtk
from vtk.util.numpy_support import vtk_to_numpy

# functions definition
def WritePolyData(input,filename):
# Write PolyData file (*.vtp)
  writer = vtk.vtkXMLPolyDataWriter()
  writer.SetInputData(input)
  writer.SetFileName(filename)
  writer.Write()

def ReadPolyData(filename):
# Read PolyData file (*.vtp)
  reader = vtk.vtkXMLPolyDataReader()
  reader.SetFileName(filename)
  reader.Update()
  return reader.GetOutput()

def computeCenterPoints(pointCoordinates):
# compute geometric center from points coordinates
   cx = np.mean(pointCoordinates[:,0])
   cy = np.mean(pointCoordinates[:,1])
   cz = np.mean(pointCoordinates[:,2])
   c = np.array([cx,cy,cz])
```

```
    return c
def computeBoundaryCoordinates(surface):
# extract boundary points coordinates from vtkpolydata surface
    FeatureEdges = vtk.vtkFeatureEdges()
    FeatureEdges.SetInputData(surface)
    FeatureEdges.BoundaryEdgesOn()
    FeatureEdges.FeatureEdgesOff()
    FeatureEdges.NonManifoldEdgesOff()
    FeatureEdges.ManifoldEdgesOff()
    FeatureEdges.Update()
    BC = FeatureEdges.GetOutput()
    return BC

def computeNormalVersor(surface):
# compute normal versor for each node of vtkpolydata surface
# output: numpy array
    normalsFilter = vtk.vtkPolyDataNormals()
    normalsFilter.SetInputData(surface)
    normalsFilter.SetAutoOrientNormals(1)
    normalsFilter.SetConsistency(1)
    normalsFilter.SplittingOff()
    normalsFilter.Update()
    normalSurface = normalsFilter.GetOutput()
    normalArray = normalSurface.GetPointData().GetArray('Normals')
    un = vtk_to_numpy(normalArray)
    N = int(np.size(un[:,0]))
    for i in range(0,N):
      if un[i,2]<0:
        un = -un
    return un

def computeRadialVersor(coordinates,center):
# compute radial versor for each node given points and center coordinates
```

```
    N = int(np.size(coordinates[:,0]))
    r_xyz = np.zeros([N,3])
    ur = np.zeros([N,3])
    for i in range(0,N):
      r_xyz[i,:] = coordinates[i,:]-center
     r_coordinates[i]=np.sqrt(np.power(coordinates[i,0]-center[0],2)+np.power(coordinates[i,1]-
center[1],2)+np.power(coordinates[i,2]-center[2],2))
    for i in range(0,N):
      ur[i,:] = r_xyz[i,:]/r_coordinates[i]
    return ur


def computeAngularVersor(un,ur):
# compute angular coordinate as cross product of normal and radial versors
    N = int(np.size(un[:,0]))
    utheta = np.zeros([N,3])
    for i in range(0,N):
        utheta[i,:] = np.cross(un[i,:],ur[i,:])
    return utheta


def computeTheta(coordinates,center):
# compute theta coordinate from points and center coordinates
    coordinates_x = coordinates[:,0] - center[0]
    coordinates_y = coordinates[:,1] - center[1]
    theta = np.arctan2(coordinates_y,coordinates_x)
    return theta


def computeRadialCoordinates(coordinates,center):
# compute radial coordinate from point and center coordinates
    N = int(np.size(coordinates[:,0]))
    r_coordinates = np.zeros(N)
    for i in range(0,N):
       r_coordinates[i]=np.sqrt(np.power(coordinates[i,0]-center[0],2)+np.power(coordinates[i,1]-
center[1],2)+np.power(coordinates[i,2]-center[2],2))
    return r_coordinates
```

```
def computeVariableRadius(surfaceTheta, boundaryTheta, r_boundary):
# variable Radius definition:
    N = int(np.size(surfaceTheta))
    Radius = np.zeros(N)
    for i in range(0,N):
        a = np.abs(boundaryTheta - surfaceTheta[i])
        b = np.where(a==np.min(a))[0][0]
        Radius[i] = r_boundary[b]
    return Radius

# Profile function definitions:
def velocityMeanValue(velocityMag):
# compute mean velocity value
    bulkIndex = np.where(velocityMag!=0)
    meanVelocity = np.mean(velocityMag[bulkIndex])
    return meanVelocity

def computeCartesianCoordinates(v,u):
# Cartesian coordinates velocity using velocity and versors
# v is velocity magnitude; u is direction versors
    v_x = v*u[:,0]
    v_y = v*u[:,1]
    v_z = v*u[:,2]
    return(v_x,v_y,v_z)

# loading inlet surface on which velocity profile hes to be imposed
name = 'okINLETFinal.vtp'
inletSurface = ReadPolyData(name)

# compute coordinates of surface, boundary and center
inletCoordinates = vtk_to_numpy(inletSurface.GetPoints().GetData())
VTKboundaryCoordinates = computeBoundaryCoordinates(inletSurface)
```

```
boundaryCoordinates = vtk_to_numpy(VTKboundaryCoordinates.GetPoints().GetData())


inletCenter = computeCenterPoints(inletCoordinates)


# Arrays' size:
N_point = int(np.size(inletCoordinates[:,0]))
# Radial coordinate computation:
r_coordinates = computeRadialCoordinates(inletCoordinates,inletCenter) #surface
r_boundary = computeRadialCoordinates(boundaryCoordinates,inletCenter) #boundary
# Angular coordinates computation:
inlet_theta = computeTheta(inletCoordinates,inletCenter) #surface
boundary_theta = computeTheta(boundaryCoordinates,inletCenter) #boundary
# Variable radius computation:
Radius = computeVariableRadius(inlet_theta,boundary_theta, r_boundary) #Adaptive Radius
# Axial,Radial and Angular versors computation
un = computeNormalVersor(inletSurface)
ur = computeRadialVersor(inletCoordinates,inletCenter)
utheta = computeAngularVersor(un,ur)


#----------------------Generalized "Cao, K. and Sucosky, P. 2016" Velocity profile STEADY----------------#
# Parameters information: Profile[Cao, K. and Sucosky, P. 2016(3.0)].py


# Sinus orientation
alphaNoCor = 0
alphaLeftCor = (np.pi*3)/4
alphaRightCor = -(np.pi*3)/4


# b definition
bNoCor = 9.82
bLeftCor = 8.40
bRightCor = 7.46
```

```
# Definition of parameters

aecc = 1

Kecc = 5

alfa = alphaNoCor

becc = bNoCor


vax_r = np.zeros(N_point)


# Implementation of the formula

for i in range(0,N_point):

   vax_r[i] = (aecc*(1-
np.power((r_coordinates[i]/Radius[i]),Kecc))+becc*(np.power((r_coordinates[i]/Radius[i]),3)-
(r_coordinates[i]/Radius[i]))*np.cos(inlet_theta[i]+alfa))


vaxg_X = vax_r*un[:,0]

vaxg_Y = vax_r*un[:,1]

vaxg_Z = vax_r*un[:,2]


# Definition of the points on the Backflow surface (they are negative <0)

surfaceBack_indx = []

boundary_indx = []


for i in range(0,N_point):

   if vax_r[i] < 0:

      surfaceBack_indx.append(i)

   if vax_r[i] == 0:

      boundary_indx.append(i)


surfaceBack_indx = np.array(surfaceBack_indx)

boundary_indx = np.array(boundary_indx)

surface_indx = np.arange(0,N_point)


# Definition of the points on the Inflow surface (positive points = all points - negative points)
```

```
surfaceIn_indx = np.array(list(set(surface_indx) - set(surfaceBack_indx) - set(boundary_indx)))
# Visualization Surface Inflow
surf1_coordinates = np.zeros((N_point,3))
surf1_points = np.zeros((len(surfaceIn_indx),3))

for i in range (0,N_point):
    for j in range(0,len(surfaceIn_indx)):
        if i == surfaceIn_indx[j]:
            surf1_coordinates[i,:] = inletCoordinates[i,:]
        surf1_points[j,:] = inletCoordinates[surfaceIn_indx[j],:]

# Visualization Surface Backflow
surf2_coordinates = np.zeros((N_point,3))
surf2_points = np.zeros((len(surfaceBack_indx),3))

for i in range (0,N_point):
    for j in range(0,len(surfaceBack_indx)):
        if i == surfaceBack_indx[j]:
            surf2_coordinates[i,:] = inletCoordinates[i,:]
        surf2_points[j,:] = inletCoordinates[surfaceBack_indx[j],:]

################################################################################
################################################################################

### CALCULATE AREA OF BACKFLOW and INFLOW SURFACES
import numpy as np
import scipy.spatial
import pylab

def heron(a,b,c):
    s = (a + b + c) / 2
    area = (s*(s-a) * (s-b)*(s-c)) ** 0.5
    return area
```

```
def distance3d(x1,y1,z1,x2,y2,z2):
    a=(x1-x2)**2+(y1-y2)**2 + (z1-z2)**2
    d= a ** 0.5
    return d

def areatriangle3d(x1,y1,z1,x2,y2,z2,x3,y3,z3):
    a=distance3d(x1,y1,z1,x2,y2,z2)
    b=distance3d(x2,y2,z2,x3,y3,z3)
    c=distance3d(x3,y3,z3,x1,y1,z1)
    A = heron(a,b,c)
    return A

# Find the ID associated to each element(cell)
GlobalElementID = vtk_to_numpy(inletSurface.GetCellData().GetArray('GlobalElementID'))
N_cells = inletSurface.GetNumberOfCells()

a = np.zeros([N_cells])
b = np.zeros([N_cells])
c = np.zeros([N_cells])
AreaToTBack = []
AreaToTIn = []

# Identification if the cell points are in inflow or backflow area
# 1 cell(triangular) --> 3 vertices points
for i in range(0,N_cells):
    cellPointIds = inletSurface.GetCell(i).GetPointIds()

    a[i] = cellPointIds.GetId(0)
    b[i] = cellPointIds.GetId(1)
    c[i] = cellPointIds.GetId(2)

for i in range(0,N_cells):
```

```
    pointBack = 0
    if (vax_r[int(a[i])] < 0):
        pointBack = pointBack + 1
    if (vax_r[int(b[i])] < 0):
        pointBack = pointBack + 1
    if (vax_r[int(c[i])] < 0):
        pointBack = pointBack + 1
    if pointBack >= 2:

        p1 = inletCoordinates[int(a[i]),:]
        p2 = inletCoordinates[int(b[i]),:]
        p3 = inletCoordinates[int(c[i]),:]

        AreaBack = areatriangle3d(p1[0], p1[1], p1[2], p2[0], p2[1], p2[2], p3[0], p3[1], p3[2])
        AreaToTBack.append(AreaBack)
    else:
        p1 = inletCoordinates[int(a[i]),:]
        p2 = inletCoordinates[int(b[i]),:]
        p3 = inletCoordinates[int(c[i]),:]

        AreaIn = areatriangle3d(p1[0], p1[1], p1[2], p2[0], p2[1], p2[2], p3[0], p3[1], p3[2])
        AreaToTIn.append(AreaIn)

# Real Area BAV and TAV
AreaToT_BAVbackflow = np.sum(np.array(AreaToTBack))
AreaToT_BAVinflow = np.sum(np.array(AreaToTIn))
AreaToT_TAV = AreaToT_BAVinflow + AreaToT_BAVbackflow

################################################################################
################################################################################

# Surface1 vector to vtk
info1 = vtk.vtkDoubleArray()
```

```
info1.SetNumberOfComponents(3)
info1.SetNumberOfTuples(N_point)
info1.FillComponent(0,0.)
info1.SetName('surface_INflow')
for i in range(0,N_point):
   info1.SetTuple3(i,surf1_coordinates[i,0],surf1_coordinates[i,1],surf1_coordinates[i,2])

# Surface2 vector to vtk
info2 = vtk.vtkDoubleArray()
info2.SetNumberOfComponents(3)
info2.SetNumberOfTuples(N_point)
info2.FillComponent(0,0.)
info2.SetName('surface_BACKflow')
for i in range(0,N_point):
   info2.SetTuple3(i,surf2_coordinates[i,0],surf2_coordinates[i,1],surf2_coordinates[i,2])

# Add array to surface
inletSurface.GetPointData().AddArray(info1)
inletSurface.GetPointData().AddArray(info2)

# Save new surface
#WritePolyData(inletSurface,'ProfilesNC_noBL_(Cao, K. and Sucosky, P. 2016)[4.0].vtp')
#WritePolyData(inletSurface,'ProfilesLEFT_noBL_(Cao, K. and Sucosky, P. 2016)[3.0].vtp')
#WritePolyData(inletSurface,'ProfilesRIGHT_noBL_(Cao, K. and Sucosky, P. 2016)[3.0].vtp')

print('\nMESSAGE: Inlet - Inflow and Bakflow - Surface DONE.')

################################################################################
################################################################################


# File '*.flow', where the velocity variation is defined
ExcelNameIN = 'flowRate2.xlsx'
```

```
SheetNameIN = 'BAV - Positive'

ExcelNameBACK = 'flowRate2.xlsx'

SheetNameBACK = 'BAV - Negative'

ExcelNameTAV = 'flowRate2.xlsx'

SheetNameTAV = 'TAV - Net'


AreaIN = AreaToT_BAVinflow #CAp info INflow surface

AreaBACK = AreaToT_BAVbackflow #CAp info BACKflow surface

AreaTAV = AreaToT_TAV #CAp info TAV surface


Nin = 8

Nback = 9

Ntav = 18


# Calculate the Fourier series

from FourierSeriesFunction import FourierSeries


t_fourier, x_flowIN, x_PulseVelocityIN = FourierSeries(ExcelNameIN, SheetNameIN, AreaIN, Nin)

t_fourier, x_flowBACK, x_PulseVelocityBACK = FourierSeries(ExcelNameBACK, SheetNameBACK,
AreaBACK, Nback)

t_fourier, x_flowTAV, x_PulseVelocityTAV = FourierSeries(ExcelNameTAV, SheetNameTAV,
AreaTAV, Ntav)


x_flowNET = x_flowIN + x_flowBACK

x_PulseVelocityNET = (x_flowNET/AreaIN)*(np.power(10,3)/60)


N_time = len(t_fourier)

# Time axis in scientific notation

t_dec = ['{:.6e}'.format(t_fourier[i]) for i in range(0, N_time)]


################################################################################

################################################################################


perimeterTAV_NC = 8.68171
```

```
perimeterBAV_NC = 8.13403

perimeterTAV_LEFT = 8.68171
perimeterBAV_LEFT = 8.21397

perimeterTAV_RIGHT = 8.68171
perimeterBAV_RIGHT = 8.35507


perimeterTAV = perimeterTAV_NC
perimeterBAV = perimeterBAV_NC

################################################################################
################################################################################

### CALCULATE HYDRAULIC DIAMETER TAV
D_hTAV = (AreaToT_TAV/perimeterTAV)*4


### CALCULATE REYNOLDS TAV
ro = 1.06 #density [g/cm^3]
mu = 0.04 #viscosity [poise]

ReynoldsTAV = (ro/mu)*(np.mean(x_PulseVelocityTAV))*D_hTAV

### CALCULATE HYDRAULIC DIAMETER BAV
D_hBAV = (AreaToT_BAVinflow/perimeterBAV)*4

### CALCULATE REYNOLDS BAV
ro = 1.06 #density [g/cm^3]
mu = 0.04 #viscosity [poise]

ReynoldsBAV = (ro/mu)*(np.mean(x_PulseVelocityNET))*D_hBAV
```

```
################################################################################
################################################################################

v_scalRe = (D_hTAV/D_hBAV)*(np.mean(x_PulseVelocityTAV))

################################################################################
################################################################################

### MODULATION INFLOW WAVEFORM-2
# Barker et al. 2010 values from literature to scale the correct Inflow velocity profile
vax_rIN = vax_r[surfaceIn_indx]
vax_rINmean = np.mean(vax_rIN)


vax_rIN_Steadymod2 = np.zeros(((len(surfaceIn_indx))))

velocityBAV_PosScaled = (PosFlow_ReScaled/AreaIN)

vax_rIN_Steadymod2 = (vax_rIN/vax_rINmean)*(velocityBAV_PosScaled)

### MODULATION BACKFLOW WAVEFORM-2
# Barker et al. 2010 values from literature to scale the correct Backflow velocity profile
vax_rBACK = vax_r[surfaceBack_indx]
vax_rBACKmean = np.mean(vax_rBACK)

vax_rBACK_Steadymod2 = np.zeros((len(surfaceBack_indx)))

velocityBAV_NegScaled = (NegFlow_ReScaled/AreaBACK)

vax_rBACK_Steadymod2 = (vax_rBACK/vax_rBACKmean)*(velocityBAV_NegScaled)

vax_r_Steady2 = np.zeros(N_point)
```

```
for j in range(0, len(surfaceIn_indx)):
    pos = surfaceIn_indx[j]
    vax_r_Steady2[pos] = vax_rIN_Steadymod2[j]

for j in range(0, len(surfaceBack_indx)):
    pos = surfaceBack_indx[j]
    vax_r_Steady2[pos] = vax_rBACK_Steadymod2[j]

vaxg_XmSTEADY2 = np.zeros((N_point))
vaxg_YmSTEADY2 = np.zeros((N_point))
vaxg_ZmSTEADY2 = np.zeros((N_point))

for k in range(0,N_time):
    vaxg_XmSTEADY2[:] = vax_r_Steady2[:]*un[:,0]
    vaxg_YmSTEADY2[:] = vax_r_Steady2[:]*un[:,1]
    vaxg_ZmSTEADY2[:] = vax_r_Steady2[:]*un[:,2]

################################################################################
################################################################################

# Trought-plane velocity vector to vtk
tPlaneVelocityArray = vtk.vtkDoubleArray()
tPlaneVelocityArray.SetNumberOfComponents(3)
tPlaneVelocityArray.SetNumberOfTuples(N_point)
tPlaneVelocityArray.FillComponent(0,0.)
tPlaneVelocityArray.SetName('tPlaneVelocityREYNOLDS')

for i in range(0,N_point):
    tPlaneVelocityArray.SetTuple3(i,vaxg_XmSTEADY[i],vaxg_YmSTEADY[i],vaxg_ZmSTEADY[i])

# Trought-plane velocity vector to vtk
tPlaneVelocityArray2 = vtk.vtkDoubleArray()
```

```
tPlaneVelocityArray2.SetNumberOfComponents(3)
tPlaneVelocityArray2.SetNumberOfTuples(N_point)
tPlaneVelocityArray2.FillComponent(0,0.)
tPlaneVelocityArray2.SetName('tPlaneVelocityREYNOLDS2')

for i in range(0,N_point):
   tPlaneVelocityArray2.SetTuple3(i,vaxg_XmSTEADY2[i],vaxg_YmSTEADY2[i],vaxg_ZmSTEADY2[i])

   # Add array to surface
   inletSurface.GetPointData().AddArray(tPlaneVelocityArray)
   inletSurface.GetPointData().AddArray(tPlaneVelocityArray2)
   # Save new surface

WritePolyData(inletSurface,'E:/VelocityPROFILES/ProfileFinal/Steady_(NET)2/PoiseuilleSteady2(NC).vtp')
#
WritePolyData(inletSurface,'E:/VelocityPROFILES/ProfileFinal/Steady_(NET)2/PoiseuilleSteady2(LEFT).vtp')
#
WritePolyData(inletSurface,'E:/VelocityPROFILES/ProfileFinal/Steady_(NET)2/PoiseuilleSteady2(RIGHT).vtp')

################################################################################################
################################################################################################

#--------------------Create a Generalized Poiseuille Steady "*.dat" file----------------------------#
# Number of points (Temporal definition)
nl = 2
# Time axis
t0 = '{:.6e}'.format(0)
t1 = '{:.6e}'.format(1)

# Surface points
GlobalNodeID = vtk_to_numpy(inletSurface.GetPointData().GetArray('GlobalNodeID'))

name = 'GeneralizedPoiseuilleSteady2(NC).dat'
```

```
#name = 'GeneralizedPoiseuilleSteady2(LEFT).dat'
#name = 'GeneralizedPoiseuilleSteady2(RIGHT).dat'

out = open (name, "w")
out.write('%d' %int(N_point) + '\t' +  '%d' %int(nl) + '\n')

for i in range(0,N_point):

   # Define surface points coordinates
   x = '{:.6e}'.format(inletCoordinates[i,0])
   y = '{:.6e}'.format(inletCoordinates[i,1])
   z = '{:.6e}'.format(inletCoordinates[i,2])
   nn = GlobalNodeID[i]

   # Define velocity coordinates
   vx = '{:.6e}'.format(vaxg_XmSTEADY2[i])
   vy = '{:.6e}'.format(vaxg_YmSTEADY2[i])
   vz = '{:.6e}'.format(vaxg_ZmSTEADY2[i])

   out.write(x + '\t' + y + '\t' + z + '\t' +  '%d' %int(nl) + '\t' + '%d' %int(nn) +'\n')
   out.write(vx + '\t' + vy + '\t' + vz + '\t' +  t0 +'\n')
   out.write(vx + '\t' + vy + '\t' + vz + '\t' +  t1 +'\n')

out.close()

print('\nMESSAGE: "Generalized Poiseuille Steady.DAT" Writing succefully performed.')
print('\nMESSAGE: "Generalized Poiseuille (NC) Steady.DAT" Writing succefully performed.')
#print('\nMESSAGE: "Generalized Poiseuille (LEFT) Pulse.DAT" Writing succefully performed.')
#print('\nMESSAGE: "Generalized Poiseuille (RIGHT) Pulse.DAT" Writing succefully performed.')
```

8. BIBLIOGRAPHY

[1] H. Anatomy, “LICENSES AND ATTRIBUTIONS CC LICENSED CONTENT , SHARED PREVIOUSLY - Anatomy & Physiology . Provided by : OpenStax CNX . Located at : http://cnx.org/contents/14fb4ad7-39a1-4eee- ab6e-3ef2482e3e22@8.25 . License : CC BY : Attribution . License Terms : Downl,” pp. 1–43, 2018.

[2] M. Heart, “Mammalian Heart and Blood Vessels Exercise 1 : Structure of the Heart,” pp. 1–8, 2018.

[3] B. T. Newman and D. Sullivan, “The heart : All you need to know,” no. January, pp. 1–7, 2018.

[4] T. Electrocardiogram, “Cardiovascular system (heart) anatomy,” pp. 1–5, 2006.

[5] U. et all Morbiducci, “BMSCV Course.”

[6] J. K. Williams and D. D. Heistad, “Structure and function of vasa vasorum,” *Trends Cardiovasc. Med.*, vol. 6, no. 2, pp. 53–57, 1996.

[7] J. M. Chalovich and E. Eisenberg, “NIH Public Access,” *Magn Reson Imaging*, vol. 31, no. 3, pp. 477–479, 2013.

[8] K. Chandran, *Cardiovascular Biomechanics*. 1992.

[9] Https://www.msdmanuals.com/home/heart-and-blood-vessel-disorders/biology-of-the-heart-and-blood-vessels/biology-of-the-blood-vessels, “Biology of the blood vessels.”

[10] American Red Cross Organization, “Blood Components,” *Am. Red Cross*, pp. 2–3, 2013.

[11] Australian Red Cross Blood, “Blood Function and Composition,” *Virtual Med. Cent.*, pp. 1–10, 2008.

[12] O. K. Baskurt, D. Ph, H. J. Meiselman, and D. Sc, “Blood rheology and hemodynamics_Baskurt,” vol. 1, no. 212, pp. 435–450, 2003.

[13] F. M. Montevecchi and P. Iii, “Fluidi biologici,” pp. 1–43.

[14] W. B. Kannel, “Overview of atherosclerosis,” *Clin. Ther.*, vol. 20, no. SUPPL.2, 1998.

[15] R. M. Wazen, S. Kuroda, C. Nishio, K. Sellin, J. B. Brunski, and A. Nanci, “NIH Public Access,” vol. 8, no. 9, pp. 1385–1395, 2014.

[16] “‘Atherogenic’. Merriam-Webster Dictionary.” .

[17] L. Aparecida and C. Veronica, “Anatomicopathological evidence of the beginning of atherosclerosis in infancy and adolescence,” *Arq Bras Cardiol*, vol. 78, no. nº 1, pp. 137–142, 2002.

[18] B. C. Nordqvist and D. R. Wilson, “Coronary heart disease : What you need to know,” no. January, pp. 1–6, 2018.

[19] A. J. Weinhaus and K. P. Roberts, “Anatomy of the Human Heart,” *Handb. Card. Anatomy, Physiol. Devices*, pp. 59–85, 2009.

[20] D. P. Statement, “Atherosclerosis (Atherosclerotic upon nition Cardiovascular Disease and Vascular Medicine,” pp. 1–7, 2018.

[21] G. K. Hansson, “Inflammation, atherosclerosis, and coronary artery disease,” *N.Engl.J.Med.*, vol. 352, pp. 1685–1695, 2005.

[22] T. B. J. of Cardiology, “Lipids module 1: lipid metabolism and its role in atherosclerosis,” pp. 1–9, 2016.

[23] H. Stary *et al.*, “AHA Medical / Scientific Statement Special Report A Definition of Initial , Fatty Streak , and Intermediate Lesions of Atherosclerosis,” *Circulation*, vol. 89, pp. 2462–2478, 1994.

[24] M. Elena R Ladich, M. M. Renu Virmani, and P. Frank Kolodgie, “Atherosclerosis Pathology,” *Medscape*, pp. 1–9, 2010.

[25] Npatchett, “Late complications of atherosclerosis.”

[26] P. Vandana, K. Shweta, J. Deepali, and G. Seema, “Histological Classification of Atherosclerosis and Correlation with Ischemic Heart Disease: A Autopsy Based Study,” *Ann. Pathol. Lab. Med.*, vol. 3, no. 2, pp. A100–A104, 2016.

[27] G. S. (March 2008). McGill HC, McMahan CA, "'Preventing heart disease in the 21st century: implications of the Pathobiological Determinants of Atherosclerosis in Youth (PDAY) study'. Circulation. 117 (9): 1216–27."

[28] H. Federation, "Global Atlas on cardiovascular disease prevention and control."

[29] Heart and Stroke Foundation, "What is coronary artery disease?," pp. 1–7, 2009.

[30] P. Waller, "Everything You Need To Know About," *Pollut. Control*, pp. 1–13, 2015.

[31] N. - NHLBI, ""How Is Atherosclerosis Treated?"

[32] B. R. Kwak *et al.*, "Biomechanical factors in atherosclerosis: Mechanisms and clinical implications," *Eur. Heart J.*, vol. 35, no. 43, pp. 3013–3020, 2014.

[33] M. Loukas *et al.*, "The clinical anatomy of high take-off coronary arteries," *Clin. Anat.*, vol. 29, no. 3, pp. 408–419, 2016.

[34] E. I. Charitos and H.-H. Sievers, "Anatomy of the aortic root: implications for valve-sparing surgery.," *Ann. Cardiothorac. Surg.*, vol. 2, no. 1, pp. 53–6, 2013.

[35] "Ventricular tachycardia and cardiac anatomy aortic cusp."

[36] M. J. Underwood, G. El Khoury, D. Deronck, D. Glineur, and R. Dion, "The aortic root : structure , function , and surgical reconstruction," no. c, pp. 376–380, 2000.

[37] A. Salica *et al.*, "The combined role of sinuses of Valsalva and flow pulsatility improves energy loss of the aortic valve," *Eur. J. Cardio-thoracic Surg.*, vol. 49, no. 4, pp. 1222–1227, 2016.

[38] N. Piazza, P. de Jaegere, C. Schultz, A. E. Becker, P. W. Serruys, and R. H. Anderson, "Anatomy of the aortic valvar complex and its implications for transcatheter implantation of the aortic valve.," *Circ. Cardiovasc. Interv.*, vol. 1, no. 1, pp. 74–81, 2008.

[39] S. K. Atkins, K. Cao, N. M. Rajamannan, and P. Sucosky, "Bicuspid aortic valve hemodynamics induces abnormal medial remodeling in the convexity of porcine ascending aortas," *Biomech. Model. Mechanobiol.*, vol. 13, no. 6, pp. 1209–1225, 2014.

[40] R. J. Cerci *et al.*, "Aligning coronary anatomy and myocardial perfusion territories

an algorithm for the core320 multicenter study," *Circ. Cardiovasc. Imaging*, vol. 5, no. 5, pp. 587–595, 2012.

[41] U. O. Radiologia and O. S. Chiara, "ANATOMIA DELLE ARTERIE CORONARIE," vol. 5, no. Figura 7, pp. 9–10, 2018.

[42] S. Arteria, "Circolo coronarico Densità capillare elevata Flusso a riposo : 60-80 ml / min / 100g tessuto (≅ 5 % GC) Flusso in attività fisica : 200-300 ml / min / 100g tessuto."

[43] A. J. Pappano, W. Gil Wier, A. J. Pappano, and W. Gil Wier, "11 – Coronary Circulation," *Cardiovasc. Physiol.*, pp. 223–236, 2013.

[44] C. I. La, "Anatomia del circolo arterioso coronarico," pp. 1–3, 2018.

[45] B. H. Foundation, "Heart Valve Disease," pp. 5–7, 2014.

[46] S. Y. Ho, "Structure and anatomy of the aortic root," *Eur. J. Echocardiogr.*, vol. 10, no. 1, pp. 3–10, 2009.

[47] A. Alexopoulos, N. Michelakakis, and H. Papadaki, "Pathophysiologic Mechanisms of Age – Related Aortic Valve Calcification," *Aortic Stenosis - Etiol. Pathophysiol. Treat.*, no. July, 2011.

[48] D. A. Lerman, S. Prasad, and N. Alotti, "Calcific Aortic Valve Disease: Molecular Mechanisms and Therapeutic Approaches.," *Eur. Cardiol.*, vol. 10, no. 2, pp. 108–112, 2015.

[49] M. S. Sacks and A. P. Yoganathan, "Heart valve function: A biomechanical perspective," *Philos. Trans. R. Soc. B Biol. Sci.*, vol. 362, no. 1484, pp. 1369–1391, 2007.

[50] M. S. Sacks, W. David Merryman, and D. E. Schmidt, "On the biomechanics of heart valve function," *J. Biomech.*, vol. 42, no. 12, pp. 1804–1824, 2009.

[51] A. Hasan *et al.*, "Biomechanical properties of native and tissue engineered heart valve constructs," *J. Biomech.*, vol. 47, no. 9, pp. 1949–1963, 2014.

[52] W. Is, H. Valve, and H. Foundation, "Heart valve disease Types of heart valve disease," pp. 1–2, 2018.

[53] B. A. Carabello and W. J. Paulus, “Aortic stenosis,” *Lancet*, vol. 373, no. 9667, pp. 956–966, 2009.

[54] C. N. Manjunath, P. Srinivas, K. S. Ravindranath, and C. Dhanalakshmi, “Incidence and patterns of valvular heart disease in a tertiary care high-volume cardiac center: A single center experience,” *Indian Heart J.*, vol. 66, no. 3, pp. 320–326, 2014.

[55] B. Iung and A. Vahanian, “Degenerative calcific aortic stenosis: A natural history,” *Heart*, vol. 98, no. SUPPL. 4, 2012.

[56] “Blausen.com staff (2014). ‘Medical gallery of Blausen Medical 2014’. WikiJournal of Medicine 1 (2): 10. doi:10.15347/wjm/2014.010. ISSN 2002-4436.”

[57] R. Mahadevia *et al.*, “Bicuspid aortic cusp fusion morphology alters aortic three-dimensional outflow patterns, wall shear stress, and expression of aortopathy,” *Circulation*, vol. 129, no. 6, pp. 673–682, 2014.

[58] S. C. Siu and C. K. Silversides, “Bicuspid Aortic Valve Disease,” *J. Am. Coll. Cardiol.*, vol. 55, no. 25, pp. 2789–2800, 2010.

[59] B. M. Schaefer *et al.*, “The bicuspid aortic valve: An integrated phenotypic classification of leaflet morphology and aortic root shape,” *Heart*, vol. 94, no. 12, pp. 1634–1638, 2008.

[60] F. Robicsek, M. J. Thubrikar, J. W. Cook, and B. Fowler, “The congenitally bicuspid aortic valve: How does it function? Why does it fail?,” *Ann. Thorac. Surg.*, vol. 77, no. 1, pp. 177–185, 2004.

[61] K. Cao, S. K. Atkins, A. McNally, J. Liu, and P. Sucosky, “Simulations of morphotype-dependent hemodynamics in non-dilated bicuspid aortic valve aortas,” *J. Biomech.*, vol. 50, no. October, pp. 63–70, 2017.

[62] C. Ward, “Clinical significance of the bicuspid aortic valve,” *Heart*, vol. 83, no. 1, pp. 81–85, 2000.

[63] K. Cao and P. Sucosky, “Effect of Bicuspid Aortic Valve Cusp Fusion on Aorta Wall Shear Stress: Preliminary Computational Assessment and Implication for Aortic Dilation,” *World J. Cardiovasc. Dis.*, vol. 05, no. 06, pp. 129–140, 2015.

[64] J. M. Cengel, Y.A.; Cimbala, “Fluid Mechanics Fundamentals and Applications,” *McGraw-Hill*, 2006.

[65] “vmtk - the Vascular Modelling Toolkit.” [Online]. Available: http://www.vmtk.org/index.html. [Accessed: 02-Nov-2018].

[66] L. Antiga, M. Piccinelli, L. Botti, B. Ene-Iordache, A. Remuzzi, and D. A. Steinman, “An image-based modeling framework for patient-specific computational hemodynamics,” *Med. Biol. Eng. Comput.*, vol. 46, no. 11, pp. 1097–1112, 2008.

[67] “SimVascular.” [Online]. Available: http://simvascular.github.io/index.html. [Accessed: 02-Nov-2018].

[68] H. Si, “TetGen, a Delaunay-Based Quality Tetrahedral Mesh Generator,” *ACM Trans. Math. Softw.*, vol. 41, no. 2, pp. 1–36, Feb. 2015.

[69] “TetGen: Features.” [Online]. Available: http://wias-berlin.de/software/tetgen/features.html. [Accessed: 03-Nov-2018].

[70] J. Zhou, Y. Shui, S. Peng, X. Li, H. Mamitsuka, and S. Zhu, “MeSHSim: An R/Bioconductor package for measuring semantic similarity over MeSH headings and MEDLINE documents,” *J. Bioinform. Comput. Biol.*, vol. 13, no. 06, p. 1542002, Dec. 2015.

[71] S. Sankaran, M. Esmaily Moghadam, A. M. Kahn, E. E. Tseng, J. M. Guccione, and A. L. Marsden, “Patient-Specific Multiscale Modeling of Blood Flow for Coronary Artery Bypass Graft Surgery,” *Ann. Biomed. Eng.*, vol. 40, no. 10, pp. 2228–2242, Oct. 2012.

[72] K. Cao and P. Sucosky, “Computational comparison of regional stress and deformation characteristics in tricuspid and bicuspid aortic valve leaflets,” *Int. j. numer. method. biomed. eng.*, vol. 33, no. 3, 2017.

[73] A. J. Barker, C. Lanning, and R. Shandas, “Quantification of hemodynamic wall shear stress in patients with bicuspid aortic valve using phase-contrast MRI,” *Ann. Biomed. Eng.*, vol. 38, no. 3, pp. 788–800, 2010.

[74] Y. Zhou, G. S. Kassab, and S. Molloi, “On the design of the coronary arterial tree: a generalization of Murray’s law,” *Phys. Med. Biol.*, vol. 44, no. 12, pp. 2929–2945,

Dec. 1999.

[75] R. S. Reneman and A. P. G. Hoeks, “Wall shear stress as measured in vivo: Consequences for the design of the arterial system,” *Med. Biol. Eng. Comput.*, vol. 46, no. 5, pp. 499–507, 2008.

[76] R. Lima, *Visualization and Simulation of Complex Flows in Biomedical Engineering*, vol. 12. 2014.

[77] S. Chien, “Mechanotransduction and endothelial cell homeostasis: the wisdom of the cell,” *Am. J. Physiol. Circ. Physiol.*, vol. 292, no. 3, pp. H1209–H1224, Mar. 2007.

[78] J.-J. Chiu and S. Chien, “Effects of Disturbed Flow on Vascular Endothelium: Pathophysiological Basis and Clinical Perspectives,” *Physiol. Rev.*, vol. 91, no. 1, pp. 327–387, Jan. 2011.

[79] C. Chiastra, S. Morlacchi, S. Pereira, G. Dubini, and F. Migliavacca, “Computational fluid dynamics of stented coronary bifurcations studied with a hybrid discretization method,” *Eur. J. Mech. B/Fluids*, vol. 35, pp. 76–84, 2012.